Electronic Structure and Statistical Mechanical Approach to Solvation Processes(Dissertation_全文)

AUTHOR(S):

Ishida, Tateki

Doctoral Thesis

Electronic Structure and Statistical Mechanical Approach to Solvation Processes

Tateki Ishida

Department of Chemistry, Graduate School of Science,

Kyoto University

Contents

Chapter 1

General Introduction

In the present thesis, the author investigates theoretically the static and dynamical solvent effects on chemical reactions in solution, and proposes the new procedure to treat the nonequilibrium process in solution. As the static solvent effects, two problems are studied: (1) solvent effects on the keto-enol tautomerization of formamide and the relation between the calculated solvation free energy and the empirical solvent parameters in aprotic solvents, (2) solvent effects on the thermodynamical properties and the large geometric change in the keto-enol tautomerization of acetylacetone in polar or nonpolar solvents.

Also, as the dynamical solvent effects, the solvation dynamics of benzonitrile at the vertical excitation and solvent effects on its process are investigated. In addition, the time-dependent reference interaction site model self-consistent field approach are proposed.

On the study of chemical equilibria and reaction processes in solution, it is one of the main subjects to understand the properties of solvents that play an important role, in addition to the detail of solute molecules. In the equilibrium state, it is considered that solvent effects appear through the solvation structure, governed by the short range

property such as hydrogen bonding and the long range one such as the electrostatic potential. For the latter, many theoretical methods have been developed, and it could be treated well by the dielectric constants which are macroscopic properties of solvent. For the former property, however, those are not enough since the short range property in solution depends on the microscopic interaction such as the solute-solvent one. The dielectric continuum model does not take the solvent geometric aspects into account, and therefore, it is unable to describe the local solute-solvent interaction. Statistical mechanics of liquids has been developed by using the integral equations. The reference interaction site model (RISM)[1] enable us to treat the solute and solvent molecular shape and, in the extended RISM (XRISM) theory[2]-[4], the Coulombic interaction was included by setting parial charges on each atomic site. The RISM equation is given as the following,

$$\boldsymbol{h} = \boldsymbol{\omega} * \boldsymbol{c} * \boldsymbol{\omega} + \rho \boldsymbol{\omega} * \boldsymbol{c} * \boldsymbol{h}, \tag{1.1}$$

where $\boldsymbol{h}$ and $\boldsymbol{c}$ represent the total and direct correlation function in the matrix form, respectively. $\boldsymbol{\omega}$ is the matrix representation for the intramolecular correlation function that defines the molecular geometry. ρ is the solvent number density. Also, the asterisk denotes the spatial convolution integral.

The XRISM theory can describe the local solute-solvent interaction such as hydrogen bonding, and the detailed solvation structures at the equilibrium state are obtained from the site-site radial distribution functions (rdfs). Also, the solute electronic structure changes due to the solvation compared to that in the gas phase, and, therefore, the solute site charges are altered. In order to take this effect into account, it is important to consider the solute electronic structure. Recently, the RISM self-consistent field (RISM-

SCF) method[5, 6] has been proposed. This is an *ab initio* electronic structure theory taking the field caused by the solvent around the solute molecule in molecular detail into account, and, by using this method, the solvation free energy and solute-solvent interaction can be analyzed from the microscopic point of view.

In nonequilibrium processes in solution, during the change from the previous equilibrium state to the new equilibrium one, the solvent distribution function around the solute molecule is represented in the time-dependent form. Then, if it is assumed that the alteration of solute electronic structure is much faster than the relaxation of solvents around the solute, it is considered that the solvent relaxation process mainly determine the nonequilibrium process. Therefore, to understand it, it is necessary to proceed the discussion based on the characteristic properties defined as the nonequilibrium ensemble average of selected dynamical variables.

In the chapter, for introducing to the subsequent chapters, reviews of theoretical treatments for solvent effects in the equilibrium state and in the nonequilibrium process, taking into the geometric aspects of solute and solvent molecules, are given.

In the chapter 2, the solvent effect on keto-enol tautomers of formamide in aprotic solvents by using the reference interaction site model self-consistent field (RISM-SCF) method is studied. The solvation free energy, solvation structures, and solute electronic structures are analyzed precisely with the RISM-SCF method. From a microscopic point of view, the relation between calculation results and the empirical solvent parameters representing solute-solvent hydrogen bonding is discussed.

In the chapter 3, a prototype β-diketone, acetylacetone, is chosen as the solute molecule, and the keto-enol tautomerization of acetylacetone in H_2O, dimethyl sulfoxide (DMSO) and carbon tetrachloride (CCl_4) is studied. The geometrical change of the

tautomers due to solvent effect taking the solute electronic structure into account is analyzed with the RISM-SCF method. The electron correlation energy of solute molecule and solute vibrational energies are considered. Based on the calculated solvent-solvent and solute-solvent total correlation functions, the thermodynamic analysis for the free energy differences between both tautomers obtained is carried out. Decomposing them into the enthalpy and entropy terms, solvent effects on tautomerization of acetylacetone is discussed considering solvent property.

In the chapter 4, the procedure to obtain the time-dependent radial distribution functions for describing the nonequilibrium process is shown based on the theory by Raineri *et al.*. Combining *ab initio* calculation method, a new treatment for treat the evolution of the solute electronic structure in solution, the time-dependent RISM-SCF approach, is proposed. This procedure is applied to the solvation dynamics of benzonitrile (C_6H_5CN) after the $2^1A_1 \leftarrow 1^1A_1$ vertical transition in H_2O, methanol(CH_3OH) and acetonitrile (CH_3CN). The solvation time correlation function and the solute charge time correlation function are calculated and analyses for them are carried out. Solvent dynamical property is discussed through the study of solvent relaxation processes considering the evolution solute electronic structure during the solvation.

1.1 Solvent Property

1.1.1 Solvent Parameters

There are many standards for determining solvent characters. Density, viscosity, heat capacity and so on, have been measured and revised for pure solvents. On the other hand, the standards that indicate functionalities of solvents in solution have been pro-

posed, too.[15] The solvent dielectric constants regard solvents as a continuum, and it is only one of the properties representing the long range interactions. The parameters to determine character of not only the long range but also the short one are needed. Of those standards, solvent parameters are famous standards, and various kinds of them have been determined. Some empirical parameters of solvent polarity are known, and, above all, solvent parameters by Taft *et al.*[8] are one of the reliable parameters and they have been determined for various kinds of organic solvents. The method applied by Taft *et al.* is interesting. They classified solvent parameters into mainly three types, α, β and π^*. The α and β parameters represent the ability of solvents to donate and accept a proton in solute-solvent hydrogen bonding, respectively. Also, π^* parameters indicate the empirical solvent dipolarity/polarizability. These three parameters are obtained from the experimental values of the equilibrium constant and so on. The remarkable point in the empirical parameters by Taft *et al.* is that solvent parameters representing the local interaction such as hydrogen bonding are defined and determined in addition to the parameter for the dielectric property. Though these empirical parameters are used to explain, for example, the energy differences of the keto-enol tautomerization and the chemical equilibrium, solvent parameters are still recognized as a phenomenological character. The physical meanings for solvent parameters themselves have not yet been analyzed from a microscopic view point.

Above-mentioned solvent parameters are often determined based on the equilibrium constant, i.e. the free energy differences. Therefore, it is necessary to evaluate the free energy and solvation energy in solution by the microscopic theory. The detail of such theory will be reviewed below.

1.1.2 Solvation Process

When a solute molecule is dissolved in solvent, solvents have an effect on a solute, that is, solvation effect. In the solvation process, it is considered that the solute molecule in the gas phase is transferred into the liquid phase. Therefore, solvents have to move and make a space (often called a cavity) for a solute immersed. Then, the solvation energy is composed of the solute-solvent interaction energy and the cavity formation (solvent reorganization) energy due to solvation. The stability of solvation energy is enhanced by the intermolecular interaction such as hydrogen bonding between solute site and solvent one, and its degree depends on the charges on solute and solvent atomic sites and the molecular shapes. In addition, the cavity formation energy have to be treated based on the site-site representation.

The solvent reorganization energy is estimated by taking the derivatives of site-site total and direct correlation function with respect to the solute density, ρ_u, at the infinite dilution. This is evaluated by the following equation:

$$\begin{aligned}\Delta\epsilon_{u,sol} = \rho_{\mathrm{v}} \sum_{\alpha=1}^{n_{\mathrm{u}}} \sum_{\gamma=1}^{n_{\mathrm{v}}} \int_0^\infty 4\pi r^2 \mathrm{d}r U_{\alpha\gamma}(r) g_{\alpha\gamma}(r) \\ + \frac{\rho_{\mathrm{v}}^2}{2} \sum_{\gamma=1}^{n_{\mathrm{v}}} \sum_{\gamma'=1}^{n_{\mathrm{v}}} \int_0^\infty 4\pi r^2 \mathrm{d}r U_{\gamma\gamma'}(r) \delta_{\rho_{\mathrm{u}}} h_{\gamma\gamma'}(r),\end{aligned} \tag{1.2}$$

where ρ_v is the solvent density and α and γ denote the interaction sites in solute and solvent molecules. n_{u} and n_{v} denote the numbers of sites in the solute and solvent molecule, respectively. $U_{\alpha\gamma}$ and $U_{\gamma\gamma'}$ are the solute-solvent and solvent-solvent site-site interaction potentials. $g_{\alpha\gamma}(r)$ is the site-site radial distribution function. $\delta_{\rho_u} h_{\gamma\gamma'}(r)$ is the first-order isothermal density derivatives. The first term in the right hand side of Eq.(1.2) represents the solute-solvent interaction energy E_{uv} and the second is the cavity formation energy

E_{cav}, which represents the solvent reorganization energy due to solvation.

Yu et al.[9, 10] proposed the method to obtain $\delta_{\rho_u} h_{\gamma\gamma'}(r)$ or $\delta_{\rho_u} h_{\gamma\gamma'}(r)$ based on the XRISM theory. From the first-order isothermal density derivatives to Eq.(1.1), the following relation is given,

$$\delta_{\rho_\eta} \hat{h}_{ss'} = \hat{w}_s \delta_{\rho_\eta} \hat{c}_{ss'} \hat{w}_{s'} + \left[\hat{w}_s \delta_{\rho_\eta} \hat{c}_{sv} + \hat{h}_{sv} \rho_v \delta_{\rho_\eta} \hat{c}_{vv}\right] \rho_v \hat{h}_{vs'} + \hat{h}_{s\eta} \hat{w}_\eta^{-1} \hat{h}_{\eta s'}, \tag{1.3}$$

where $\hat{h}, \hat{c}$ and $\hat{w}$ represent h, c and w in k-space, respectively, with $\{s, s'\} = \{u, v\}$. The corresponding relation to the HNC closure is given by:

$$\delta_{\rho_\eta} h_{\alpha\gamma}(r) = \left[\delta_{\rho_\eta} h_{\alpha\gamma}(r) - \delta_{\rho_\eta} c^*_{\alpha\gamma}(r)\right] \left[h_{\alpha\gamma}(r) + 1\right], \tag{1.4}$$

where η represents u or v, and $\delta_{\rho_\eta} \hat{c}^* = \delta_{\rho_\eta} \hat{c} - \hat{\phi}^\eta$, $\hat{\phi}^\eta = \delta_{\rho_\eta} \hat{\phi}$. $\hat{\phi}$ represents the Coulombic interaction.

The enthalpy term $\delta h_{u,sol}$ is calculated by the following equation,

$$\begin{aligned} \Delta h_{u,sol} = \Delta\epsilon_{u,sol} + T\alpha_{v,P} \{ & \Delta\mu_{u,sol} \\ + & \frac{\rho_v^2}{2\beta} \sum_{\alpha=1}^{n_u} \sum_{\gamma=1}^{n_v} \int_0^\infty 4\pi r^2 \mathrm{d}r \left[h_{\alpha\gamma}(r) \delta_{\rho_v} c_{\alpha\gamma}(r) - c_{\alpha\gamma}(r) \delta_{\rho_v} h_{\alpha\gamma}(r)\right] \Bigg\}, \end{aligned} \tag{1.5}$$

where $\alpha_{v,P}$ is the isobaric thermal expansion coefficient of the pure solvent. Also, the excess chemical potential is represented as[11, 12]

$$\Delta\mu_u = \frac{\rho}{2\beta} \sum_{\alpha\in u} \sum_{\gamma\in v} \int_0^\infty 4\pi r^2 \mathrm{d}r (h_{\alpha\gamma}^2 - 2c_{\alpha\gamma} - h_{\alpha\gamma} c_{\alpha\gamma}). \tag{1.6}$$

where $\beta = 1/k_B T$ with k_B being the Boltzmann constant and T being temperature. $h_{\alpha\gamma}$ and $c_{\alpha\gamma}$ are total and direct correlation function, respectively. From these equations, the solvation entropy is defined by

$$\Delta S_{u,sol} = (\Delta h_{u,sol} - \Delta \mu_{sol})/T. \tag{1.7}$$

As shown in above-mentioned equations, the solvation energy and solvation enthalpy depend on the site-site correlation functions and solute-solvent or solvent-solvent interactions. Therefore, by using the results obtained with the interaction site model, it enables us to discuss solvent effects on the thermodynamic property considering the geometric aspects of solute and solvent molecules.

1.1.3 Solute Electronic Structure on Solvation Processes

In the transfer process of a solute molecule from in the gas phase to in solvents, the solute electronic structure is affected by the field coming from solvent distribution around a solute molecule. Along with the change of the solute electronic structure, the variations of charges on solute atomic sites can occur. Therefore, the solute-solvent interactions have effects on the solvation structure. In order to take the solute electronic structure into account, many procedures have been proposed, and the some methods which attempts to treat solvents with the shape have appeared. Recently, the RISM-SCF method[5, 6] has been developed and applied to some chemical systems. The outline of the RISM-SCF method is summarized below briefly.

In the RISM-SCF theory, the total free energy of the system is defined by,

$$G = \langle \Psi \mid \hat{H}_{gas} + \Delta \hat{\mu}_{sol} \mid \Psi \rangle, \tag{1.8}$$

where Ψ is the solute electronic wave function and $\hat{H}_{gas}$ is the solute electronic Hamiltonian in the gas phase. $\Delta \hat{\mu}_{sol}$ is the operator that determines the excess chemical potential due

to the solvation, Eq.(1.6). From the variation of Eq.(1.8) with respect to the solute molecular orbitals and the correlation functions, the Fock equation is obtained as,

$$\hat{F}_{sol}\phi_i = \varepsilon_i\phi_i, \tag{1.9}$$

where $\hat{F}_{sol}$ is the solvated Fock operator. $\hat{F}_{sol}$ is defined in the form

$$\hat{F}_{sol} = \hat{\mathrm{h}} + 2\hat{J} - \hat{K} - \sum_{\alpha} V_\alpha \hat{b}_\alpha, \tag{1.10}$$

where $\hat{\mathrm{h}}$, $\hat{J}$ and $\hat{K}$ are the usual one electron, Coulomb and exchange operators and $\hat{b}_\alpha$ is the population operator which generates the partial charge on the solute atomic site α. The averaged electrostatic potential acting on the site α is given by

$$V_\alpha = \rho \sum_{\gamma} \int \mathrm{d}r \frac{q_\gamma}{r} g_{\alpha\gamma}(r), \tag{1.11}$$

where $g_{\alpha\gamma}(r)$ is the radial distribution function.

Also, under the variational condition, the RISM Ornstein-Zernike (OZ) equation:

$$h_{uv} = w_u * c_{uv} * \omega_v + \rho\omega_u * c_{uv} * h_{vv} \tag{1.12}$$

and the hypernetted chain (HNC) closure relation is obtained. In Eq.(1.12), the indices u and v denote the solute and solvent, ρ is the number density of solvent. w is the intramolecular correlation function that defines the molecular geometry. The solvent-solvent correlation function, h_{vv}, is determined from the RISM OZ equation for the pure solvent:

$$h_{vv} = \omega_v * c_{vv} * \omega_v + \rho\omega_v * c_{vv} * h_{vv}. \tag{1.13}$$

1.2 Solvent Dynamical Property

1.2.1 Surrogate Theory

In order to describe the nonequilibrium process such as solvation dynamics, Raineri *et al.*[13]-[15] have proposed the surrogate description. In the equilibrium states, the Hamiltonian in the equilibrium that governs the solvent in the field of the solute is described as

$$H = H_w + \hat{\Psi}^* + \hat{\Psi}^l, \tag{1.14}$$

where H_w is the Hamiltonian of the pure solvent. $\hat{\Psi}^*$ and $\hat{\Psi}^l$ are the short range and the long range parts of the solute-solvent interactions, respectively. In the surrogate theory, they modify above Hamiltonian and define the following one as the surrogate Hamiltonian,

$$H_\Sigma^{\mathcal{D}} = H_w + \hat{\Psi}_\Sigma^{\mathcal{D}}, \ (\ \mathcal{D} = \mathcal{P} \ or \ \mathcal{S}) \tag{1.15}$$

where $\hat{\Psi}_\Sigma^{\mathcal{D}}$ represent renormalized solute-solvent interaction. The supersubscript P denotes the precursor state which is the equilibrium state before a sudden change of the solute charge distribution and S represents the new equilibrium states at $t = \infty$.

Based on the surrogate Hamiltonian, Eq.(1.15), the nonequilibrium distribution function of the state Γ at time t, is given as

$$f^h(\Gamma, t) = f^{\mathcal{S}}(\Gamma) + \beta f_{eq}^w(\Gamma)\delta\hat{\mathcal{E}}(-t), \tag{1.16}$$

where the superscript h denotes the homogeneous approximation.[13]-[15] Here $f^{\mathcal{S}}$ is the

equilibrium distribution at $\mathcal{S}$ state and f_{eq}^{w} is that for the homogeneous solvent. $\hat{\mathcal{E}}$ is the surrogated energy gap and defined as

$$\hat{\mathcal{E}} = H_{\Sigma}^{\mathcal{S}} - H_{\Sigma}^{\mathcal{P}} = \hat{\Psi}_{\Sigma}^{\mathcal{S}} - \hat{\Psi}_{\Sigma}^{\mathcal{P}}. \tag{1.17}$$

Here, the renormalized pair interaction, $\hat{\Psi}_{\Sigma}^{\mathcal{D}}$, is chosen so that a dynamical variable, $\hat{\mathcal{G}}$, satisfies the following equation,

$$\langle\langle \hat{\mathcal{G}} \rangle\rangle^{\mathcal{D}} = \langle \hat{\mathcal{G}} \rangle^{\mathcal{D}}, \ (\mathcal{D} = \mathcal{P} \ or \ \mathcal{S}) \tag{1.18}$$

where $\langle\langle \cdots \rangle\rangle$ is the nonequilibrium ensemble average with Eq.(1.16). $\langle \cdots \rangle$ is the equilibrium ensemble average with f_{eq}^{w}.

Raineri *el at.*[13]-[15] chose the site number densities of the solvent as the dynamical variable,

$$\hat{n}_{u,\lambda} = \sum_{i} \delta(\boldsymbol{r} - \boldsymbol{r}_{i\lambda} + \boldsymbol{r}_{u}), \tag{1.19}$$

where the summation runs all over the solvent molecules, and they defined $\hat{\Psi}_{\Sigma}^{\mathcal{D}}$ in the following form,

$$\hat{\Psi}_{\Sigma}^{\mathcal{D}} = \sum_{u} \sum_{i} \int \mathrm{d}^{3}\boldsymbol{r}\, \hat{n}_{u\lambda}(\boldsymbol{r}) \phi_{u\lambda}^{\mathcal{D}}(\boldsymbol{r}). \tag{1.20}$$

Here, renormalized pair interactions $\phi_{u\lambda}^{\mathcal{D}}(\boldsymbol{r})$ is not defined. They showed that the following relation was confirmed under Eq. (1.18),

$$-\beta \phi_{u\lambda}^{\mathcal{D}}(r) = c_{u\lambda}^{\mathcal{D}}(r), \tag{1.21}$$

where $c_{u\lambda}^{\mathcal{D}}(r)$ is the direct correlation function, evaluated by using the XRISM equation.

It is in advance of the computer simulation that, in the surrogate theory, the calculation of the nonequilibrium ensemble average can carried out easily with the equilibrium distributions. The surrogate theory are applied to the problem of solvation dynamics in some systems, and it shows the good agreement with the nonequilibrium molecular dynamics (MD) simulation. However, in this theory, since it is difficult to take solute site charge variations during the solvation process into account, the detail information of solute-solvent interactions at every time step can not be obtained. Therefore, in order to the changes of solute site charges at every time step, it is necessary to calculate the time-dependent solute electronic structure of the solute molecule.

Bibliography

[1] D. Chandler and H. C. Andersen, J. Chem. Phys. **57**, 1930 (1972).

[2] F. Hirata and P. J. Rossky, Chem. Phys. Lett. **83**, 329 (1981).

[3] F. Hirata, B. M. Pettitt and P. J. Rossky, J. Chem. Phys. **77**, 509 (1982).

[4] F. Hirata, P. J. Rossky and B. M. Pettitt, J. Chem. Phys. **78**, 4133 (1983).

[5] S. Ten-no, F. Hirata and S. Kato, Chem. Phys. Lett. **214**, 391 (1993).

[6] S. Ten-no, F. Hirata and S. Kato, J. Chem. Phys. **100**, 7443 (1994).

[7] C. Reichardt, *Solvents and Solvent Effects in Organic Chemistry, 2nd ed* (VCH Verlagsgesellschaft, Weinheim, 1988).

[8] M. J. Kamlet, J.-L. M. Abboud, M. H. Abraham and R. W. Taft, J. Org. Chem. **48**, 2877 (1983).

[9] H. A. Yu and M. Karplus, J. Chem. Phys. **89**, 2366 (1988).

[10] H. A. Yu, B. Roux, and M. Karplus, J. Chem. Phys. **92**,5020 (1990).

[11] S. J. Singer and D. Chandler, Mol. Phys. **55**, 621 (1985).

[12] D. A. Zichi and P. J. Rossky, J. Chem. Phys. **84**, 1712 (1986).

[13] F. O. Raineri, H. Resat, B.-C. Perng, F. Hirata, and H. L. Friedman, J. Chem. Phys. **100**, 1477 (1994).

[14] F. O. Raineri, B.-C. Perng, and H. L. Friedman, Chem. Phys. **183**, 187 (1994).

[15] H. L. Friedman, F. O. Raineri, F. Hirata, and B.-C. Perng, J. Stat. Phys. **78**, 239 (1995).

Chapter 2

Molecular Theory of Solvent Effect on Keto-Enol Tautomers of Formamide in Aprotic Solvents: RISM-SCF Approach

2.1 Introduction

Solvent effects on chemical equilibria and reactions have long been one of the important subjects in physical organic chemistry. Several empirical relations have been proposed to characterize the properties of various protic and aprotic solvents.[1] Among them, the solvent parameters that Taft and co-workers[2] determined taking solute-solvent hydrogen bonding and solvent polarity into account have been applied to rationalize experimentally observed solvent effects. Although these parameters have been qualitatively related to the physical properties of solvent molecules such as hydrogen bonding and solvent polarities

in their studies, it seems still far from satisfactory to interpret them on the basis of microscopic information of the solute-solvent interaction and solvation free energy. In particular, the theoretical interpretation based on statistical mechanical treatments of solute-solvent systems is virtually nonexistent to our knowledge. In this respect, it would be worthwhile to carry out theoretical studies on the solvent effects for various protic and aprotic solvents from a unified microscopic point of view.

There has been remarkable progress in the electronic structure theories of solute molecules in solution in the last two decades. Various versions of self-consistent reaction field (SCRF) methods have been advanced[3] to utilize them in interpreting the effects of polar solvents on chemical phenomena. However, many of these methods[4] employ the dielectric continuum model for solvent, characterized by the dielectric constants, and are unable to describe the local solute-solvent interaction such as hydrogen bonding.

Statistical mechanics of liquids has been developed by the approach with the integral equations. The reference interaction site model (RISM) by Chandler and Andersen[5] takes the geometric aspect of molecules into account with the site - site representation for intra- and intermolecular interactions. The extended RISM (XRISM) theory[6]-[8] has been further devised to include the Coulombic interaction between molecules by setting partial charges on each atomic site.

Recently, the RISM self-consistent field (RISM-SCF) method[9]–[11] has been developed by combining the electronic structure calculations of solute molecules with the RISM theory for solvents and applying it to various problems in solution chemistry.[12]-[14]. This method describes the solute-solvent interaction as the sum of site - site interactions between the constituent atoms in solute and solvent molecules and thus has an advantage in providing a microscopic view of solute-solvent interaction. It is noted that the RISM-SCF

method has been applied so far only to the aqueous solutions.[12]-[14]

Many examples of the solvent effects on chemical equilibria and reactions have been observed. Among them, the solvent effect on the keto-enol tautomerism has been extensively studied.[15, 16] Experimentally, it is known that the keto-enol equilibrium constants change depending on the solvent polarity in solution.[17]-[20] Theoretical studies of the specific systems such as 2-pyridone[1, 21] ,formamide[1, 21, 22] have been reported, but, in most of them, the solvent was treated as a dielectric continuum and little information was obtained on the structure of solvents around the solute. In these studies, the solvation free energy has been interpreted in relation to the dielectric constants, which are macroscopic properties of solvents and could not be treated from the viewpoint of microscopic picture.

In this article, we present a theoretical study on the keto-enol tautomerism of formamide in a series of aprotic solvents. We adopted six aprotic solvents including carbon tetrachloride (CCl_4) and carbon disulfide (CS_2) as nonpolar ones, and dimethyl ether (DME), tetrahydrofuran (THF), acetonitrile (CH_3CN), and dimethyl sulfoxide (DMSO) as polar ones. We carried out RISM-SCF calculations to obtain the geometries and solvation free energies of the keto and enol tautomers of formamide in these aprotic solvents. In the following section, the details of calculations are presented. In Sec. 2.3, we present the results of calculations and the origin of the energy difference between the keto and enol tautomers is discussed by relating the solvation free energy to the characteristics of solvent molecules. We further give a microscopic interpretation of Taft's solvent parameters based on the present calculations. The conclusion is given in Sec. 2.4.

2.2 Method

(a) Calculation of the Total Correlation Functions of Pure Aprotic Solvents

In applying the XRISM theory to the solute - solvent systems, it is necessary to solve the RISM Ornstein-Zernike equations:

$$h^{vv} = \omega^v * c^{vv} * \omega^v + \rho\omega^v * c^{vv} * h^{vv} \tag{2.1}$$

$$h^{uv} = \omega^u * c^{uv} * \omega^v + \rho\omega^u * c^{uv} * h^{vv} \tag{2.2}$$

where the asterisk denotes the spatial convolution integral, h and c stand for the site-site intermolecular pair correlation functions and the direct correlation functions, respectively, and ρ is the number density of solvent. The indices u and v denote the solute and solvent, respectively. ω is the intramolecular correlation function that defines the molecular geometry. As the total correlation function, h^{vv}, for solvent in Eq.(2.2), the solutions of Eq.(2.1) for pure solvents are used.

The total correlation functions of pure aprotic solvents were obtained by solving Eq.(2.1) with the hypernetted chain (HNC) approximation. The geometric parameters, the partial charges on the sites, and the parameters of the 6-12 type potential functions of aprotic solvents were those used in the computer simulations.[23]-[29] All the parameters employed in the present calculations are summarized in Table 1. The Lennard-Jones parameters of solute atoms[30, 31] are also included in Table 1.

(b) RISM-SCF calculation

The details of the RISM-SCF method have been presented in previous papers.[9]-[11] In determining partial charges on the solute sites, we generated grid points based on the

Voronoi polyhedrons[32] and applied the least square fitting procedure to the electrostatic potential coming from the solute charge distribution. All the ab initio calculations were performed at the restricted Hartree-Fock (RHF) level by using the double zeta plus polarization (DZP) basis set.[39] The geometry of the solute molecule was optimized using the analytical energy gradient technique[11] in each solvent studied.

The solvation free energies were calculated with the equation for HNC closure[34, 35]:

$$\Delta F_{HNC} = \frac{\rho}{2\beta} \sum_{\alpha \in u} \sum_{\gamma \in v} \int_0^\infty 4\pi r^2 \mathrm{d}r (h_{\alpha\gamma}^2 - 2c_{\alpha\gamma} - h_{\alpha\gamma} c_{\alpha\gamma}) \tag{2.3}$$

and the total free energy was defined by

$$E_{total} = E^{sol}(solute) + \Delta F_{HNC} \tag{2.4}$$

where $E^{sol}(solute)$ represents the electronic energy of the solute in solution. In solution, the solute electronic structure changes from that in the gas phase due to the solute-solvent interaction. The energy change associated with the relaxation in the geometry and the electronic structure of the solute is defined as the following:

$$\Delta E_{re} = E^{sol}(solute) - E^{gas}(solute) \tag{2.5}$$

where $E^{gas}(solute)$ is the solute energy in the gas phase.

2.3 Results and Discussion

2.3.1 Solvation Structure

(a) Pure Solvent Radial Distribution Function

We carried out RISM calculations to obtain the radial distribution functions (rdfs), the total correlation functions, for six aprotic solvents. We used the potential parameters listed in Table 1. The geometric parameters were taken from the literature for all the solvents.[23]-[29, 36] The temperature was set to be 295.15K for CCl_4 and 298.15K for other solvents except DME, respectively, and that of DME was 248.35K. Although the RISM calculations have been reported previously for CCl_4, CS_2, the partial charges on the sites were not taken into account in these calculations.[23] Therefore the results of the present calculations are different from those in the previous ones.

Since the present calculations of solvents are aimed to use in the calculations for solutions, we only discuss here the results for THF and DMSO. In Figure 1, the calculated rdfs for pure THF and DMSO are shown and are compared with the computer simulation results for pure THF[27] and DMSO[29]. For THF, the positions and heights of the first and second peaks are in qualitative accord with those obtained by the computer simulation. The rdf for DMSO is rather complicated as seen in Figure 1(b), but the positions and heights of three peaks and the whole profile are similar to those by the computer simulation. Also in both cases, the long range behavior which appears in the simulation results is reproduced.

(b) Radial Distribution Functions of Solvent around Solute

Some of the rdfs between the solute hydrogen atoms, H(4) and H(5) in Figure 2, and solvent atoms are shown in Figure 3(a) - 3(c). The rdfs in polar aprotic solvents show distinct peaks representing the first and second solvation shells. The height of the first peak is greater than that of the second peak. In solutions of nonpolar aprotic solvents, however, the first peak does not appear clearly and the whole profiles of the rdfs are structureless. In determining the solvation structure, the Coulombic interactions between

the solute and the solvents in the neighborhood of the first peak are very important. Especially, the hydrogen atoms with positive partial charges attractively interacts with the solvent atoms with negative partial charges and repulsively with the solvent atoms positively charged. Since, as seen in Table 2, H(4) and H(5) of formamide have modest positive charges, the interactions with the nitrogen of acetonitrile and the oxygen of DMSO, which have large negative charges, are attractive due to the Coulombic interaction. These attractive forces produce distinct peaks in the rdfs. Since the chlorine site of CCl_4 has a small positive charge, the structureless behavior in the rdfs in CCl_4 solution is caused by the repulsive interaction between positive charges on solute and solvent sites, and this behavior shows that the tendency of forming a solute-solvent hydrogen-bond is low.

2.3.2 Solvation Energy

(a) Comparison of Solvations for Keto and Enol Tautomers

In Table 3, the optimized geometries of formamide and its tautomer in solutions are shown. In nonpolar aprotic solvents, the structures of both tautomers are very close to the gas phase ones due to weak solute-solvent interactions. In polar aprotic solvents, the C=O distance in formamide is stretched while the C-N bond is shortened. This structural change increases the solute dipole moment and results in a stronger solute-solvent interaction.

In the enol form (formidic acid), the intramolecular hydrogen bonding between the nitrogen and hydroxyl hydrogen atom is formed in the gas phase. Its strength seems to be weak, but it affects the distance between the nitrogen and hydrogen. As seen in Table 3, the N$\cdots$H distance does not change compared with that in the gas phase in the nonpolar

solvents. However, the distance becomes longer in polar solvents than in the gas phase by about 0.05 Å . This is because the intramolecular hydrogen bond is weakened because of the formation of solute-solvent hydrogen bonding. The O-H bond and the OCN bending angle are slightly increased in polar solvents which enhance the solute dipole moment.

The differences in the total free energies between the keto and enol tautomers at the optimized geometries, denoted by ΔG, are shown in Table 4. For the solutions of nonpolar solvents, the energy differences between the keto and enol tautomers are almost the same as that in the gas phase. This is because the solvation free energies as well as the solute electronic reorganization energies are very small since the electrostatic potentials acting on the solute sites are very small in these solvents.

On the other hand, in the solutions of polar aprotic solvents, ΔG is larger than that in the gas phase. As seen in Table 4, the differences in the solvation free energies are larger than those in the solute reorganization energies in all solutions. Therefore it is considered that ΔG is dominated by the solvation free energy differences. For the keto-enol equilibria, the keto tautomer is stabilized in comparison with the enol one, which is consistent with the larger dipole moment of the keto tautomer than the enol one. This is in qualitative accord with the experimental findings on similar tautomeric systems.[16, 18]

(b) Solvation Free Energy Analyses

In Table 4, the solvation free energies of the keto and enol form of formamide in aprotic solvents are shown. In nonpolar aprotic solvents, the solvation free energies are of positive values. These are consistent with the tendency that the solubilities of polar solutes in nonpolar solvents are very low. In polar aprotic solvents, the magnitude of the solvation free energy does not increase monotonically as the solvent polarities increase. Especially, as seen in Table 4, the irregularity of the solvation free energy in acetonitrile

is remarkable both for the keto and enol forms. This irregularity in acetonitrile cannot be explained by the conventional dielectric continuum model, because the magnitude of the solvation free energy increases with the increase of the dielectric constant of solvents[37] (see Table 4).

We further estimated the solvation free energies with the assumption of Gaussian fluctuations (GF) by Chandler et al.[38] Although the solvation free energies by the GF approximation are systematically larger than the HNC results in Table 4, the qualitative tendency is the same and the irregularity is also observed for acetonitrile. Therefore we will use the results by the HNC equation for further analyses.

In order to clarify the origin of irregular order of solvation energy, we carried out the decomposition analyses of solvation free energy. Since the expression for solvation free energy, Eq.(2.3), is "formally" a sum of the solute-solvent site - site interactions, we define the contribution of solute atom, for example, atom α, to the solvation free energy by:

$$\Delta F^{\alpha}_{HNC} = \frac{\rho}{2\beta} \sum_{\gamma \in v} \int_0^{\infty} 4\pi r^2 \mathrm{d}r (h^2_{\alpha\gamma} - 2c_{\alpha\gamma} - h_{\alpha\gamma} c_{\alpha\gamma}) \tag{2.6}$$

It should be noted that ΔF^{α}_{HNC} is not the same as the solvation free energy of atom α when the atom is placed in the solvent by itself. The results for ΔF^{α}_{HNC} are shown in Table 5. In the keto form, the stabilization energies assigned to the solute hydrogen sites, H(4) and H(5), are the largest. Also the solvation free energies for the solute carbon and oxygen sites have negative values though the contributions are smaller than those of the solute H(4) and H(5) sites. Although the solvation energy at the solute nitrogen site is positive, the negative values for the remaining sites make the total solvation energy to be negative. Similar results were obtained for the enol tautomer. These indicate that the

characteristics of the solvent effect are dominated by the hydrogen-bonding.

(c) Characterization of Solvent Effect by Hydrogen-Bond

The empirical solvent parameters derived by Taft and co-workers[2] are well-known as a measure of hydrogen bonding abilities of solvents. For various kinds of solvents, they determined the parameters for the ability of solvents to donate or accept a proton in solute-solvent hydrogen bonding, the α parameter (for donating) and β parameter (for accepting). Since we treat aprotic solvents here, it is appropriate to take the β parameter. The values of β parameter are reported to be 0.31, 0.55, and 0.76 for acetonitrile, THF, and DMSO, respectively[2], indicating that the strength of hydrogen bonding in THF or DMSO solutions is larger than in acetonitrile. The β parameter for CCl_4 is zero. As seen in Figure 3(b), 3(c), the height of the first peak is smaller for the acetonitrile solution than that for the DMSO solution. This suggests that the hydrogen bonding ability of acetonitrile is weaker than that of DMSO. Considering that the solute-solvent hydrogen bonding is represented by the first peak of rdfs and the peak height is related to the well-depth of mean potential, it would be appropriate to take the logarithm of the height of the first peak as a measure of the strength of hydrogen bonding. In Figure 4, we plotted the heights of the first peaks in the logarithmic scale against Taft's β parameters for CCl_4, THF, acetonitrile, and DMSO solutions. As easily seen, linear correlation is obtained both for the keto and enol tautomers. This indicates that the Taft's parameters are in fact good measures of hydrogen-bonding. It is not surprising that the solvation free energy in the acetonitrile solution shows a remarkable irregularity. With these relations, we could qualitatively explain the origin of empirical solvent parameters representing the ability of the solvent to form hydrogen bonding at a molecular level. It is noted that the solvent geometric structures as well as the partial charges on the sites play an important

role in determining the solvent parameters.

As seen in Table 3, the calculated solute dipole moments in polar aprotic solvents are larger than that in the gas phase while those in nonpolar aprotic solvents are not different from the gas phase value. It is observed that the dipole moment of the keto form is much enhanced than the enol form in polar aprotic solvents. The calculated solute dipole moments, in both of the tautomers, increase as solvent polarities increase. These tendencies show good correlation with the empirical solvent dipolarity / polarizability parameters, the π^* parameter by Taft et al. They are 0.28, 0.58, 0.75, and 1.00 for CCl_4, THF, CH_3CN, and DMSO, respectively[2]. Therefore it is indicated that the enhancement of the solute dipole moment is related to bulk properties of solvents and our calculations also reproduce qualitatively the tendency of the π^* parameter.

2.4 Conclusion

By using the RISM-SCF method, the optimized geometries and solvation free energies of the keto and enol tautomers of formamide were calculated in six organic aprotic solvents (CS_2, CCl_4, DME, THF, acetonitrile, and DMSO). From the analysis of the solvation free energies, it is shown that the solute-solvent hydrogen bonding largely contributes to them and that the ability of the solvent to form hydrogen bonding is very important. It is also shown that Taft's β parameters are well-correlated to the calculated well-depth of the hydrogen bonding. The results that the solvation free energies for both of the tautomers show the irregularity in the acetonitrile solution are in qualitative accord with the empirically determined solvent parameters. The empirical measure of the solvent ability to form hydrogen-bonding with solute is explained at a molecular level.

The solvent effects on the energy difference between the keto-enol tautomers were examined. It is found that the keto tautomer is stabilized largely compared to the enol form. These tendencies are consistent with the experimental and previous theoretical results. In the both tautomers, the dipole moments of solutes are enhanced in polar solvents and the geometric structures are changed, so as to increase the solute dipole moment. It is found that the tendency of solute dipole moments is correlated to Taft's parameters with respect to the solvent polarity.

Acknowledgment

We are grateful to Mr. K. Naka for his coding of the grid point generation based on the Voronoi polyhedrons and Professor N. Hirota for valuable discussion in preparing the manuscript. We also thank Professor W. L. Jorgensen for sending the data of simulation of THF to us and Dr. A. Luzar for the data of simulation of DMSO.

This work was supported by the Grant in Aid for Scientific Research from the Ministry of Education.

Bibliography

[1] C. Reichardt, *Solvents and Solvent Effects in Organic Chemistry, 2nd ed* (VCH Verlagsgesellschaft, Weinheim, 1988).

[2] M. J. Kamlet, J.-L. M. Abboud, M. H. Abraham and R. W. Taft, J. Org. Chem. **48**, 2877 (1983).

[3] C. J. Cramer and D. G. Truhlar, in *Solvent Effects and Chemical Reactivity*, edited by O. Tapia and J. Bertrán (Kluwer, Dordrecht, 1996) and references cited therein.

[4] J. Tomasi and M. Persico, Chem. Rev. **94**, 2027 (1994).

[5] D. Chandler and H. C. Andersen, J. Chem. Phys. **57**, 1930 (1972).

[6] F. Hirata and P. J. Rossky, Chem. Phys. Lett. **83**, 329 (1981).

[7] F. Hirata, B. M. Pettitt and P. J. Rossky, J. Chem. Phys. **77**, 509 (1982).

[8] F. Hirata, P. J. Rossky and B. M. Pettitt, J. Chem. Phys. **78**, 4133 (1983).

[9] S. Ten-no, F. Hirata and S. Kato, Chem. Phys. Lett. **214**, 391 (1993).

[10] S. Ten-no, F. Hirata and S. Kato, J. Chem. Phys. **100**, 7443 (1994).

[11] H. Sato, F. Hirata and S. Kato, J. Chem. Phys. **105**, 1546 (1996).

[12] M. Kawata, S. Ten-no, S. Kato and F. Hirata, Chem. Phys. Lett. **240**, 199 (1995).

[13] M. Kawata, S. Ten-no, S. Kato and F. Hirata, J. Am. Chem. Soc. **117**, 1638 (1995).

[14] M. Kawata, S. Ten-no, S. Kato and F. Hirata, J. Phys. Chem. **100**, 1111 (1996).

[15] A. I. Kol'tsov and G. M. Kheifets, Russ. Chem. Revs. **40**, 773 (1971).

[16] A. I. Kol'tsov and G. M. Kheifets, Russ. Chem. Revs. **41**, 452 (1972).

[17] P. Beak, F. S. Fry, Jr., J. Lee and F. Steele, J. Am. Chem. Soc. **98**, 171 (1976).

[18] P. Beak, Acc. Chem. Res. **10**, 186 (1977).

[19] P. Beak, J. B. Covington and J. M. White, J. Org. Chem. **45**, 1347 (1980).

[20] J. Emsley, Structure and Bonding **57**, 147 (1984).

[21] M. W. Wong, K. B. Wiberg and M. J. Frisch, J. Am. Chem. Soc. **114**, 1645 (1992).

[22] H. Sato and S. Kato, J. Mol. Struct. (THEOCHEM) **310**, 67 (1994).

[23] L. J. Lowden and D. Chandler, J. Chem. Phys. **61**, 5228 (1974).

[24] T.-M. Chang, K. A. Peterson and L. X. Dang, J. Chem. Phys. **103**, 7502 (1995).

[25] S.-B. Zhu, J. Lee and G. W. Robinson, Mol. Phys. **65**, 65 (1988).

[26] W. L. Jorgensen and M. Ibrahim, J. Am. Chem. Soc. **103**, 3976 (1981).

[27] J. M. Briggs, T. Matsui and W. L. Jorgensen, J. Comput. Chem. **11**, 958 (1990).

[28] W. L. Jorgensen and J. M. Briggs, Mol. Phys. **63**, 547 (1988).

[29] A. Luzar, A. K. Soper and D. Chandler, J. Chem. Phys. **99**, 6836 (1993).

[30] W. L. Jorgensen and C. J. Swenson, J. Am. Chem. Soc. **107**, 569 (1985).

[31] S. J. Weiner, P. A. Kollman, D. A. Case, U. C. Singh, C. Ghio, G. Alagona, S. Profeta, Jr. and P. Weiner, J. Am. Chem. Soc. **106**, 765 (1984).

[32] R. A. Friesner, J. Phys. Chem. **92**, 3091 (1988).

[33] T. H. Dunning, Jr. and P. J. Hay, in *Modern Electronic Structure Theory*, edited by H. F. Schaefer III (Plenum, New York, 1977).

[34] S. J. Singer and D. Chandler, Mol. Phys. **55**, 621 (1985).

[35] D. A. Zichi and P. J. Rossky, J. Chem. Phys. **84**, 1712 (1986).

[36] J. A. Riddick, W. B. Bunger and T. K. Sakano, *ORGANIC SOLVENTS, 4th ed* (Wiley-Interscience, New York, 1986).

[37] C. J. F. Böttcher, *Theory of Electric Polarization vol.1* (Elsevier, Amsterdam, 1973) pp 129-157.

[38] D. Chandler, Y. Singh and D. M. Richardson, J. Chem. Phys. **81**, 1975 (1984).

Figure captions

Figure 1. (a) O-O radial distribution functions for pure THF. Circles indicates computer simulation results (ref 27). (b) S-O radial distribution functions for pure DMSO. Circles indicates computer simulation results (ref 29).

Figure 2. Molecular form and site assignment of keto-enol tautomers of formamide.

Figure 3. Radial distribution functions between the H(4) and H(5) sites of the keto form (formamide) and solvent sites. (a) H-Cl (solvent: CCl_4), (b) H-N (solvent: CH_3CN), (c) H-O (solvent: DMSO).

Figure 4. Plots of the logarithms of the heights of the first peaks in the rdfs against Taft's β parameters. The abscissa is logarithmic scale. (a) For the keto form, the positions of the first peaks are 2.8, 2.2, 2.3, and 2.0 Å for CCl_4, THF, CH_3CN, and DMSO (for the both H(4) and H(5)). (b) For the enol form, the positions of the first peaks are 2.9, 2.0, 2.2, and 1.8 Å for CCl_4, THF, CH_3CN, and DMSO (for the both H(4) and H(5)).

Table 1. Parameters for aprotic solvents and solute

solvent [a]	site	q	σ / Å	ε / kcal mol^{-1}
CCl_4	C	-0.1616	3.2	0.10
	Cl	0.0404	3.4	0.26
CS_2	C	-0.308	3.2	0.101
	S	0.154	3.52	0.395
DME	O	-0.50	3.0676	0.179
	CH_3	0.25	3.8609	0.181
THF	O	-0.50	3.000	0.170
	CH_2^{α}	0.25	3.800	0.118
	CH_2^{β}	0.00	3.905	0.118
CH_3CN	CH_3	0.15	3.775	0.206
	C	0.28	3.650	0.150
	N	-0.43	3.200	0.169
DMSO	O	-0.459	2.80	0.0715
	S	0.139	3.40	0.238
	CH_3	0.160	3.80	0.293

[a] Data from ref 23, 24 for CCl_4, ref 25 for CS_2, ref 26 for DME, ref 27 for THF, ref 28 for CH_3CN, ref 29 for DMSO.

solute	site	σ / Å	ε / kcal mol^{-1}
	N [b]	3.25	0.170
	C [b]	3.75	0.105
	O [b]	2.96	0.210
	H [c]	1.78	0.02

[b] Reference 30. [c] Reference 31.

Table 2. Partial Charges on Atom Sites in CCl_4, CH_3CN, DMSO (Units in Electronic Charges)

	keto						enol					
solvent	C	N	O	H(4)	H(5)	H(6)	C	N	O	H(4)	H(5)	H(6)
CCl_4	0.74	-1.06	-0.60	0.47	0.44	0.01	0.58	-0.87	-0.64	0.48	0.38	0.07
CH_3CN	0.75	-1.04	-0.67	0.48	0.46	0.02	0.63	-0.94	-0.68	0.51	0.41	0.07
DMSO	0.76	-1.07	-0.69	0.49	0.48	0.03	0.66	-1.00	-0.72	0.54	0.45	0.07

Table 3. Optimized Geometries of Keto-Enol Tautomers in Solutions

	keto			enol			
solvent	l (C=O)[a]	l (C-N)[a]	dipole[b]	l (O-H(4))[a]	l (N··· H(4))[a]	∠OCN[c]	dipole[b]
CCl_4	1.196	1.353	4.22	0.948	2.312	122.58	1.25
CS_2	1.198	1.351	4.38	0.949	2.321	122.76	1.28
DME	1.204	1.347	4.86	0.952	2.369	123.91	1.37
THF	1.202	1.347	4.73	0.951	2.353	123.50	1.26
CH_3CN	1.206	1.343	4.99	0.952	2.351	123.23	1.43
DMSO	1.208	1.340	5.21	0.951	2.358	123.28	1.51
gas	1.196	1.353	4.23	0.948	2.309	122.54	1.23

[a] In angstrom. [b] In D. [c] In degree.

Table 4. Total Free Energy Diffrences, Solvation Free Energies, and Reorganization Energies

solvent	ΔG(keto-enol)[a,b]	ΔF_{HNC} (keto)[b]	ΔF_{HNC} (enol)[b]	ΔE_{re} (keto)[b]	ΔE_{re} (enol)[b]	ε[c]
CCl_4	-12.60	2.39	2.33	0.00033	0.0012	2.237
CS_2	-12.77	0.51	0.64	0.054	0.040	2.643
DME	-13.37	-4.95	-4.19	0.74	0.69	5.02
THF	-14.41	-5.57	-3.72	0.39	0.28	7.58
CH_3CN	-14.57	-2.51	-0.084	0.97	0.45	35.94
DMSO	-13.35	-7.78	-6.81	1.70	1.41	46.45
gas	-12.66					

[a] ΔG is the difference of Eq.(4) between the keto and enol form. [b] In kcal / mol-1. [c] Dielectric constant for each solvent. Data from reference 36.

Table 5. Contributions of Solute (keto) Atom to the Solvation Free Energies in CCl_4, CH_3CN, DMSO (Units in kcal / mol)

	solute site					
solvent	C	N	O	H(4)	H(5)	H(6)
CCl_4	1.00	-0.60	-0.47	0.86	0.97	0.63
CH_3CN	-1.64	11.34	-1.81	-4.38	-6.50	0.49
DMSO	-4.51	16.17	-2.37	-7.26	-10.24	0.42

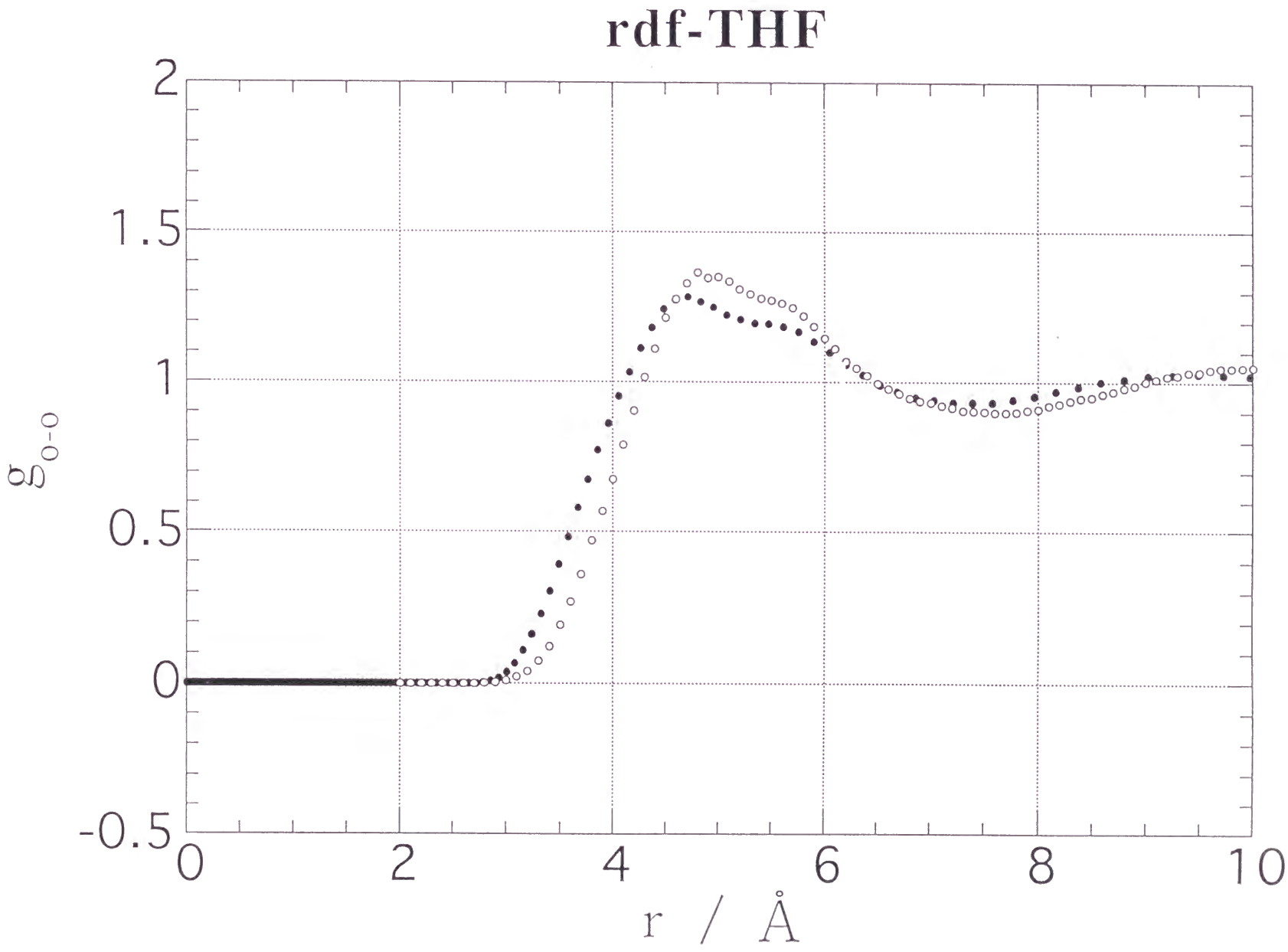

Figure 1. (a)

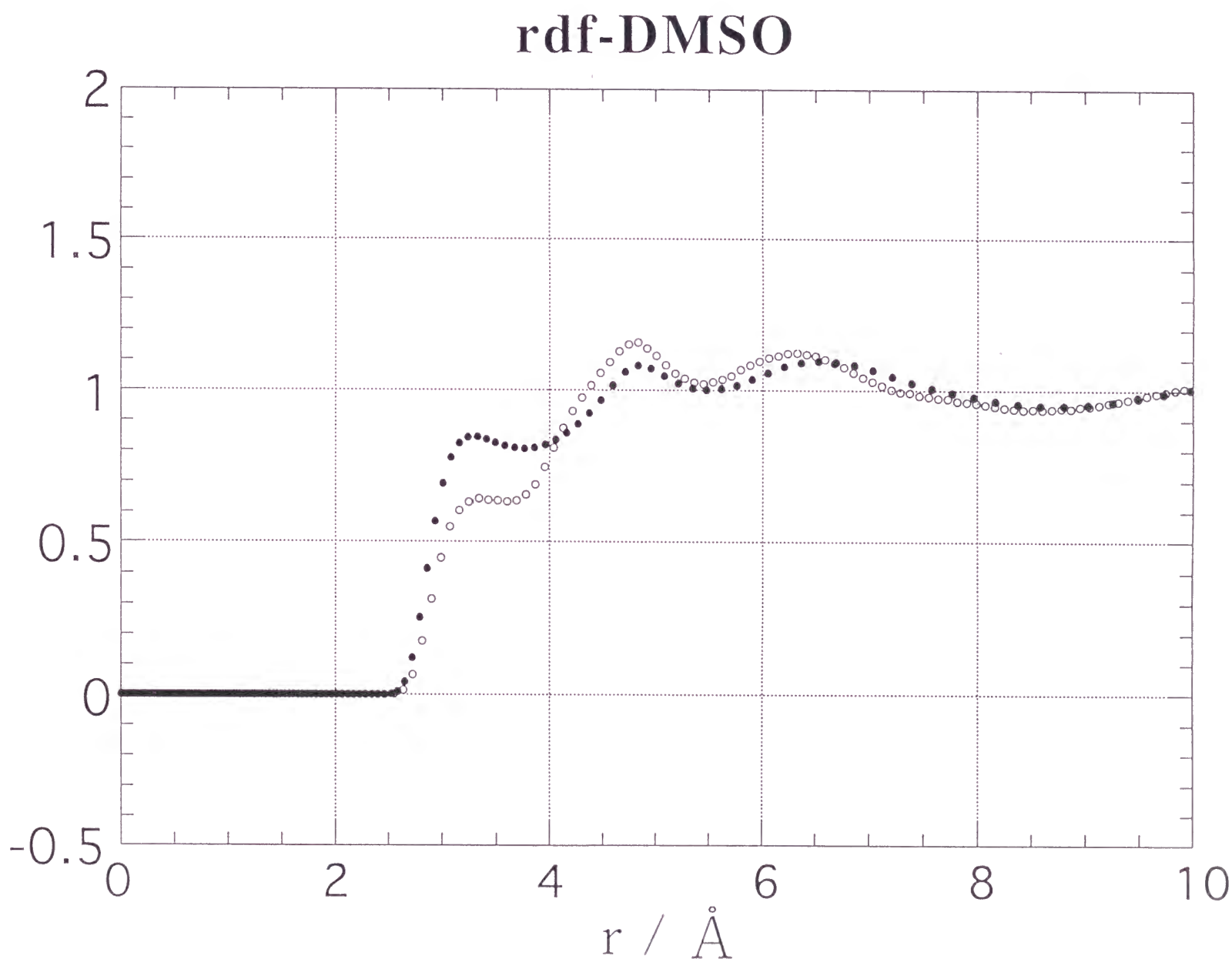

Figure 1.(b)

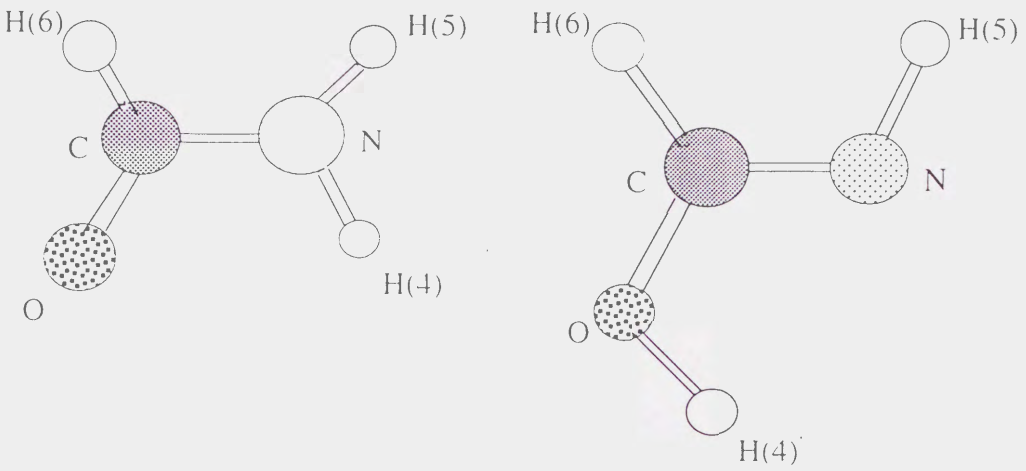

keto (formamide) enol (formidic acid)

Figure 2.

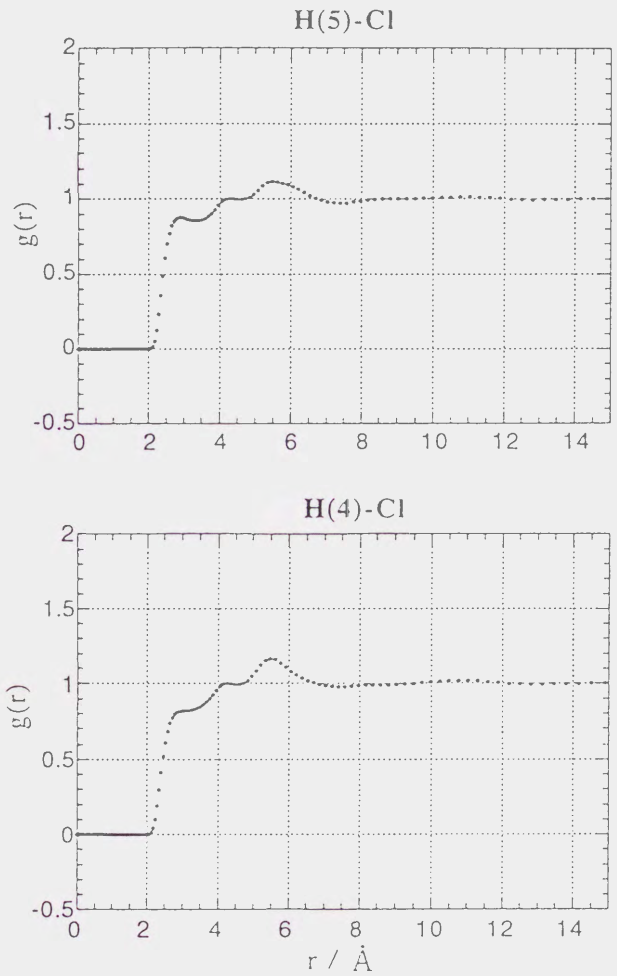
H(5)-Cl
g(r)
2
1.5
1
0.5
0
-0.5
0
2
4
6
8
10
12
14
H(4)-Cl
g(r)
2
1.5
1
0.5
0
-0.5
0
2
4
6
8
10
12
14
r / Å

Figure 3. (a)

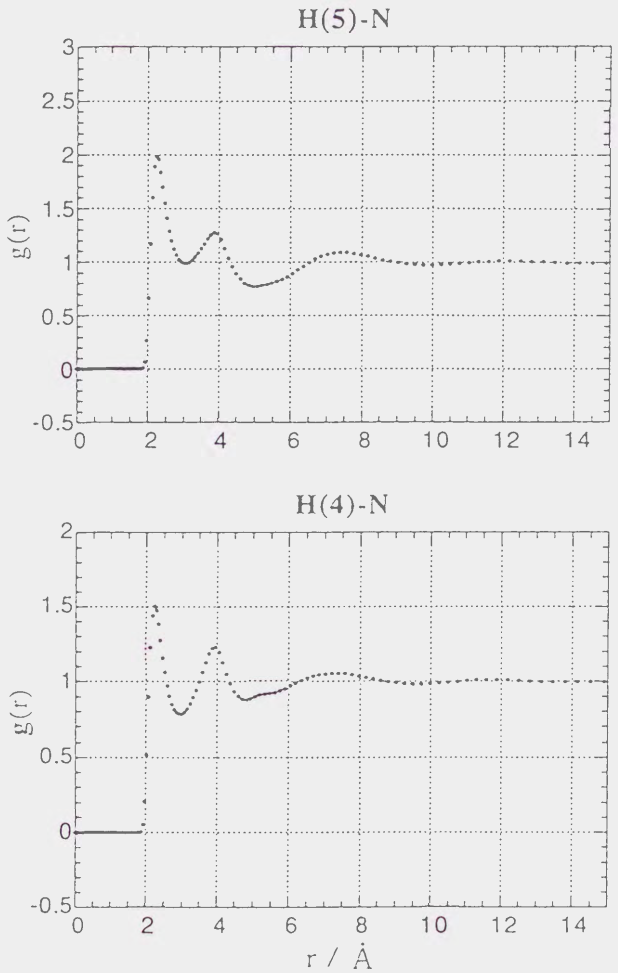
H(5)-N
g(r)
3
2.5
2
1.5
1
0.5
0
-0.5
0
2
4
6
8
10
12
14
H(4)-N
g(r)
2
1.5
1
0.5
0
-0.5
0
2
4
6
8
10
12
14
r / Å

Figure 3.(b)

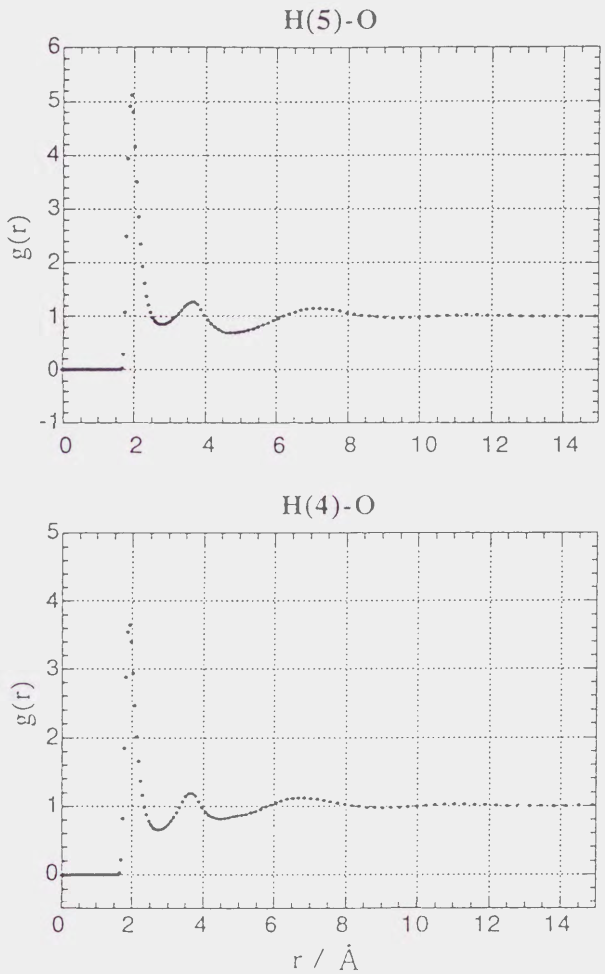

Figure 3. (c)

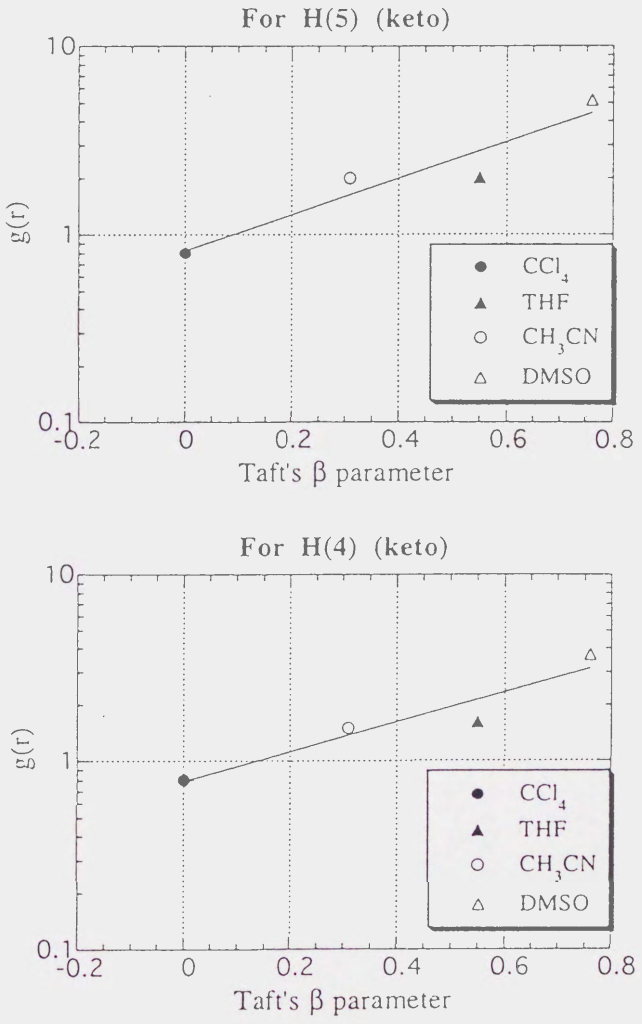
For H(5) (keto)
10
1
0.1
g(r)
-0.2
0
0.2
0.4
0.6
0.8
Taft's β parameter
CCl4
THF
CH3CN
DMSO
For H(4) (keto)
10
1
0.1
g(r)
-0.2
0
0.2
0.4
0.6
0.8
Taft's β parameter
CCl4
THF
CH3CN
DMSO

Figure 4. (a)

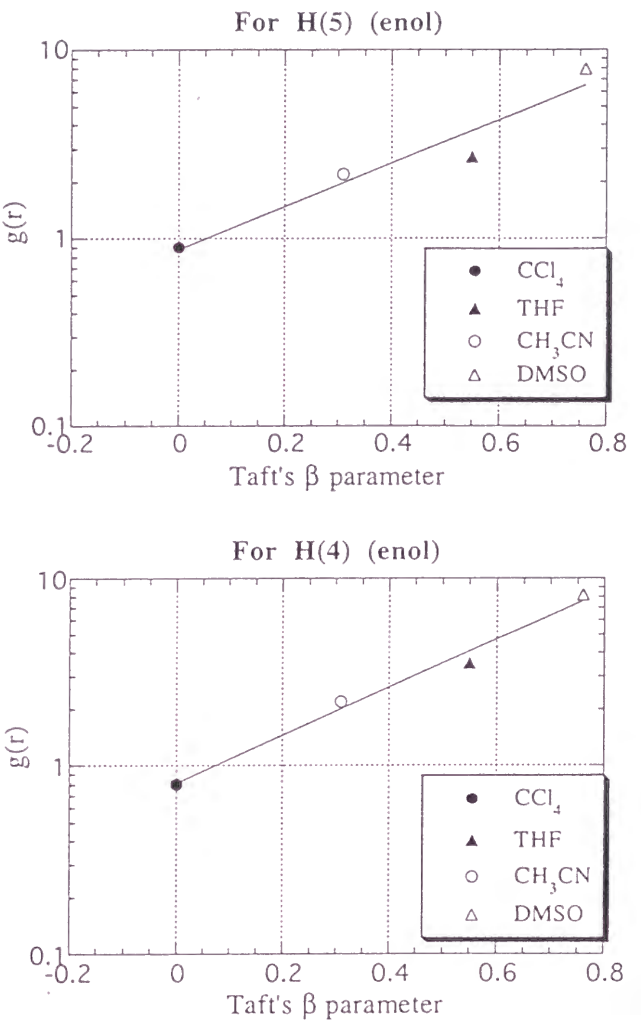
For H(5) (enol)
10
1
0.1
g(r)
-0.2
0
0.2
0.4
0.6
0.8
Taft's β parameter
CCl4
THF
CH3CN
DMSO
For H(4) (enol)
10
1
0.1
g(r)
-0.2
0
0.2
0.4
0.6
0.8
Taft's β parameter
CCl4
THF
CH3CN
DMSO

Figure 4.(b)

Chapter 3

Thermodynamic analysis of the solvent effect on tautomerization of acetylacetone: An ab initio approach

3.1 Introduction

Chemical equilibria and reactions in solution have been one of the most important subjects in theoretical chemistry and various methods have been developed for studying such a problem[1]. Computer simulation studies employing molecular dynamics and Monte Carlo techniques have provided a wealth of information on the thermodynamic properties for various processes in solution. Analyses of the solvation free energies derived from these simulations have been utilized for interpreting the origin of thermodynamic stability of chemically equilibrium systems at a molecular level[1]. It has been also emphasized that

the electronic structure of solute molecule and the geometry itself are largely influenced through the interaction with surrounding solvent molecules[2]. In this respect, quantum chemical methods incorporating the solvation effects in the electronic structure calculations of solute have also been advanced to elucidate the importance of solute electronic polarization effect for understanding the mechanism of chemical equilibria in solution.[2, 3]

The keto-enol tautomerization is among the most well-studied subjects both from experimental and theoretical points of view. Theoretical calculations have been so far performed for some specific systems such as formamide[4, 5] and 2-pyridone[5], and many of them have been based on the dielectric continuum model characterizing the solvent by the dielectric constant. In the present work, we performed a theoretical study on the keto-enol tautomerization of acetylacetone in polar and nonpolar solvents using the reference interaction site model self-consistent-field (RISM-SCF) method[6, 7], which is an ab initio electronic structure theory taking account of the solvent reaction field in molecular detail.

The keto-enol tautomerization of acetylacetone, a prototype β-diketone, has been extensively studied experimentally[8]-[13], and the attention has been paid to its solvent effect. Although the enol form is more stable than the keto in the gas phase due to the intramolecular hydrogen bonding, the equilibrium is known to shift toward the keto in solution as the solvent polarity increases.[14]-[18] Several theoretical studies of acetylacetone have been carried out. Dannenberg and Rios[19] employed various levels of ab initio electronic structure methods to predict the geometries and stabilities of the keto and enol tautomers in the gas phase. Solvent effects on the tautomerism have been also studied with the self-consistent reaction field method (SCRF)[20]-[22], in which semiempirical level of electronic structure calculations was used. Most importantly, Cramer and Truhlar predicted[23] that the keto form could cause a large geometric change so as to increase the

solute dipole moment in polar solvents. However, as mentioned by them, more elaborate ab initio calculations utilizing a microscopic solvent model would be required for further understanding the solvation effect since they employed a semiempirical level electronic structure theory with the dielectric continuum model.

The purpose of the present paper is to provide detailed analysis to the thermodynamic property for the keto-enol tautomerization of acetylacetone in solution based on the ab initio electronic structure calculations. We chose H_2O and dimethyl sulfoxide (DMSO), and carbon tetrachloride (CCl_4), representing respectively protic polar, aprotic polar and nonpolar solvents. The solvation free energies in these solvents were analyzed by decomposing them into the enthalpic and entropic contributions based on the scheme proposed by Yu et al.[24, 25] The effect of changes in solute geometry and vibrations due to the solvation was also examined. The organization of the paper is as follows. In the following section, the theoretical methods employed are presented. In Sec. 3.3, we present the results of calculations. The solvent effect on the solute geometries and vibrational frequencies are discussed. The thermodynamic analysis of the solvation free energies in the tautomerization is performed to study the stabilities of the keto and enol tautomers in solution. The origin of geometric change of the keto form is also discussed. Conclusions are summarized in Sec. 3.4.

3.2 Theoretical Methods

3.2.1 RISM-SCF method

Since the details of RISM-SCF method have been presented in the previous papers[6, 7], we only describe the outline of theory pertinent to the calculations of the electron correlation

energy of solute molecule and the thermodynamic analyses of solvation free energies.

In the RISM-SCF theory, the total free energy of the system considered is defined by

$$G = \langle \Psi \mid \hat{H}_{gas} + \Delta\hat{\mu}_{sol} \mid \Psi \rangle, \tag{3.1}$$

where Ψ is the solute electronic wave function and $\hat{H}_{gas}$ is the electronic Hamiltonian of solute in the gas phase. The operator $\Delta\hat{\mu}_{sol}$ determines the excess chemical potential due to the solvation, which is the functional of the solute-solvent correlation functions $h_{\alpha\gamma}$, the direct correlation functions $c_{\alpha\gamma}$, and the t-bonds $t_{\alpha\gamma}$. Here, α and γ denote the interaction sites in solute and solvent molecules.

The variation of the free energy, Eq.(3.1), with respect to the solute molecular orbitals (MO) ϕ_i and the correlation functions $h_{\alpha\gamma}$, $c_{\alpha\gamma}$ and $t_{\alpha\gamma}$ automatically provides the Fock equation:

$$\hat{F}_{sol}\phi_i = \varepsilon_i\phi_i, \tag{3.2}$$

the RISM Ornstein-Zernike (OZ) equation:

$$h_{uv} = w_u * c_{uv} * \omega_v + \rho\omega_u * c_{uv} * h_{vv} \tag{3.3}$$

and the hypernetted chain (HNC) closure relation. In Eq.(3.3), the indices u and v denote the solute and solvent, ρ is the number density of solvent, and $\beta = 1/k_BT$ with k_B being Boltzmann constant. w is the intramolecular correlation function that defines the molecular geometry. The solvent-solvent correlation function, h_{vv}, is determined by solving the RISM OZ equation for the pure solvent:

$$h_{vv} = \omega_v * c_{vv} * \omega_v + \rho\omega_v * c_{vv} * h_{vv} \tag{3.4}$$

At convergence, the excess chemical potential[26, 27] is represented as:

$$\Delta\mu_u = \frac{\rho}{2\beta} \sum_{\alpha\in u} \sum_{\gamma\in v} \int_0^\infty 4\pi r^2 \mathrm{d}r (h_{\alpha\gamma}^2 - 2c_{\alpha\gamma} - h_{\alpha\gamma}c_{\alpha\gamma}). \tag{3.5}$$

The solvated Fock operator is given in the form:

$$\hat{F}_{sol} = \hat{\mathrm{h}} + 2\hat{J} - \hat{K} - \sum_\alpha V_\alpha \hat{b}_\alpha, \tag{3.6}$$

where $\hat{\mathrm{h}}$, $\hat{J}$ and $\hat{K}$ are the usual one electron, Coulomb and exchange operators and $\hat{b}_\alpha$ is the population operator which generates the partial charge on the solute atomic site α. The averaged electrostatic potential acting on the site α is given by

$$V_\alpha = \rho \sum_\gamma q_\gamma 4\pi r \int g_{\alpha\gamma}(r)\mathrm{d}r, \tag{3.7}$$

where $g_{\alpha\gamma}(r), h_{\alpha\gamma}(r) + 1$, is the radial distribution function between the solute site α and the solvent site γ with the partial charge q_γ.

To calculate the electron correlation energy of the solute molecule in solution, we employ the Møller-Plesset (MP) perturbation expansion. We consider here up to the second-order correction. The Hamiltonian is partitioned into

$$H = \hat{H}_{gas} + \Delta\hat{\mu}_{sol} = \sum_i \hat{F}_{sol}(i) + \hat{V} \tag{3.8}$$

where the zero-th order Hamiltonian is defined by the sum of solvated Fock operators and $\hat{V}$ corresponds to the perturbation. Since $\Delta\hat{\mu}_{sol}$ and $\hat{b}_\alpha$ in the perturbation term $\hat{V}$ is

the one-electron operators, it is straightforward to show that the second-order correlation energy is represented by

$$E_{MP2}^{sol}(u) = \frac{1}{4}\sum_{abrs}\frac{|\langle ab||rs\rangle|^2}{\varepsilon_a + \varepsilon_b - \varepsilon_r - \varepsilon_s} \tag{3.9}$$

where ε_a and ε_b are the occupied orbital energies, and ε_r and ε_s the unoccupied orbital energies, respectively. The integral $\langle ab||rs\rangle$ is the anti-symmetrized two-electron integral.

All the ab initio calculations were performed at the restricted Hartree-Fock (RHF) level by using the (9s5p1d/4s1p)/[3s2p1d/2s1p] basis set, which has a valence double zeta plus polarization quality.[28] The geometry of solute molecule was optimized using the analytical energy gradient technique[29] in each solvent studied. The MP2 calculations were repeated at the RISM-SCF optimized geometries to estimate the electron correlation effect.

All the parameters[30]-[32] employed for describing the solute-solvent interaction are summarized in Table I. Especially, for H_2O, the simple point charge (SPC)-like[33] model was used where the Lennard-Jones parameters, σ=1.0 Åand ϵ=0.056 kcal/mol, were added on the H site. The Lennard-Jones parameters for the solute atoms[34] were also included in Table I. We used the standard combination rule to construct the solute-solvent van der Waals interaction. The temperature was set to be 295.15 K for CCl_4, and 298.15 K for the other solvents.

We further calculated the harmonic vibrational frequencies of solute for estimating the zero point energy of solute molecule, $E_{ZPE}(u)$, and the vibrational contribution to the free energy, ΔG_{vib}. The Hessian matrix was obtained by the numerical differentiation of analytically calculated gradients of RISM-SCF free energy at the optimized geometry in each solvent.

3.2.2 Thermodynamic analysis

The solvation free energy is defined as the sum of the solute term ΔG_{solute} and the excess chemical potential $\Delta\mu_{sol}$. The solute term is given by

$$\Delta G_{solute} = \Delta E_{re} + \Delta ZPE + \Delta G_{vib} \tag{3.10}$$

where ΔE_{re} is the solute electronic reorganization energy given as the change of solute electronic energy from the gas phase to the solution, and ΔZPE and ΔG_{vib} are the changes of the zero-point energy and vibrational free energy. It is noted that the change of solute electron correlation energy due to the solvation is included in ΔE_{re}.

The enthalpy and entropy contributions to the excess chemical potential were calculated using the method proposed by Yu et al..[24, 25] Taking the derivatives of h and c with respect to the solute or solvent density, ρ_u or ρ_v, the solvation energy $\Delta\epsilon_{u,sol}$ and the enthalpy $\Delta h_{u,sol}$ are calculated with the equations by the following:

$$\begin{aligned}\Delta\epsilon_{u,sol} = {} & \rho_{\mathrm{v}} \sum_{\alpha=1}^{n_{\mathrm{u}}} \sum_{\gamma=1}^{n_{\mathrm{v}}} \int_0^\infty 4\pi r^2 \mathrm{d}r U_{\alpha\gamma}(r) g_{\alpha\gamma}(r) \\ & + \frac{\rho_{\mathrm{v}}^2}{2} \sum_{\gamma=1}^{n_{\mathrm{v}}} \sum_{\gamma'=1}^{n_{\mathrm{v}}} \int_0^\infty 4\pi r^2 \mathrm{d}r U_{\gamma\gamma'}(r) \delta_{\rho_{\mathrm{u}}} h_{\gamma\gamma'}(r),\end{aligned} \tag{3.11}$$

$$\begin{aligned}\Delta h_{u,sol} = {} & \Delta\epsilon_{u,sol} + T\alpha_{v,P} \{\Delta\mu_{u,sol} \\ & + \frac{\rho_{\mathrm{v}}^2}{2\beta} \sum_{\alpha=1}^{n_{\mathrm{u}}} \sum_{\gamma=1}^{n_{\mathrm{v}}} \int_0^\infty 4\pi r^2 \mathrm{d}r \left[h_{\alpha\gamma}(r)\delta_{\rho_{\mathrm{v}}} c_{\alpha\gamma}(r) - c_{\alpha\gamma}(r)\delta_{\rho_{\mathrm{v}}} h_{\alpha\gamma}(r)\right]\Bigg\},\end{aligned} \tag{3.12}$$

where n_{u} and n_{v} denote the numbers of sites in the solute and solvent molecule, respectively. $U_{\alpha\gamma}$ and $U_{\gamma\gamma'}$ are the solute-solvent and solvent-solvent site-site interaction potentials. $\alpha_{v,P}$ is the isobaric thermal expansion coefficient of the pure solvent. In the

present study, the experimental data for $\alpha_{v,P}$[35], $2.57\times10^{-4}\mathrm{K}^{-1}$ for H_2O, 9.28×10^{-4} for DMSO and 1.22×10^{-3} for CCl_4, respectively, were employed. The first term in the right hand side of Eq.(3.11) represents the solute-solvent interaction energy E_{uv} and the second is the cavity formation energy E_{cav}, which represents the solvent reorganization energy due to solvation.

The solvation entropy is defined by

$$\Delta S_{u,sol} = (\Delta h_{u,sol} - \Delta\mu_{sol})/T \tag{3.13}$$

Based on the extended RISM theory[36]-[38], the first-order isothermal density derivatives to Eqs.(3.3) and (3.4) provide the relation:

$$\delta_{\rho_\eta}\hat{h}_{ss'} = \hat{w}_s\delta_{\rho_\eta}\hat{c}_{ss'}\hat{w}_{s'} + \left[\hat{w}_s\delta_{\rho_\eta}\hat{c}_{sv} + \hat{h}_{sv}\rho_v\delta_{\rho_\eta}\hat{c}_{vv}\right]\rho_v\hat{h}_{vs'} + \hat{h}_{s\eta}\hat{w}_\eta^{-1}\hat{h}_{\eta s'}, \tag{3.14}$$

where $\hat{h}, \hat{c}$ and $\hat{w}$ represent h, c and w in k-space, respectively, with $\{s, s'\} = \{u, v\}$. The corresponding relation to the HNC closure is given by:

$$\delta_{\rho_\eta}h_{\alpha\gamma}(r) = \left[\delta_{\rho_\eta}h_{\alpha\gamma}(r) - \delta_{\rho_\eta}c^*_{\alpha\gamma}(r)\right]\left[h_{\alpha\gamma}(r) + 1\right], \tag{3.15}$$

where η represents u or v, and $\delta_{\rho_\eta}\hat{c}^* = \delta_{\rho_\eta}\hat{c} - \hat{\phi}^\eta$, $\hat{\phi}^\eta = \delta_{\rho_\eta}\hat{\phi}$.

The free energy difference between the keto and enol tautomers is defined by

$$\Delta G(k-e) = \Delta G_{solute}(k) - \Delta G_{solute}(e) + \Delta\mu_{sol}(k) - \Delta\mu_{sol}(e) + \Delta G_{gas}(k-e) \tag{3.16}$$

where $\Delta G_{gas}(k-e)$ is the free energy difference in the gas phase. With the free energy partitioning scheme discussed above, the differences of the enthalpy and entropy terms between tautomers are easily derived.

The solvation enthalpy is defined by

$$\Delta H_{sol} = \Delta h_{u,sol} + \Delta E_{re} + \Delta E_{vib}^{sol} - \Delta E_{vib}^{gas} - 3k_B T, \tag{3.17}$$

and then, the enthalpy difference is calculated by

$$\Delta H(k-e) = \Delta H_{sol}(k) - \Delta H_{sol}(e) + \Delta H_{gas}(k-e) \tag{3.18}$$

where $\Delta H_{gas}(k-e)$ is the energy difference in the gas phase including the vibrational energy. The enthalpy difference, $\Delta H(k-e)$, is related to $\Delta G(k-e)$ by

$$\Delta G(k-e) = \Delta H(k-e) - T\Delta S(k-e) \tag{3.19}$$

where $\Delta S(k-e)$ is the entropy difference.

3.3 Results and Discussion

3.3.1 Solute property.

Figure 1 shows the geometries of the keto and enol tautomers of acetylacetone along with the site numberings. The optimized geometric parameters in the gas phase and in each solvent are summarized in Table II.

For the keto tautomer, we found the two geometries in the gas phase; one with the dihedral angles, τ_{3256}, of 140.4° and the other of 102.4° , respectively. The former is more stable than the latter by 1.87 kcal/mol at MP2 level, which is consistent with the result by Dannenberg et al.[19], 1.1 kcal/mol. We also obtained two optimized structures in CCl_4, and their geometries are very close to those in the gas phase as seen in Table II. Since the conformer with τ_{3256}=140.4° is lower in energy by 1.35 kcal/mol than the other

with τ_{3256}=101.6°, we consider only the former in later discussion.

The geometry of the keto tautomer undergoes a drastic change in polar solvents. The stable conformer with a larger dihedral angle observed in the gas phase and CCl_4 disappeared and the torsional angle, τ_{3256}, significantly decreased to 56.4° in H_2O and to 75.2° in DMSO. The calculated torsional angle in H_2O is similar to the predicted value, 59°, by Cramer and Truhlar[23] with the semiempirical calculations. These results indicate that the dihedral angle changes so as to increase the solute dipole moment with the increase of solvent polarity. Table II shows that the C=O bond length in the carbonyl group becomes longer in polar solvent, though the average C−C bond length becomes slightly short compared with that in the gas phase. The bending angle, θ_{245}, also increases, which is because the repulsion between lone pair electrons in the two carbonyl groups becomes large as the dihedral angle decreases and thus the bending angle becomes wide in order to reduce such repulsive interaction. The origin of these geometric changes in polar solvents will be discussed in Sec.III.D.

In the enol tautomer, the geometric change due to the solvation is smaller than that in the keto one. All the atoms except for the methyl hydrogens lie in the same plane in all the solvents as in the gas phase. The change of bending angle, θ_{245}, is also small. As seen in Table II, R_{23} and R_{56} become longer in the polar solvents than in the gas phase, while the change of their lengths is small in CCl_4. It is considered that these changes occur in order to make the solute dipole moment increase in DMSO and H_2O. The distance $R_{3\cdots12}$ characterizing the intramolecular hydrogen bonding was calculated to be 1.685 Å in the gas phase, which is comparable to the experimental value, 1.626Å.[10] While $R_{3\cdots12}$ becomes slightly shorter in CCl_4 and DMSO compared with the gas phase value, it is elongated by 0.04 Å in H_2O, indicating that the intramolecular hydrogen bonding is weakened in

aqueous solution. The intramolecular hydrogen bonding in the enol remains intact even in polar solvents, these results being consistent with the experimental observation by Emsley and Freeman.[15]

The calculated dipole moments in the solvents as well as in the gas phase are shown in Table III. The dipole moment of the keto is larger than that of the enol in the gas phase. This tendency agrees with the previous studies.[23, 13] In solutions, the dipole moment of the keto form is enhanced as the solvent polarity increases since the dihedral angle between the planes containing two carbonyl groups becomes smaller. For the enol, the degree of enhancement of dipole moment induced by the solvation is not so large, since such marked change in geometry observed in the keto form do not occur. The dipole moment, however, is appreciably larger in H_2O than in gas phase.

The harmonic vibrational frequencies were calculated in all the solvents considered as well as in the gas phase. The frequencies in CCl_4 were close to the gas phase values, while those in H_2O changed appreciably from the gas phase ones. In Table IV, we only showed the vibrations which undergo large frequency shifts, more than 20 cm^{-1}, due to solvation. In the keto, the frequency of $C_2C_4C_5$ bending vibration decreases with increasing the solvent polarity, which is consistent with the result that bond angle θ_{245} becomes large by the solvation. The frequencies for C=O stretching are remarkably reduced by $\sim$ 100 cm^{-1} in H_2O. This is because the hydrogen bonding between the carbonyl O and water H atoms is formed in aqueous solution and thus the C=O bond distances lengthen. Experimentally, it was observed that the C=O stretching frequency was lower by about 100 cm^{-1} in aqueous solution.[39]-[41] In the enol, the frequencies of C_4C_5 and C_2O_3 stretching modes decrease in the polar solvents. In particular, the shifts of these frequencies are more than 100 cm^{-1} in the aqueous solution, corresponding to

the significant increases of R_{45} and R_{23} distances as seen in Table II. The OH stretching frequency also decreases in the polar solvents. Although the frequency change is only 30 cm^{-1} in DMSO, it is reduced by 190 cm^{-1} in H_2O, indicating that a strong hydrogen bond is formed between the water O atom and the H atom of OH group in the enol tautomer.

3.3.2 Keto-Enol equilibrium

Table V shows the calculated free energy differences between the keto and enol tautomers along with the available experimental values. In H_2O, the free energy of the keto form was calculated to be lower than that of the enol by -1.37 kcal/mol, which is in good agreement with the experiment, -1.18 kcal/mol. For DMSO solution, the stability of two tautomers became comparable each other, 0.14 kcal/mol, as in the experiment. The free energies were also very close in CCl_4, which is slightly different from the experiment where the enol form is more stable than the keto by 1.76 kcal/mol. This discrepancy in the free energy difference in CCl_4 solution may come from the underestimation of solute electronic energy difference between the tautomers. In the present calculation, the electronic energy of the enol form is lower than that of the keto only by 1.04 kcal/mol in the gas phase, which provides the free energy difference of -0.69 kcal/mol. As shown by Bauer and Wilcox[42], the electronic energy difference becomes larger by employing the complete basis set method. Considering that the solute geometries are very similar to those in the gas phase and the electric field is weak in CCl_4, the error in the gas phase energy is the origin of small difference in the free energies for CCl_4 solution.

We further tabulated the components of free energy differences in Table V. The electronic energy difference, $\Delta E_{sol}(k-e)$, increases with the solvent polarity, which is mainly attributed to the geometric change of the keto form due to the solvation. It was

also found that the electron correlation energy becomes smaller in polar solvents than in the gas phase and such a solvent effect is remarkable in the keto form. This is because the electrostatic potential coming from the surrounding solvent enlarges the energy gap between occupied and unoccupied MOs of the solute and thus the correlation energy is reduced for the keto due to strong solvation. As shown in Table IV, there are some solute normal vibrations whose frequencies are reduced in polar solvents and thus the zero point energy becomes smaller in solution than that in the gas phase. The calculated zero point energy changes due to the solvation were -0.07, -0.39 and -0.75 kcal/mol in CCl_4, DMSO and H_2O, respectively, for the keto, while those for the enol were -0.04, -0.34 and -1.12 kcal/mol. The relatively larger negative value of the enol ZPE attributed to the formation of the hydrogen bonding with H_2O molecules is remarkable, which provides the smaller difference in ZPEs between the tautomers in water compared to the other solvent as well as the gas phase (Table V). The solvent effect on the vibrational frequencies also changes the solute vibrational contribution to the free energy difference, $\Delta G_{vib}(k-e)$. As shown in Table V, $\Delta G_{vib}(k-e)$ is negative in all the solvents as well as in the gas phase, indicating that the keto form has low frequency vibrational modes more than the enol. It is worth noting that the present calculations reproduced the experimental estimates of the free energy differences in the solutions fairly well by including the solute electronic reorganization energies and vibrational free energies.

The keto-enol difference of the excess chemical potentials, $\mu_{sol}(k-e)$, becomes more negative with the solvent polarity. This implies that the keto is more stabilized by the solvation, which is consistent with large enhancement of the keto dipole moment in polar solvent accompanied by the drastic geometric change. As seen in Table V, the stabilization by $\mu_{sol}(k-e)$ is comparable to the destabilization of solute electronic energy, $\Delta E_{sol}(k-e)$,

in the aqueous solution.

3.3.3 Thermodynamic analysis

The solvation enthalpies, ΔH_{sol}, of the two tautomers in solutions are shown in Table VI. In DMSO and CCl_4, the calculated values are comparable to the experimental ones. However, we found a large discrepancies between the calculation and experiment for those in H_2O. Although the calculated enthalpies are positive for both the tautomers, the experiments provided negative values of the enthalpies, which are close to those for DMSO and CCl_4 solutions. Moreover, the enol is enthalpically unstable than the keto by 6.5 kcal/mol in the calculations, while the experimental estimate is reversed.

In order to clarify the origins of such discrepancies in the enthalpies for the aqueous solution, we examined the components of ΔH_{sol}, which are included in Table VI. According to Eq.(3.17), the solvation enthalpy is composed of two contributions; one is $\Delta h_{u,sol}$ coming from the solute-solvent interaction and another is the solute term including the electronic and vibrational contributions as well as those from the translation and rotation in the gas phase. As seen in Table VI, the differences in the solute-solvent term $\Delta h_{u,sol}$ are rather small and are further cancelled out by the solute terms to give similar values of ΔH_{sol} for the two tautomers in DMSO and CCl_4. On the other hand, in the aqueous solution, there is a large difference in $\Delta h_{u,sol}$ between the tautomers, and the solvation enthalpies ΔH_{sol} of the enol is still larger than that of the keto even after including the solute terms. Considering that the errors in the solute terms are relatively small because we estimated them by ab initio calculations, the discrepancies should be attributed to the solute-solvent term $\Delta h_{u,sol}$.

As in Eq.(3.12), $\Delta h_{u,sol}$ is given as the sum of two terms. The first term ϵ_{sol}, the

solvation energy, is further decomposed into the solute-solvent interaction energy E_{uv} and the cavity formation energy (solvent reorganization energy) E_{cav}, i.e. Eq.(3.11). Yu et al.[43] pointed out that the RISM integral equation theory provides comparable results for E_{uv} to the computer simulations, while E_{cav} is overestimated with the HNC approximation in aqueous solution. The present calculations yielded considerably large values of E_{uv} in water in comparison with those in DMSO and CCl_4, indicating the existence of hydrogen bonding in solvent-solvent and solute-solvent in the aqueous solution causes an overestimation of E_{cav}, while such an effect is small in DMSO and CCl_4, typical aprotic solvents, having a small ability of hydrogen bonding. It is noted that the second term in Eq.(3.12) might be overestimated in the present treatments, because this term also originated from the reorganization of solvent water.

Only the overestimations of E_{cav} and the second term in Eq.(3.12) may not resolve a large discrepancy in the calculated solvation enthalpies between the tautomers because the error in E_{cav} is considered to be larger for the keto than the enol. As pointed out by Spencer et al.[14], the enol tautomer can be enthalpically stabilized through self-association. Although the self-association of enol might be one of the possibilities for interpreting the discrepancy between the present calculation and the experiment for both the tautomers in the solvation enthalpies, we have not examined this possibility because such an effect is beyond the scope of the present study.

The changes of the enthalpy and entropy terms caused by the keto-enol tautomerization are shown in Table V. The calculated results are comparable to the experiments for DMSO and CCl_4 solutions as in the case of solvation enthalpies discussed above. For the aqueous solution, the calculations gave the enthalpy and entropy changes with the opposite signs to the experiments. The calculated results implies that the keto form is

enthalpically more stable but entropically unstable than the enol, which can be easily understood considering the stronger solute-solvent interaction in the keto.

3.3.4 Driving force for the geometric change of the keto tautomer in solutions

As shown in Subsec. 3.3.1, the keto tautomer undergoes a large geometry change going from the gas phase to the polar solvents. We discuss here the driving force to cause such a change in geometry. For this purpose, the free energy ΔG and solvation enthalpy ΔH_{sol} calculated at the gas phase optimized geometry, hereafter denoted as **a**, were compared with those in the polar solvents, **b**, and the results are summarized in Table VII. For the geometry in the gas phase, we took the optimized one with a smaller torsional angle (τ_{3256}= 102.4°). Note that the solute vibrational contributions were omitted in calculating ΔG and ΔH_{sol} though the electron correlation energies were included.

The free energy ΔG at **b** is more stable than that of **a** because the geometry **b** corresponds to the minimum free energy point in each solvent. However, the difference of the enthalpies between **a** and **b** obtained with Eq.(3.18), $\Delta H(\mathbf{b}-\mathbf{a})$, is positive in DMSO, indicating that the geometry **b** is enthalpically unstable compared with **a** and thus the geometric change observed for DMSO solution is driven by the entropy term. In the aqueous solution, the situation is quite different from the DMSO case: the calculated $\Delta H(\mathbf{b}-\mathbf{a})$ is −4.81 kcal/mol and the entropy change is also negative as going from **a** to **b**. We can thus conclude that the enthalpy term is responsible to cause the geometric change in H_2O.

In order to clarify such a difference of the driving forces for the geometric change

between the DMSO and aqueous solutions, we examined the solvation structures, i.e. the radial distribution functions (rdfs). Figure 2 compares the rdfs between the O_3 site of acetylacetone and the water H site obtained at the geometries **a** and **b** because the solute O_3 and O_6 sites participate in the solute-solvent interaction most strongly. In DMSO, the height of the first peak is almost the same between **a** and **b**, as seen in Figure 2(a). This means that the solvation structure around the solute does not undergo a large modification by the geometric change from **a** to **b** and the positive enthalpy change, $\Delta H(\mathbf{b} - \mathbf{a})$, is attributed to the increase of solute electronic energy. On the contrary, the solvation becomes stronger after the geometric change in the aqueous solution. The first peak is higher at **b** than **a** as illustrated in Figure 2(b), which implies that the hydrogen bonding becomes strong by the geometry change and the stabilization due to the increase of solute-solvent interaction energy overcomes the increase of solute electronic reorganization energy. The difference of solvation structures between the DMSO and aqueous solutions can be rationalized if we see the change of the partial charges on the O_3 and O_6 sites caused by the solute geometric change form **a** to **b**: the partial charges change from -0.74 to -0.79 in H_2O, while the change in DMSO is very small, from -0.62 to -0.63.

3.4 Conclusions

In the present paper, we studied the keto-enol tautomerization equilibrium of acetylacetone in CCl_4, DMSO and H_2O with the RISM-SCF method. The solvation free energies were analyzed by decomposing them into the enthalpy and entropy contributions as well as the solute electronic and vibrational ones. The conclusions derived from the calculations are summarized as follows.

(1) The geometry of keto tautomer undergoes a large change in polar solvents from that in the gas phase. Especially, the dihedral angle between the planes containing two carbonyl groups becomes small, 56.4° and 75.2° in H_2O and DMSO, respectively. In CCl_4, the geometry was almost the same as in the gas phase. For the enol, the solvent induced geometry change was rather small even in polar solvents.

(2) The calculated keto-enol free energy difference in solution was in good agreement with the experiments, including the vibrational free energy difference and zero point energy contributions as well as the electron correlation effect of solute. It was found that the equilibrium shifts to the keto form in aqueous solution while the enol is still dominant in CCl_4 as in the gas phase.

(3) The calculated solvation enthalpies for both tautomers were comparable to the experimental estimates in CCl_4 and DMSO. However, we observed a large discrepancy in the solvation enthalpies in H_2O between the calculations and experiments, which was attributed to the overestimation of the cavity formation energy in water solvent.

(4) The origin of a large geometric change of the keto form in polar solvents was examined. It was found that such a geometric change is driven by the enthalpy term for aqueous solution while the entropy term is important in DMSO.

Acknowledgement

We thank Dr. A. Morita for valuable discussions. This work was supported by the Grant in Aid for Scientific Research from the Ministry of Education.

Bibliography

[1] W. L. Jorgensen, Acc. Chem. Res. **22**, 184 (1989)

[2] J. Gao, Acc. Chem. Res. **29**, 298 (1996)

[3] J. Tomasi and M. Persico, Chem. Rev. **94**, 2027 (1994)

[4] T. Ishida, F. Hirata, H. Sato and S. Kato, J. Phys. Chem. B **102**, 2045 (1998).

[5] M. W. Wong, K. B. Wiberg and M. J. Frisch, J. Am. Chem. Soc. **114**, 1645 (1992).

[6] S. Ten-no, F. Hirata and S. Kato, Chem. Phys. Lett. **214**, 391 (1993).

[7] S. Ten-no, F. Hirata, and S. Kato, J. Chem. Phys. **100**, 7443 (1994).

[8] J. Emsley, Structure and Bonding **57**, 147 (1984).

[9] A. H. Lowrey, C. George, P. D'Antonio and J. Karle, J. Am. Chem. Soc. **93**, 6399 (1971).

[10] K. Iijima, A. Ohnogi and S. Shibata, J. Mol. Struct. **156**, 111 (1987).

[11] J. Powling and H. J. Bernstein, J. Am. Chem. Soc. **73**, 4353 (1951).

[12] S. L. Wallen, C. R. Yonker, C. L. Phelps and C. M. Wai, J. Chem. Soc. Faraday Trans. **93**, 2391 (1997).

[13] M. M. Folkendt, B. E. Weiss-Lopez, J. P. Chauvel, Jr. and N. S. True, J. Phys. Chem. **89**, 3347 (1985).

[14] J. N. Spencer, E. S. Holmboe, M. R. Kirshenbaum, D. W. Firth and P. B. Pinto, Can. J. Chem. **60**, 1178 (1982).

[15] J. Emsley and N. J. Freeman, J. Mol. Struct. **161**, 193 (1987).

[16] W. Blokzijl and J. B. F. N. Engberts, J. Chem. Soc. Perkin Trans. 2 455 (1994).

[17] E. Iglesias, J. Chem. Soc. Perkin Trans. 2 431 (1997).

[18] M. T. Rogers and J. L. Burdett, Can. J. Chem. **43**, 1516 (1965).

[19] J. J. Dannenberg and R. Rios, J. Phys. Chem. **98**, 6714 (1994).

[20] G. Buemi and C. Gandolfo, J. Chem. Soc. Faraday Trans. 2 **85**, 215 (1989).

[21] M. Karelson, Adv. Quant. Chem. **28**, 141 (1997).

[22] M. A. Rios and J. Rodríguez, J. Mol. Struct. (THEOCHEM) **204**, 137 (1990).

[23] C. J. Cramer and D. G. Truhlar, in *Solvent Effects and Chemical Reactivity*, edited by O. Tapia and J. Bertrán (Kluwer, Dordrecht, 1996).

[24] H. A. Yu and M. Karplus, J. Chem. Phys. **89**, 2366 (1988).

[25] H. A. Yu, B. Roux, and M. Karplus, J. Chem. Phys. **92**,5020 (1990).

[26] S. J. Singer and D. Chandler, Mol. Phys. **55**, 621 (1985).

[27] D. A. Zichi and P. J. Rossky, J. Chem. Phys. **84**, 1712 (1986).

[28] T. H. Dunning, Jr. and P. J. Hay, in *Modern Electronic Structure Theory*, edited by H. F. Schaefer III (Plenum, New York, 1977).

[29] H. Sato, F. Hirata and S. Kato, J. Chem. Phys. **105**, 1546 (1996).

[30] L. J. Lowden and D. Chandler, J. Chem. Phys. **61**, 5228 (1974).

[31] T.-M. Chang, K. A. Peterson and L. X. Dang, J. Chem. Phys. **103**, 7502 (1995).

[32] A. Luzar, A. K. Soper and D. Chandler, J. Chem. Phys. **99**, 6836 (1993).

[33] H. J. C. Brendsen, J. P. M. Postma, W. F. von Gustern, and J. Hermas, *in Intermolecular Forces*, edited by B. Pullman (Reidel, Dordrecht, 1981).

[34] S. J. Weiner, P. A. Kollman, D. A. Case, U. C. Singh, C. Ghio, G. Alagona, S. Profeta, Jr. and P. Weiner, J. Am. Chem. Soc. **106**, 765 (1984).

[35] J. A. Riddick, W. B. Bunger and T. K. Sakano, *ORGANIC SOLVENTS, 4th ed* (Wiley-Interscience, New York, 1986).

[36] F. Hirata and P. J. Rossky, Chem. Phys. Lett. **83**, 329 (1981).

[37] F. Hirata, B. M. Pettitt and P. J. Rossky, J. Chem. Phys. **77**, 509-520 (1982).

[38] F. Hirata, P. J. Rossky and B. M. Pettitt, J. Chem. Phys. **78**, 4133 (1983).

[39] R. Mecke and E. Funck, Z. Elecktrochem. **60**, 1124 (1956).

[40] K. L. Wierzchowski and D. Shugar, Spectrochim. Acta. **21**, 943 (1965).

[41] E. E. Ernstbrunner, J. Chem. Soc.(A) 1558 (1970).

[42] S. H. Bauer and C. F. Wilcox, Chem. Phys. Lett. **279**, 122 (1997).

[43] H. A. Yu, B. M. Pettitt and M. Karplus, J. Am. Chem. Soc. **113**, 2425 (1991).

Figure captions

Figure 1. Molecular geometry and site assignment for tautomers of acetylacetone (a) Keto form (b) Enol form.

Figure 2. Radial distribution functions between the O_3 site of the keto and the solvent sites. Arrows indicate the change of the first peak. (a) O-CH_3 (solvent: DMSO), (b) O-H (solvent: H_2O).

Table.I: Parameters for Solvents and Solute

solvent[a]	site	q	σ/Å	$\epsilon/kcalmol^{-1}$
H_2O	H	0.41	1.000	0.056
	O	−0.82	3.166	0.155
DMSO	O	−0.459	2.80	0.0715
	S	0.139	3.40	0.238
	CH_3	0.160	3.80	0.293
CCl_4	C	−0.1616	3.2	0.10
	Cl	0.0404	3.4	0.26

parameter for solute site[b]

	σ/Å	$\epsilon/kcalmol^{-1}$
C	3.562	0.1499
C(C_2 and C_5)[c]	3.296	0.1199
O	2.850	0.1999
H	2.450	0.0379

[a] Data from refs 30, 31 for CCl_4, ref 32 for DMSO, ref 33 for H_2O.
[b] Reference 34.
[c] See Figure 1.

Table.II: Selected Geometric Parameters for Both Tautomers in the Gas Phase and Solutions. (Units: R in Å, τ and θ in degree.)

Keto form	gas phase	in CCl_4	in DMSO	in H_2O
$R^a_{24\ or\ 45}$	1.529 (1.529)[b]	1.527 (1.526)[b]	1.520	1.522
$R^a_{12\ or\ 57}$	1.510 (1.508)	1.508 (1.506)	1.504	1.504
$R^a_{23\ or\ 56}$	1.195 (1.194)	1.195 (1.194)	1.197	1.213
τ_{3256}	140.4 (102.4)	140.4 (101.6)	75.2	56.4
θ_{245}	108.6 (109.9)	108.6 (110.0)	112.8	115.8
R_{36}	3.787 (3.259)	3.783 (3.249)	2.940	2.763

Enol form	gas phase	in CCl_4	in DMSO	in H_2O
R_{12}	1.514	1.510	1.509	1.508
R_{23}	1.218	1.217	1.223	1.246
R_{24}	1.459	1.456	1.454	1.455
R_{45}	1.356	1.355	1.355	1.368
R_{56}	1.316	1.315	1.318	1.329
R_{57}	1.497	1.496	1.495	1.496
θ_{245}	121.5	121.4	121.7	122.8
τ_{12-654}	0.0	0.0	0.0	0.0
R_{6-12}	0.961	0.960	0.961	0.973
$R_{3\cdots12}$	1.685	1.680	1.672	1.727

[a]Averaged values. [b]Parenthesises represent parameters for the other keto conformer.

Table.III: Dipole Moment in the Gas Phase and Solutions (Units in D)

	keto	enol
CCl_4	1.752 (3.767)[a]	3.186
DMSO	6.014	3.928
H_2O	8.863	5.311
gas	1.744 (3.724)[a]	3.157

[a] Values in parenthesis are for the other keto conformer(τ_{3256} = 102.4°).

Table.IV: Selected Solute Vibrational Frequencies.[a]

Keto form	gas phase	in CCl_4	in DMSO	in H_2O
$C_2C_4C_5$ bending	152.3	153.8	128.3	106.0
C=O anti-symmetric	1986.0	1988.5	1964.0	1862.8
C=O symmetric	2009.2	2011.8	2001.9	1923.6
Enol form	**gas phase**	**in CCl_4**	**in DMSO**	**in H_2O**
C_4-C_5 stretching	1779.2	1771.7	1751.9	1669.8
C_2-O_3 stretching	1904.4	1894.4	1862.7	1765.3
O_6-H_{12} stretching	3871.4	3871.2	3846.5	3686.8

[a]Units in cm^{-1}.

Table.V: Differences of Total Free Energies between the Keto and Enol and Their Components.

solvent	$\Delta G(k-e)$	$\Delta H(k-e)^a$	$T\Delta S(k-e)^a$	$\Delta G_{exp}(k-e)^b$
H_2O	−1.37	−6.05 (2.7±0.3)	−4.68 (3.7)	−1.18(−0.98)
DMSO	0.14	0.55 (1.8±0.2)	0.41 (1.5)	−0.16(0.29)
CCl_4	0.11	1.02 (2.5±0.3)	0.91 (0.80)	1.76(1.74)
gas	−0.69	–	–	2.20[c]

Components of $\Delta G(k-e)$.

solvent	$\Delta E_{sol}(k-e)^d$	$\Delta ZPE(k-e)$	$\Delta G_{vib}(k-e)$	$\mu_{sol}(k-e)$
H_2O	17.71(11.57)	−0.47	−1.08	−17.53
DMSO	6.46(3.08)	−0.89	−1.27	−4.16
CCl_4	1.00(−0.35)	−0.87	−0.98	0.96
gas	1.04(−0.35)	−0.84	−0.89	–

[a] Values in parenthesises are the experimental data in ref 14. [b] Data from ref 15. Data in parenthesis from ref 14. [c] Reference 13. [d] Values in parenthesis are the RHF level results.

Table.VI: Solvation Enthalpy Terms. (Units in kcal/mol)

	Keto					Enol				
solvent	ΔH^a_{sol}	$\Delta h_{u,sol}$	E_{uv}	E_{cav}	experimental	ΔH^a_{sol}	$\Delta h_{u,sol}$	E_{uv}	E_{cav}	experimental
H_2O	5.02	−17.23	−84.72	35.67	−10.6	11.56	6.48	−46.60	19.81	−11.1
DMSO	−13.95	−17.88	−40.10	7.49	−9.8	−14.01	−12.54	−30.63	3.97	−9.4
CCl_4	−5.38	−2.61	−18.56	1.47	−8.2	−5.91	−3.82	−19.40	1.63	−8.5

[a] Values include MP2 energies.

Table.VII: $\Delta G(\mathbf{b}-\mathbf{a})$, $\Delta H(\mathbf{b}-\mathbf{a})$ and $T\Delta S(\mathbf{b}-\mathbf{a})$ with **a.** the optimized geometry in gas phase and **b.** the optimized geometry in solution. (Units in kcal/mol)[a]

solvent	$\Delta G(\mathbf{b}-\mathbf{a})$	$\Delta H(\mathbf{b}-\mathbf{a})$[b]	$T\Delta S(\mathbf{b}-\mathbf{a})$
DMSO	−0.44	0.58	1.02
H_2O	−3.35	−4.81	−1.46

[a] For all values, the electron correlation energies are included.
[b] $\Delta H_{gas}(\mathbf{b}-\mathbf{a})$s are 0.67 kcal/mol in DMSO, 0.75 kcal/mol in H_2O.

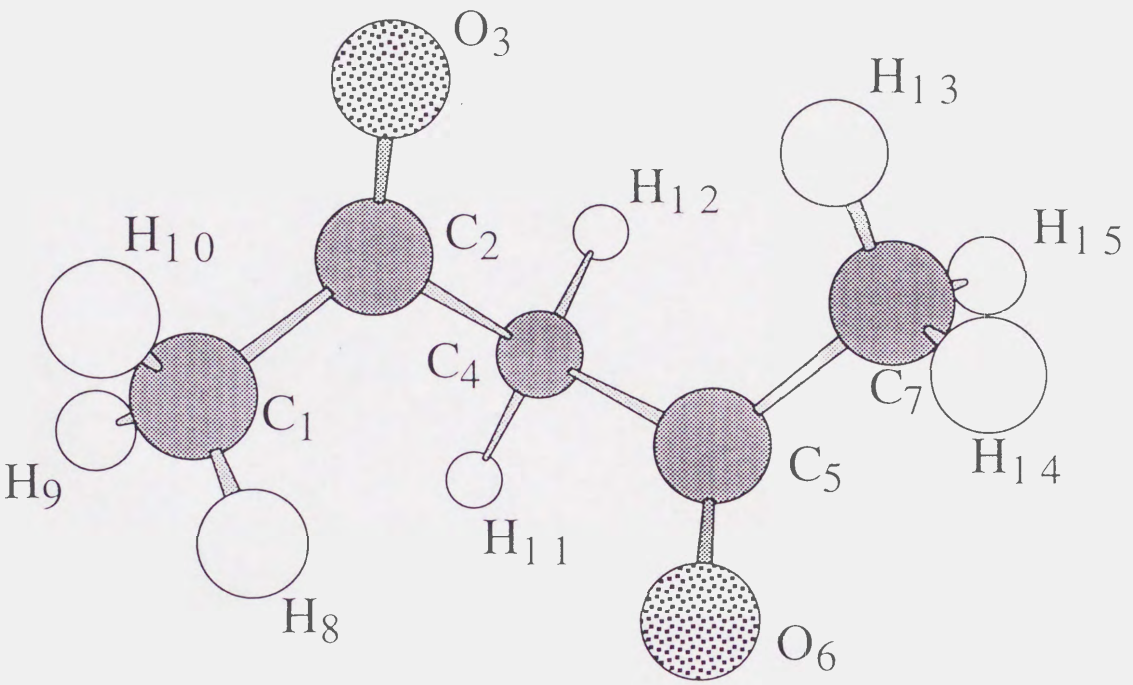

FIG.1. (a)

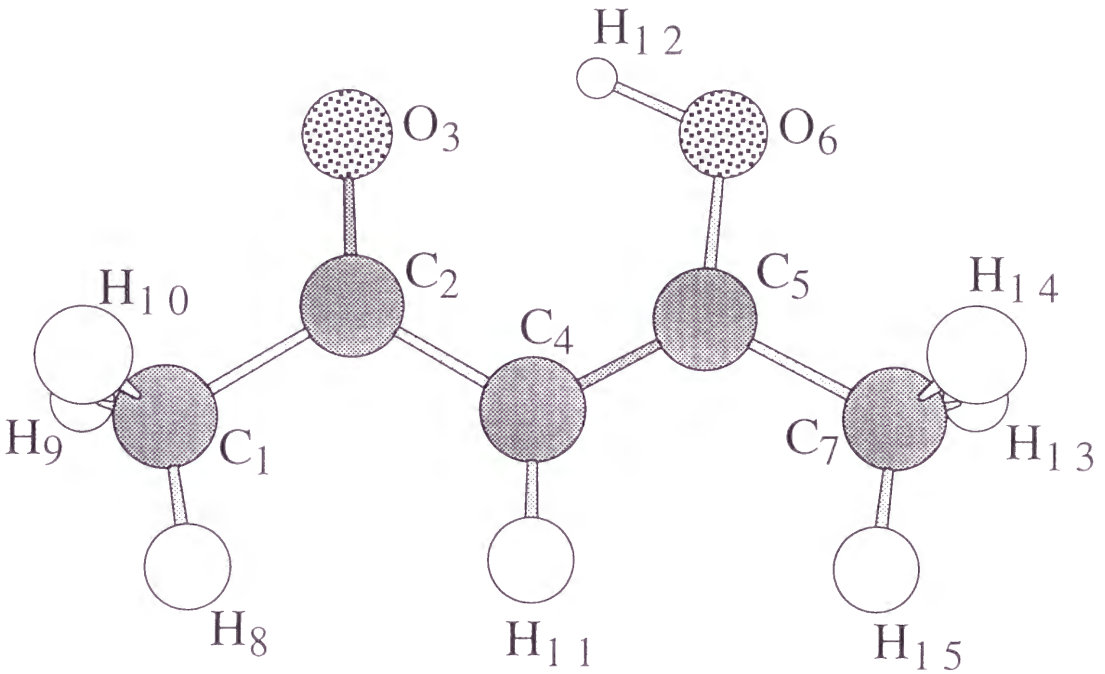

FIG.1. (b)

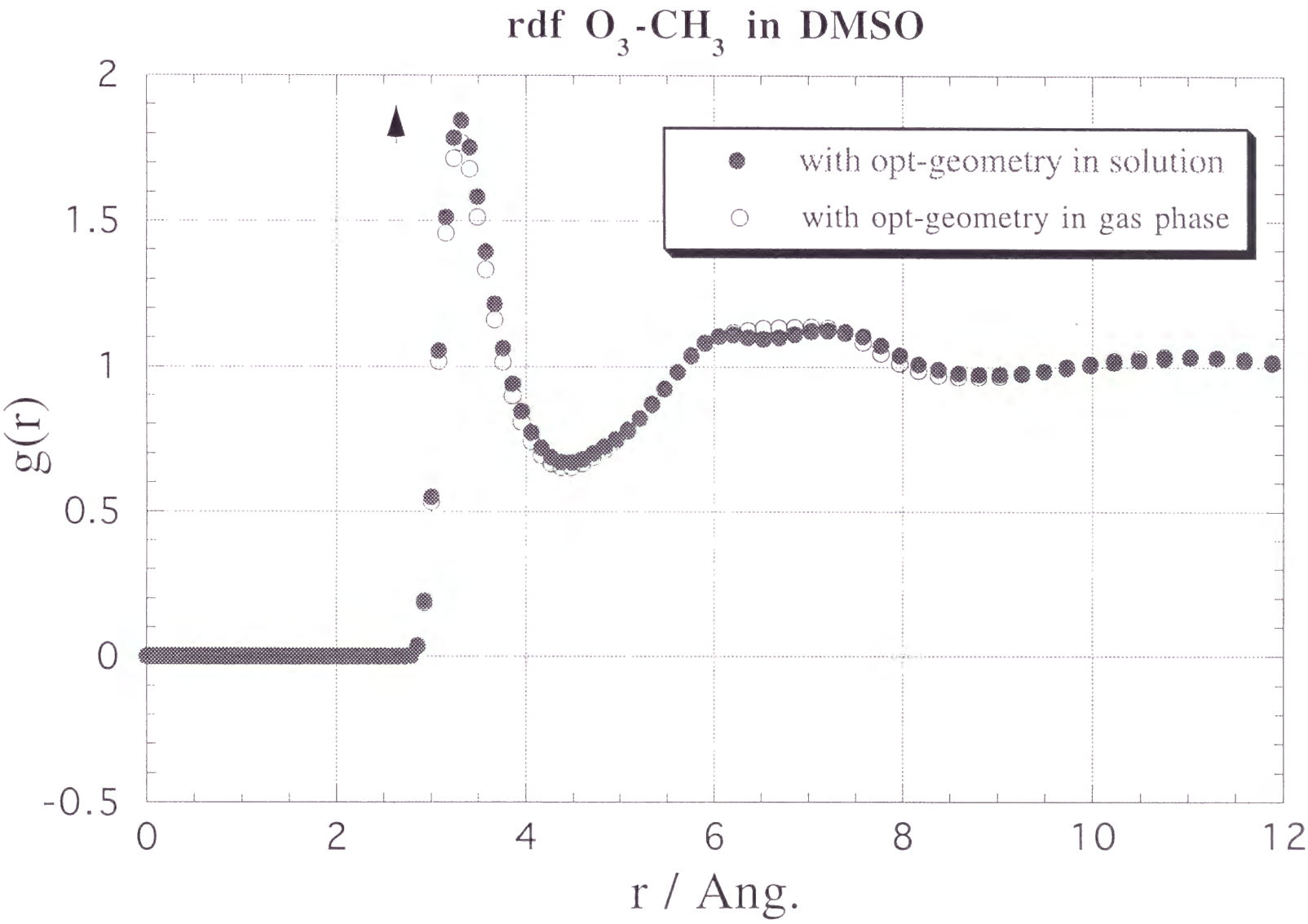
rdf O3-CH3 in DMSO
with opt-geometry in solution
with opt-geometry in gas phase
g(r)
r / Ang.
2
1.5
1
0.5
0
-0.5
0
2
4
6
8
10
12

FIG.2. (a)

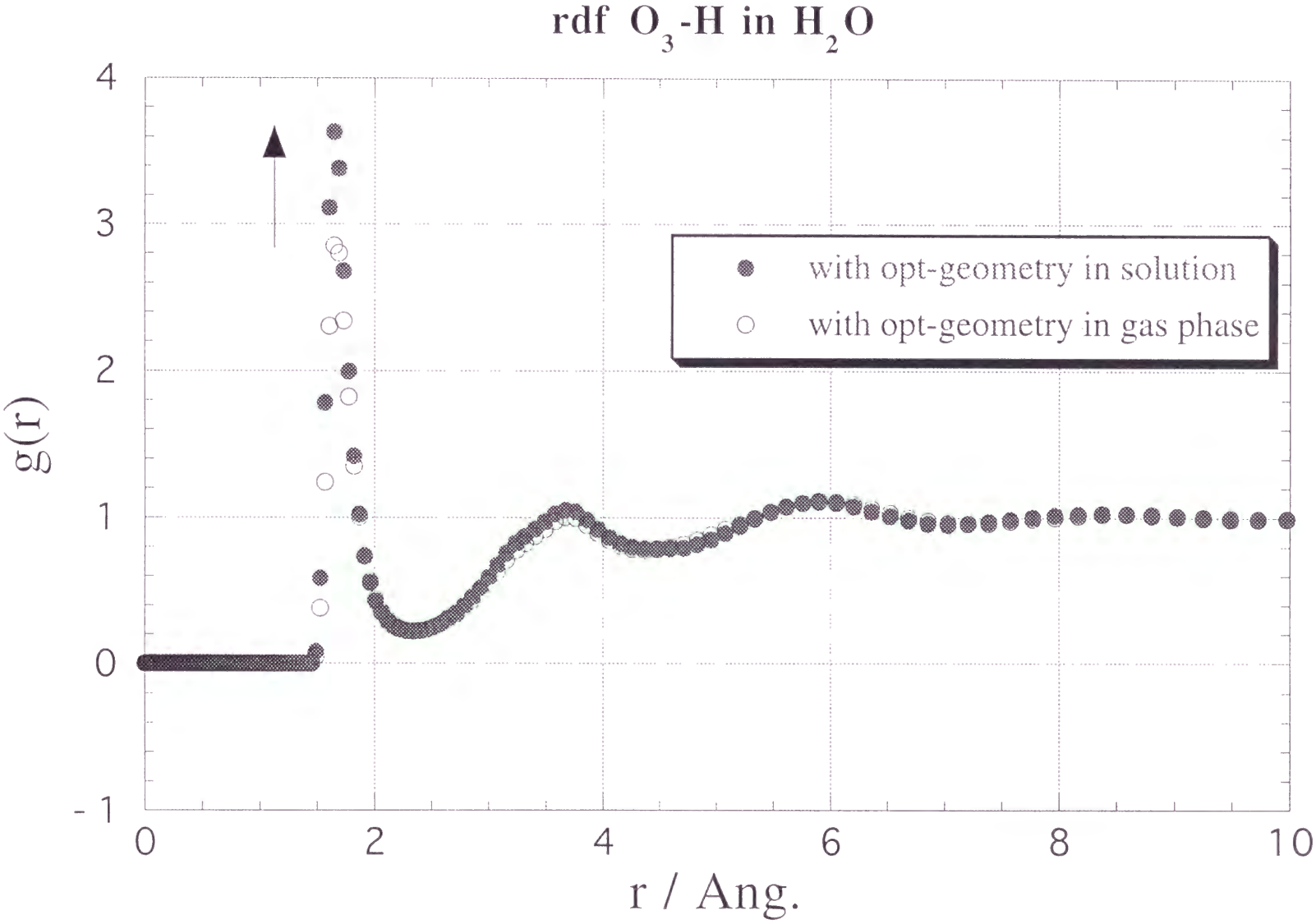
rdf O3-H in H2O
g(r)
r / Ang.
with opt-geometry in solution
with opt-geometry in gas phase
4
3
2
1
0
-1
0
2
4
6
8
10

FIG.2. (b)

Chapter 4

Solvation dynamics of benzonitrile excited state in polar solvents: A time-dependent reference interaction site model self-consistent field approach

4.1 Introduction

The role of molecular properties of solvent such as the shape and polarity in solvation dynamics has long received considerable attention from experimental and theoretical points of view, because of its importance in understanding the dynamics of chemical reactions in solution.[1]-[3] Experimentally, with the recent development of ultrafast laser spectroscopy in a femtosecond order, it has become feasible to explore the solvation dynamics

in a short time scale initiated by the electronic excitation of the probe molecule, providing that the relaxation time scale of solvent molecules in the vicinity of solute molecule differs from that of the overall solvation process.[4]-[10] On the theoretical ground, many studies including the approaches from molecular theories of liquids and computer simulations have been performed in order to clarify the importance of solute-solvent interactions in rationalizing the mechanism of solvation dynamics.[3]-[12]

Molecular dynamics (MD) simulation calculations have been carried out so far for the systems consist of atomic and molecular solutes in polar solvents such as water, alcohols and nitriles, for investigating the solvation dynamics induced by the change of solute charge distribution.[13]-[19] Although those studies have provided wealth of information on the solvent relaxation dynamics at a microscopic level in terms of the solute-solvent and solvent-solvent intermolecular interactions, many of them are based on the assumption that the charge distribution of probe molecule prepared just after the excitation does not change during the solvent relaxation. Considering that polarizable dye molecules with π electrons have been utilized as the probe molecules in many experimental measurements of the dynamic Stokes shift,[20] such an approximation seems to be too crude for describing the real molecular processes because the electronic states of the probe molecules are very sensitive to the external field originating from the solvent. In this respect, it would be worthwhile to pay more attention to the change of the electronic structure in the probe molecules caused by the solvent relaxation.

Recently there have been noticeable progresses in *ab initio* electronic structure theories for solute molecules in solution including the polarizable continuum (PCM) model,[21] reference interaction site model self-consistent field (RISM-SCF) method[22]-[24] and combined quantum mechanics/molecular mechanics (QM/MM) method.[25] Those have been

successfully applied to calculate solute molecular properties as well as free energy surfaces of chemical reactions in solution, which are obtained under the equilibrium solvation condition. In view of the importance of the solute electronic structure variation during the solvent relaxation as mentioned above, [19] it would be highly desired to extend those *ab initio* methods to be capable of dealing with the time dependent nonequilibrium solvation processes.

In the present paper, we propose a method, referred to as a time-dependent RISM-SCF approach, by incorporating the time-dependent solute-solvent radial distribution functions (rdfs) into the RISM-SCF theory, and apply it to study the dynamic Stoke shifts of benzonitrile (C_6H_5CN) in water (H_2O), methanol (CH_3OH) and acetonitrile (CH_3CN) solvents. For calculating the time-dependent rdfs, we adopt the recent theory proposed by Raineri *et al.*[26]-[28] dealing with solvent relaxation processes based on statistical mechanics of molecular liquids, in which the surrogated form is developed closely relating to the extended reference interaction site model (XRISM).[29]-[31] With the surrogate formalism, one can obtain the time-dependent solvent distribution around the solute connecting the initial and final states, which has been shown to be in good agreement with the simulation results for model solution systems.

Benzonitrile molecule is one of the popular benzene-derivatives and its amino substituted compounds are well-known to show dual fluorescence in polar solvents. Electronic structure calculations have been performed for low-lying excited states of C_6H_5CN employing semiempirical[32] and *ab initio* methods.[33, 34] The lowest singlet excited state is the 1^1B_2 one located at ~ 4.5 eV measured from the ground state. Because the dipole moment of this state is very close to that of the ground state, one can not expect a large Stokes shift for the transition to this state even in polar solvents. The second excited

state is the 2^1A_1, which has a large dipole moment with the strong transition intensity from the ground state. We therefore chose the $2^1A_1 \leftarrow 1^1A_1$ transition as the probe for investigating the solvation dynamics. A theoretical study on the solvation of excited states of C_6H_5CN in polar solvents may provide an insight in resolving the still controversial mechanism of intramolecular charge transfer in aminobenzonitriles.[35, 36]

This paper is organized as follows. In the following section, we present the theoretical method to calculate the time evolution of rdfs which is incorporated into the RISM-SCF method. Details of *ab initio* computational procedures are also given. In Sec. 4.3, the calculated results of the solvation of C_6H_5CN in H_2O, CH_3OH and CH_3CN solvents are presented. We discuss the electronic distributions in the solute and the solvation structures obtained at the ground and vertical excited states. The evolution of solute electronic states caused by the solvent relaxation is characterized by the energy difference between these states. The variation of solute electronic distribution during the solvation process is also examined. Conclusions of the present paper follow in Sec. 4.4.

4.2 Theoretical Methods

4.2.1 Time-dependent RISM-SCF

We consider a solute molecule immersed in a solvent media. The time evolution of solute electronic states driven by solvent motions may be described by the Hamiltonian,

$$\begin{aligned} \hat{H}(t) &= \hat{H}_0 + \hat{V}(t) \\ &= \hat{H}_0 + \sum_u^{N_u} \hat{Q}_u V_u(t), \end{aligned} \tag{4.1}$$

where $\hat{H}_0$ is the solute electronic Hamiltonian in the gas phase and V_u is the electrostatic potential acting on the solute site u with N_u being the number of solute interaction sites. $\hat{Q}_u$ is the population operator generating the partial charge Q_u on the site u, which is determined by a least-square-fitting to the electrostatic potential around the solute as usual. In order to obtain the time-dependent electrostatic potential $V_u(t)$, it is required to calculate the time-dependent radial distribution functions $g_{u\lambda}(r,t)$ between the solute-solvent interaction sites, *i.e.*

$$V_u(t) = \rho \sum_{\lambda}^{N_v} \int \mathrm{d}\boldsymbol{r} \frac{Q_\lambda}{r} g_{u\lambda}(r,t), \tag{4.2}$$

where ρ is the solvent density. Here Q_λ is the partial charge at the solvent site λ and N_v is the number of sites in a solvent molecule.

In many experimental and theoretical studies, the solvation dynamics has been examined in terms of the solvation time correlation function (STCF):

$$S(t) = \frac{\Delta E(t) - \Delta E(0)}{\Delta E(\infty) - \Delta E(0)}, \tag{4.3}$$

where $\Delta E(t)$ is the energy difference between the excited and ground states. In the present approach, the energy difference is calculated by

$$\Delta E(t) = < \Psi_e(t) \mid \hat{H}(t) \mid \Psi_e(t) > - < \Psi_g(t) \mid \hat{H}(t) \mid \Psi_g(t) > . \tag{4.4}$$

Here $\Psi_e(t)$ and $\Psi_g(t)$ are the solute electronic wave functions for the excited and ground states.

We use the surrogate linear response theory proposed by Raineri *et al.*[26]-[28] for calculating the time-dependent radial distribution functions in Eq.(4.2) as the response to a sudden change of solute charge distribution caused by the solute electronic excitation. Although they took the energy gap between the solute excited and ground states as the

dynamic variable and derived directly the dynamic solvation time correlation function (STCF), we adopt here a matrix with the element of $\widehat{\mathcal{G}}_{u\lambda}$ representing the fluctuation of solvent site number density $\delta\hat{n}_{u,\lambda}$ in the following,

$$\widehat{\mathcal{G}}_{u\lambda} = \sum_{u'}^{N_u}\sum_{\eta}^{N_v}\int \mathrm{d}^3\boldsymbol{r}'\delta\hat{n}_{u',\eta}(\boldsymbol{r}')\delta_{uu'}\delta_{\lambda\eta}\delta(\boldsymbol{r}-\boldsymbol{r}') \tag{4.5}$$

or in the Fourier k-space

$$\widehat{\mathcal{G}}_{u\lambda} = \frac{1}{(2\pi)^3}\sum_{u'}^{N_u}\sum_{\eta}^{N_v}\int \mathrm{d}^3\boldsymbol{k}\ \delta\hat{n}_{u',\eta}(\boldsymbol{k})\delta_{uu'}\delta_{\lambda\eta}\mathrm{e}^{i\boldsymbol{k}\cdot(\boldsymbol{r}-\boldsymbol{r}')}, \tag{4.6}$$

with

$$\delta\hat{n}_{u,\lambda} = \hat{n}_{u,\lambda} - \langle\hat{n}_{u,\lambda}\rangle, \tag{4.7}$$

where $\langle\ \cdots\ \rangle$ means the equilibrium ensemble average. The suffices u and u' denote the solute sites, and λ and η the solvent sites, respectively. The microscopic number density of solvent site λ at a position $\boldsymbol{r}$ relative to solute site u is defined as

$$\hat{n}_{u,\lambda} = \sum_i \delta(\boldsymbol{r}-\boldsymbol{r}_{i\lambda}+\boldsymbol{r}_u), \tag{4.8}$$

where the summation runs over all the solvent molecules.

Introducing the time dependent fluctuation of solvent number density,

$$\widehat{\mathcal{G}}_{u\lambda}(t) = \frac{1}{(2\pi)^3}\sum_{u'}^{N_u}\sum_{\eta}^{N_v}\int \mathrm{d}^3\boldsymbol{k}\ \delta\hat{n}_{u',\eta}(\boldsymbol{k},t)\delta_{uu'}\delta_{\lambda\eta}\mathrm{e}^{i\boldsymbol{k}\cdot(\boldsymbol{r}-\boldsymbol{r}')}, \tag{4.9}$$

one can obtain the equilibrium time correlation function for the fluctuation of solvent number density as follows,

$$\begin{aligned} C_{\mathcal{G}_{u\lambda}}(t) &= \langle\widehat{\mathcal{G}}_{u\lambda}(t)\widehat{\mathcal{E}}(0)\rangle \\ &= \frac{1}{(2\pi)^3}\sum_{u'}^{N_u}\sum_{\eta}^{N_v}\int \mathrm{d}^3\boldsymbol{k}\ \hat{\omega}_{uu'}(\boldsymbol{k})\Delta\phi_{u'\eta}(-\boldsymbol{k})F_{\eta\lambda}(\boldsymbol{k},t)\mathrm{e}^{i\boldsymbol{k}\cdot(\boldsymbol{r}-\boldsymbol{r}')}, \end{aligned} \tag{4.10}$$

and

$$C_{\mathcal{G}}(0) = \frac{1}{(2\pi)^3} \sum_{u'}^{N_u} \sum_{\eta}^{N_v} \int \mathrm{d}^3\boldsymbol{k}\ \hat{\omega}_{uu'}(\boldsymbol{k}) \Delta\phi_{u'\eta}(-\boldsymbol{k}) S_{\eta\lambda}(\boldsymbol{k}) \mathrm{e}^{i\boldsymbol{k}\cdot(\boldsymbol{r}-\boldsymbol{r}')}, \tag{4.11}$$

where $-\beta\Delta\phi_{u'\eta}(r) \equiv c^{\mathcal{S}}_{u'\eta}(r) - c^{\mathcal{P}}_{u'\eta}(r)$ and $\beta = 1/k_B T$ (see Appendix). Note that we used the relation,[28]

$$\delta\hat{n}_{u,\lambda}(\boldsymbol{k}) = \mathrm{e}^{-i\boldsymbol{k}\cdot\boldsymbol{r}_u} \delta\hat{n}_{\lambda}(\boldsymbol{k}), \tag{4.12}$$

where $\delta\hat{n}_\lambda$ is the fluctuation of pure solvent number density. In Eqs.(4.10) and (4.11), $\hat{\omega}_{uu'}$ is the solute intramolecular correlation function in k-space. $F_{\eta\lambda}$ is the intermediate site-site structure factor,[28]

$$F_{\eta\lambda}(k,t) = \left\{ \frac{1}{V} \langle \delta\hat{n}_\eta(k,t) \delta\hat{n}_\lambda(-k) \rangle \right\}_\infty, \tag{4.13}$$

where $\{\cdots\}_\infty$ means taking the thermodynamic limit, and V is the volume. $S_{\eta\lambda}$ is the static site-site structure factor,

$$S_{\eta\lambda}(k) = F_{\eta\lambda}(k,0). \tag{4.14}$$

The supersubscript $\mathcal{P}$ or $\mathcal{S}$ denotes the precursor or successor state, respectively. The precursor state corresponds to the vertical excited state with the solvent distribution in equilibrium to the solute charge in the ground state. On the other hand, the successor one represents the new equilibrium state achieved by the solvent relaxation following to the electronic transition. The solute-solvent direct correlation function $c^{\mathcal{D}}_{u'\eta}(r)$ ($\mathcal{D}$=$\mathcal{S}$ or $\mathcal{P}$) can be evaluated by the XRISM equation for the equilibrium solvation corresponding to the ground or excited state:

$$\boldsymbol{h}^{\mathcal{D}} = \boldsymbol{\omega} * \boldsymbol{c}^{\mathcal{D}} * \boldsymbol{\omega} + \rho\boldsymbol{\omega} * \boldsymbol{c}^{\mathcal{D}} * \boldsymbol{h}^{\mathcal{D}}, \tag{4.15}$$

where $\boldsymbol{h}^{\mathcal{D}}$ is the solute-solvent correlation function and the asterisk means the convolution. Note that the bold variables represent the matrices.

The static structure factor $S_{\eta\lambda}$ in Eq.(4.14) is obtained from the XRISM calculations for the pure solvent. In calculating $F_{\eta\lambda}$, we employ the site-site Smoluchowski-Vlasov (SSSV) theory,[37, 38] which provides the diffusion equation for the fluctuation of solvent site-site number densities, $\delta\hat{\boldsymbol{n}}(k,t)$, derived from the generalized Langevin equation,

$$\frac{\partial^2\delta\hat{\boldsymbol{n}}(k,t)}{\partial t^2} = -\hat{\boldsymbol{D}}(k)\hat{\boldsymbol{\xi}}(k)k^2\rho\hat{\boldsymbol{\chi}}(k)^{-1}\delta\hat{\boldsymbol{n}}(k,t) - \hat{\boldsymbol{\xi}}(k)\frac{\partial\delta\hat{\boldsymbol{n}}(k,t)}{\partial t}, \tag{4.16}$$

where

$$\hat{\boldsymbol{\chi}}(k)^{-1} = [\rho\hat{\boldsymbol{\omega}}(k)]^{-1} - \hat{\boldsymbol{c}}(k). \tag{4.17}$$

Here $\hat{\boldsymbol{D}}(k)$ and $\hat{\boldsymbol{\xi}}(k)$ are the diffusion and friction coefficient matrices represented in k-space, respectively. In the present study, the inertia term corresponding to the left-hand side in Eq.(4.16) is omitted, indicating that the solvent fluctuation is treated in the diffusion limit. Thus the intermediate structure factor is evaluated by

$$\hat{\boldsymbol{F}}(k,t) = \hat{\boldsymbol{S}}(k)\frac{1}{2\pi i}\int_{-i\infty}^{+i\infty}[k^2\hat{\boldsymbol{D}}(k)\hat{\boldsymbol{\chi}}(k)^{-1} + iz\boldsymbol{I}]^{-1}e^{izt}\mathrm{d}z, \tag{4.18}$$

where $\boldsymbol{I}$ is the unit matrix.

Employing the linear response approximation, the nonequilibrium ensemble average of the dynamical variable $\widehat{\mathcal{G}}_{u\lambda}(r,t)$ denoted as, in the matrix form, $\langle\langle\widehat{\boldsymbol{G}}(r,t)\rangle\rangle$ is derived to be

$$\langle\langle\widehat{\boldsymbol{G}}(r,t)\rangle\rangle = \langle\widehat{\boldsymbol{G}}(r)\rangle^{\mathcal{S}} + [\langle\widehat{\boldsymbol{G}}(r)\rangle^{\mathcal{P}} - \langle\widehat{\boldsymbol{G}}(r)\rangle^{\mathcal{S}}] * \boldsymbol{\Phi}(r,t), \tag{4.19}$$

as shown in Appendix. In the k-space, it is represented in the form,

$$\langle\langle\widehat{\boldsymbol{G}}(k,t)\rangle\rangle = \langle\widehat{\boldsymbol{G}}(k)\rangle^{\mathcal{S}} + [\langle\widehat{\boldsymbol{G}}(k)\rangle^{\mathcal{P}} - \langle\widehat{\boldsymbol{G}}(k)\rangle^{\mathcal{S}}] \cdot \boldsymbol{\Phi}(k,t), \tag{4.20}$$

where the matrix $\boldsymbol{\Phi}$(k,t) has the element

$$\Phi_{\eta\lambda}(k,t) = \frac{F_{\eta\lambda}(k,t)}{S_{\eta\lambda}(k)}. \tag{4.21}$$

It is straightforward to show that Eq.(4.20) is further rewritten into

$$\langle\langle \delta\hat{n}_{u,\lambda}(k,t)\rangle\rangle = \langle \delta\hat{n}_{u,\lambda}(k)\rangle^{\mathcal{S}} + \sum_{\eta}^{N_v}[\langle \delta\hat{n}_{u,\eta}(k)\rangle^{\mathcal{P}} - \langle \delta\hat{n}_{u,\eta}(k)\rangle^{\mathcal{S}}] \cdot \Phi_{\eta\lambda}(k,t), \tag{4.22}$$

and one can finally obtain the desired relation represented in the matrix form,

$$\hat{\boldsymbol{h}}(\boldsymbol{k},t) = \hat{\boldsymbol{\omega}}^{\mathcal{S}}\hat{\boldsymbol{c}}^{\mathcal{S}}\boldsymbol{S}(\boldsymbol{k}) - [\hat{\boldsymbol{\omega}}^{\mathcal{S}}\hat{\boldsymbol{c}}^{\mathcal{S}} - \hat{\boldsymbol{\omega}}^{\mathcal{P}}\hat{\boldsymbol{c}}^{\mathcal{P}}]\boldsymbol{F}(\boldsymbol{k},t), \tag{4.23}$$

where we used the relation $\langle \delta\hat{n}_{u,\lambda}(k)\rangle^{\mathcal{D}} = \rho\hat{h}^{\mathcal{D}}_{u,\lambda}(k)$ ($\mathcal{D} = \mathcal{S}$ or $\mathcal{P}$). The time dependent radial distribution functions between the solute-solvent site pairs are thus evaluated by

$$g_{u,\lambda}(r,t) = h_{u,\lambda}(r,t) + 1, \tag{4.24}$$

where $h_{u,\lambda}(r,t)$ is the Fourier transform of $\hat{h}_{u,\lambda}(k,t)$.

4.2.2 Computational Details

The electronic wave functions of the solute C_6H_5CN were calculated by the complete active space (CAS)SCF method with the (9s5p1d/4s1p)/[3s2p1d/2s1p] basis set, which is of valence double zeta plus polarization (DZP) equality.[39] The CASSCF wave functions were constructed by distributing eight electrons in the eight active orbitals, *i.e.*, the π and π^* orbitals on the benzene ring and those on the cyano group. In order to obtain more accurate estimation of the excitation energies, we further employed a multi-configurational quasi-degenerate perturbation theory (MCQDPT),[40, 41] which is a second order Møller-Plesset (MP2) perturbation method for the CASSCF reference wave functions.

The RISM-SCF calculations were performed in H_2O, CH_3OH and CH_3CN solvents in order to obtain the equilibrium solvent distributions both in the ground and 2^1A_1 excited states employing the same CASSCF wave functions as mentioned above. The

solute geometry was optimized using the energy gradient technique[24] for the RISM-SCF free energy. The partial charges on the solute atomic sites were determined by a least square fitting to the electrostatic potentials evaluated at a number of grid points around the solute. For the solvent molecule, we adopted three site models regarding the methyl group as an united atom. The simple point charge[42] (SPC)-like model was used by augmenting the Lennard-Jones parameters, $\sigma = 1.0$ $\AA$ and $\epsilon = 0.056$ kcal/mol, on the H sites for H_2O. All the solvent parameters[42]-[45] are summarized in Table I along with the Lennard-Jones parameters for the solute atoms.[46] The standard combination rule was applied to construct the solute-solvent van der Waals interaction. The hyper-netted chain (HNC) closure relation was employed in solving the XRISM integral equation under the condition that the temperature was 298.15 K for all the solvents.

The evolution of solute electronic states were calculated by the CASSCF wave functions with the Hamiltonian, Eq.(4.1), with the time step of 0.1 ps. We first carried out the XRISM calculations for the pure solvents to obtain the static site-site structure factors $S_{\eta\lambda}(k)$. The intermediate structure factors $F_{\eta\lambda}(k,t)$ were evaluated at every time step by the SSSV theory with the diffusion constants of 3.9×10^{-5} cm^2/s for H_2O and CH_3OH[38] and 4.3×10^{-5} for CH_3CN.[47] The same value for the diffusion constants for H_2O and CH_3OH was used here because those are very close with each other at 298.15 K from the experiment.[48, 49] Note that the diffusion coefficient matrix in Eq.(4.16) is given by the unit matrix multiplied by the corresponding diffusion constant. The time-dependent radial distribution functions $g_{u,\lambda}(r,t)$ were calculated by Eq.(4.23) using the direct correlation functions for the precursor and successor states, $c^{\mathcal{P}}_{u,\lambda}(r)$ and $c^{\mathcal{S}}_{u,\lambda}$(r), obtained by the RISM-SCF calculations for the respective state, with the structure factors, $F_{\eta\lambda}$ and $S_{\eta\lambda}$, and were then substituted into Eq.(4.2) to generate the electrostatic potential acting

on the solute sites $V_u(t)$.

4.3 Results and Discussion

4.3.1 Solute electronic states

The ground state geometry of C_6H_5CN optimized in the gas phase at the CASSCF level is shown in Fig 1, which is in good agreement with the experimental results.[50] The partial charges on solute atomic sites obtained by fitting to the electrostatic potential around the molecule are listed in Table II. The dipole moment derived from the partial charges, 4.34 D, is consistent with that directly calculated from the ab initio wave function, 4.52 D.

The vertical excitation energy corresponding to the $2^1A_1 \leftarrow 1^1A_1$ transition was calculated to be 7.46 eV in the gas phase from the present CASSCF calculations. Since the electronic wave function of 2^1A_1 state is mainly described by the combination of two configurations representing the $3b_1 \rightarrow 4b_1$ and $1a_2 \rightarrow 2a_2$ orbital excitations, the 2^1A_1 state is considered to be of ionic character as in the case of benzene 1^1B_{1u} state. Actually, the dipole moment increased by 2.41 D due to excitation, which is attributed to the change in the partial charge distribution going from the ground state to the excited one as seen in Table II.

It is well known that the dynamic electron correlation effect, particularly the $\sigma - \pi$ polarization effect, is important in estimating the energies of ionic type excited states such as the $1^1B^+_{1u}$ state of benzene. In order to estimate the importance of dynamic correlation effect, the MCQDPT calculations were carried out for the ground and excited $^1A_1$ states at the ground state CASSCF optimized geometry. The vertical excitation energy is reduced to 6.64 eV.

RISM-SCF calculations were carried out to obtain the ground state equilibrium geometries of C_6H_5CN in all three solvents. The changes in the geometry due to the solvation was very small; less than 0.005 $\AA$ in the bond lengths and 1.0° in the angles. The solute dipole moment was enhanced to be 5.80, 5.34 and 5.04 D in H_2O, CH_3OH and CH_3CN, respectively. Using the solute-solvent rdfs which are in equilibrium to the ground state solute electronic distribution, the vertical excitation energy was calculated in each solvent. Compared with the gas phase excitation energy, the vertical excitation energy was reduced by 0.81, 0.79 and 0.77 eV in H_2O, CH_3OH and CH_3CN. These correspond to the red shifts of 6500, 6350 and 6230 cm^{-1}, respectively. Such large red shifts in the vertical excitation energy seem to be reasonable considering that the excited state dipole moment is further increased to 9.29, 8.60 and 8.15 D in those solvents. Note that a blue shift of $\sim$1900 cm^{-1} for the $n\pi^*$ transition of acetone in aqueous solution is attributed to the decrease in the dipole moment by $\sim$1.5 D caused by the electronic excitation.

We further calculated the rdfs which are in equilibrium to the 2^1A_1 electronic state. As seen in Fig. 2, the peak at 1.8 Å for the rdf between the N_8 site in C_6H_5CN and H in H_2O becomes higher due to the orientational polarization of water, indicating the hydrogen bonding is strengthen between those sites. The enhancement of the C_7-H peak at 2.8 Å is attributed to the formation of stronger hydrogen bond between the N_8 and H sites in the excited state equilibrium solvation. In methanol, as shown in Fig. 3, the N_8-H peak at 1.8 Å is higher than that in water both in the ground and excited states, in spite that the positive charge on the H site is larger in H_2O than CH_3OH as seen in Table I. One can also observe the growth at 2.6 Å for the C_7-H rdf coming from the solvation in the excited state as in the case of aqueous solution. The rdfs in CH_3CN solvent are much different from those in the protic solvents, H_2O and CH_3OH. As shown in Fig. 4, there is

no distinct peak between the N_8 or C_7 site in C_6H_5CN and N atom in CH_3CN. The heights of those peaks decrease with proceeding the solvation. On the other hand, the CH_3 group has peaks at 3.3 Å with the N_8 site and at 4.0 Å with the C_7 one, representing rather weak electrostatic interactions with the solute molecule, whose heights slightly increase due to the solvation in the excited state.

The solvation in the excited state induces the electronic polarization in the solute molecules. The partial charges after completing the solvation are summarized in Table II, where the appreciable positive charges are induced on the C_1, C_6 and C_7 sites, while the negative charge on the N_8. The solute dipole moment in the equilibrium solvation was calculated to be 12.6, 10.5 and 9.4 D in H_2O, CH_3OH and CH_3CN. The enhancement of solute dipole moment induced by the solvent relaxation is thus 3.3, 1.9 and 1.3 D in these solvents, indicating that the solute electronic polarization is very important in the present systems. We obtained the energy difference between the excited and ground state under the influence of electrostatic potential coming from the solvent distribution in equilibrium to the excited state solute charges, which was 6.93, 7.16 and 7.27 eV in H_2O, CH_3OH and CH_3CN. The magnitudes of Stokes shifts thus became 0.44, 0.22 and 0.14 eV. It is noted that the Stokes shifts do not change by including the dynamic electron correlation energies if we assume that the electron correlation energies are the same before and after the solvent relaxation.

4.3.2 Solvation dynamics

(a) Solvation time correlation functions

We calculated the time-dependent solute-solvent rdfs up to 20 ps with the time step of 0.1 ps in all the three solvents, initiated by the vertical excitation of the solute with its geometry being fixed to the ground state one optimized in each solvent. At the initial stage of the relaxation, $t < 1$ ps, the distribution functions changed rapidly particularly in the vicinity of solute molecule and then the overall rdfs gradually approached to those for the final state. In H_2O and CH_3CN, the change in the rdfs was very small after $t = 5$ ps though the rdfs showed a slow variation up to more than 10 ps in CH_3OH. Figure 5 displays the calculated STCFs, which show a multi-exponential behavior in all the solvents. In a short time region (< 1ps), water shows the fastest decay among the three solvents and more than 70 % of the relaxation occurs within 1 ps. It is also found that the STCF decays more rapidly in CH_3OH than in CH_3CN on the short time scale. However, the decay curve for CH_3OH shows a longwinded tail which continues up to 20 ps though the relaxation in aqueous and CH_3CN solutions almost complete within 5 ps.

Computer simulation calculations have been performed to explore the mechanism of solvation in polar solvents as treated in the present work. Those studies have revealed that the solvent relaxation takes place on two widely separated time scales. The fast component is attributed to the underdamped or inertial motions of solvent molecules, whose time scale is reported to be 0.1 and 0.2 ps in CH_3CN and CH_3OH while it is 0.02 ps in water. It has been also observed an oscillatory behavior in STCF at the initial stage of the relaxation. As seen in Fig. 5, the present STCFs decay more slowly, 0.2, 0.3 and 0.5 ps in H_2O, CH_3OH and CH_3CN, compared with the simulation results. This is

mainly because we employed the SSSV theory in calculating the intermediate structure factors $F_{u,\lambda}$, in which the solvent motions were described in the overdamped diffusive limit neglecting the inertia term. It is also noted that the vibrational and librational relaxations, which are not taken into account in the present treatment, are known to be responsible to the ultrafast relaxations to some extent. Considering this, the decay time scale in Fig. 5 corresponds to the slow component in the solvent relaxation.

Recently Kumar and Maroncelli[18] carried out MD simulation calculations for the benzene-like solute molecule in CH_3OH and CH_3CN solvents and the resultant STCFs were decomposed to the contributions from the fast inertial component and the slower diffusive one. In order to estimate the slow decay component from the present calculations, we fitted the STCFs in the time range $t > 1$ ps to the bi-exponential functions of the form

$$S(t) = a_1 \exp(-\tau_1^{-1} t) + a_2 \exp(-\tau_2^{-1} t). \tag{4.25}$$

The results are 1.27 (0.54) and 5.45 (0.05) ps in H_2O, 3.28 (0.43) and 24.7 (0.003) ps in CH_3OH and 2.08 (0.96) ps in CH_3CN, respectively, where the values in parentheses are the weights of the exponential functions. The long-time tail observed in the CH_3OH STCF is represented by the exponential function with the longest time constant, 24.7 ps. In contrast to those protic solvents, the STCF in CH_3CN was well fitted by the single exponential function. Using the fitting parameters in Eq.(4.25), we calculated the average decay rate,

$$\bar{\tau} = \frac{a_1\tau_1 + a_2\tau_2}{a_1 + a_2}, \tag{4.26}$$

and the results were 1.62, 3.43 and 2.08 ps for H_2O, CH_3OH and CH_3CN. The average decay rates for CH_3OH and CH_3CN solutions are comparable to the results by Kumar and Maroncelli.[18]

(b) Evolution of solute electronic states

Figure 6 shows the excited state solute dipole moment evolved by the solvent relaxation, where one can observe the increase of dipole moments in the similar time-dependent behaviors as in the STCFs. Those in H_2O and CH_3CN solution saturate within 10 ps, while it takes a longer time to achieve the dipole moment of the new equilibrium solvated state in CH_3OH. In order to see the evolution of solute electronic states in more detail, we defined the solute charge time correlation function, $C_Q^u(t)$, (CTCF) as

$$C_Q^u(t) = \frac{Q_u(t) - Q_u(\infty)}{Q_u(0) - Q_u(\infty)}, \tag{4.27}$$

where $Q_u(t)$ is the partial charge on the site u at time t and $Q_u(0)$ and $Q_u(\infty)$ correspond to the solute site charge in the precursor and successor states given in Table II, respectively. The calculated CTCFs on the C_1, C_6, C_7 and N_8 atomic sites are shown in Fig. 7. As seen in Fig. 7(a), the CTCF at the C_6 site gradually decreases with the progress of solvation while the charge on N_8 changes rapidly at an early stage of the relaxation followed by a slow decay to the asymptotic value in water solvent. In contrast to those atomic charges, the CTCFs for the C_1 and C_7 sites suddenly decrease after the vertical excitation and reach the minimums at $t = 0.2 \sim 0.3$ ps and become the maximum at $t = \sim 1$ ps followed by a slow decrease. Similar behaviors of CTCFs to the water case are observed in CH_3OH though the electronic polarization at the N_8 site in the cyano group is larger. Slow decaying tails of the CTCFs in CH_3OH correspond to the slow decay of STCF in a long time region. The acetonitrile solution shows a different behavior from the protic solvents particularly on the C_1 site whose CTCF does not have a minus sign as seen in Fig. 7(c).

In order to see the origin of the sudden changes in the solute atomic charges at the

initial stage of relaxation, we examined the solvent charge polarization by defining the function

$$\Delta V_u(r,t) = \sum_{\lambda}^{N_v} \frac{Q_\lambda}{r}\{g_{u\lambda}(r,t) - g_{u\lambda}(r,0)\}, \tag{4.28}$$

which is related to the electrostatic potential acting on the solute sit u as $V_u(t) - V_u(0) = \int d\boldsymbol{r}\Delta V_u(r,t)$. The result for aqueous solution is displayed in Fig. 8, where one can observe that large positive charge polarization at $r = 1.8$ Å around the N_8 site increases very rapidly after the excitation and becomes very close to that of the final state at 0.2 ps while smaller charge polarization in the vicinity of C_7 and C_1 sites are still ~ 60 % of the final ones. Considering that the negative charge on the N_8 site is mainly supplied from the C_7 and C_1 sites, the rapid decrease of CTCFs at C_7 and C_1 as seen in Fig. 7(a) is attributed to the charge transfer from these site to N_8 induced by fast charge polarization around the N_8 site. After those sudden changes in the charge distribution at C_1-C_7-N_8 region, the charge polarization is readjusted by the subsequent slower solvent polarization as seen in the variation of N_8 charge at t $>$ 0.5 ps in Fig. 7 (a). A rather gradual change in the CTCF at C_6 comes from a slow solvent polarization around this site. The similar behavior was observed in CH_3OH solution. Very large decrease of the C_7 CTCF is caused by a larger positive charge polarization around N_8 compared with the water solvent. In CH_3CN, the solute-solvent interaction is rather smaller than those in the protic solvents. The smaller extent in the C_1 CTCF decay at the initial stage of relaxation is due to such a weak solute-solvent site-site interaction in CH_3CN.

Non-uniform decays observed in the CTCFs indicate that the electric field coming from the solute molecule such as C_6H_5CN can not be treated by a simple dipole model and it is important to take account of the local charge distribution and its polarization at the individual atomic site in order to obtain a realistic description of the solvation process. It

is also emphasized that a microscopic model of the solvent reflecting its molecular aspects as employed in the present work are required to describe a non-uniform solvent charge polarization in the vicinity of solute molecules as seen in Fig.8.

4.4 Conclusions

In the present paper, we proposed a time-dependent RISM-SCF method incorporating the time-dependent rdfs obtained based on the surrogate linear response theory and applied it to study the solvation dynamics of the 2^1A_1 excited state of C_6H_5CN in H_2O, CH_3OH and CH_3CN solvents. We mainly focused the evolution of solute electronic state during the solvent relaxation following to the vertical transition to the 2^1A_1 state. The main findings of the present study are as follows:

(1) The 2^1A_1 excited state was found to be of ionic character with the dipole moment of 6.75 D in the gas phase, which was enhance to 9.29, 8.60 and 8.15 D in H_2O, CH_3OH and CH_3CN solvents just after the vertical excitation to this state. The red shift of $6230 \sim 6500$ cm^{-1} was obtained for the vertical excitation energy in solution, which is attributed to a large difference in the dipole moment between the excited and ground states. After the solvent relaxation, the solute dipole moment further increased to 12.6, 10.5 and 9.4 D in the respective solvent, indicating that the electron distribution of 2^1A_1 state is very sensitive to the change of electrostatic field coming from the solvent polarization.

(2) The calculated STCFs showed non-exponential behaviors characterized by the fast and slow components of relaxation time scale. The fast components obtained were slower than the experimental and MD simulation values, because we neglected the inertial contribution in evaluating the intermediate structure factors. The slow components were

consistent with those by MD calculations for a model benzene-like solute in CH_3OH and CH_3CN. A long-time tail was observed with the decay rate of 24.7 ps in CH_3OH, while the solvent relaxation almost completed within 5 ps in H_2O and CH_3OH.

(3) The evolution of solute electronic state during the solvent relaxation was examined by observing the time-dependent behavior of CTCF. The resultant CTCF changes very rapidly at the initial stage of relaxation particularly at C_1, C_7 and N_8 sites in contrast to monotonic decays as observed for the STCFs.

As discussed above, we employed the SSSV theory which neglects the inertial effect in calculating the intermediate structure factors and therefore a rather slower solvent relaxation at the initial stage just after the vertical excitation was resulted. It would be required to improve the present method taking into account the inertial effect correctly. For such a purpose, the intermediate structure factors derived from MD simulations or more sophisticated theories as the mode-coupling theory might be promising.

In the present treatment, we only considered the vertical electronic transition of solute in solution with fixing the solute geometry. It is known that the vibrational and librational relaxations contribute to the dynamics at the initial stage of relaxations. In this respect, it would be required to further extend the present approach so as to treat the nuclear dynamics of solute, for describing the processes where the solute geometric change and vibrational relaxation play an important role such as photochemical reactions in solution. In spite of those limitations, we could show in this work the importance of treating the electronic states of solute molecule explicitly with solvent models taking account of their molecular aspects in order to describe the solvation dynamics of polarizable aromatic molecule as C_6H_5CN.

Acknowledgments

The authors are grateful to Dr. H. Nakano for the MCQDPT program. This work was supported by the Joint Studies Program (1998 $\sim$ 1999) of the Institute for Molecular Science and the Grant in Aid for Scientific Research from the Ministry of Education.

Appendix

In the surrogate linear response theory of solvation dynamics,[26]-[28] the nonequilibrium distribution function of the solvent in the field of the solute is given by

$$f^h(\Gamma, t) = f^{\mathcal{S}}(\Gamma) + \beta f^w_{eq}(\Gamma)\delta\hat{\mathcal{E}}(-t), \tag{4.29}$$

where the superscript h denotes the homogeneous approximation.[28] Here $f^{\mathcal{S}}$ is the equilibrium distribution at the successor state $\mathcal{S}$ and f^w_{eq} is that for the homogeneous solvent. The surrogated energy gap $\delta\hat{\mathcal{E}}(t)$ is represented with the renormalized pair interaction, $\phi^{\mathcal{D}}_{u\lambda}(\mathbf{r})$ ($\mathcal{D}$=$\mathcal{S}$ or $\mathcal{P}$),

$$\delta\hat{\mathcal{E}}(t) = \frac{1}{(2\pi)^3}\int \mathrm{d}^3\boldsymbol{k} \sum_u^{N_u}\sum_\lambda^{N_v} \delta\hat{n}_{u,\lambda}(\boldsymbol{k}, t)(\phi^{\mathcal{S}}_{u\lambda}(-\boldsymbol{k}) - \phi^{\mathcal{P}}_{u\lambda}(-\boldsymbol{k})) \tag{4.30}$$

where $\phi^{\mathcal{D}}_{\eta\lambda}$ is related to the solute-solvent direct correlation function:

$$-\beta\phi^{\mathcal{D}}_{\eta\lambda}(\boldsymbol{k}) = c^{\mathcal{D}}_{\eta\lambda}(\boldsymbol{k}). \tag{4.31}$$

Using Eq.(4.29), the nonequilibrium ensemble average for a dynamical variable $\widehat{\mathcal{G}}$ is given by

$$\langle\langle\widehat{\mathcal{G}}\rangle\rangle = \langle\widehat{\mathcal{G}}\rangle^{\mathcal{S}} + \beta\langle\delta\widehat{\mathcal{G}}(t)\delta\widehat{\mathcal{E}}(0)\rangle, \tag{4.32}$$

where $\langle\widehat{\mathcal{G}}\rangle^{\mathcal{S}}$ is the ensemble average under the distribution $f^{\mathcal{S}}$, and $\langle\delta\widehat{\mathcal{G}}(t)\delta\widehat{\mathcal{E}}(0)\rangle$ is the equilibrium time correlation function denoted as $C_{\mathcal{G}}(t)$.

Substituting Eq.(4.10), Eq.(4.32) is thus written in the form:

$$\langle\langle\widehat{\mathcal{G}}\rangle\rangle = \langle\widehat{\mathcal{G}}\rangle^{\mathcal{S}} + [\langle\widehat{\mathcal{G}}\rangle^{\mathcal{P}} - \langle\widehat{\mathcal{G}}\rangle^{\mathcal{S}}]\cdot\Phi_{\mathcal{G}}(t) \tag{4.33}$$

where

$$\Phi_{\mathcal{G}}(t) = \frac{C_{\mathcal{G}}(t)}{C_{\mathcal{G}}(0)}. \tag{4.34}$$

Bibliography

[1] P. F. Barbara and W. Jarzeba, Adv. Photochem. **15**, 1 (1990).

[2] R. Jimenz, G. R. Fleming, P. V. Kumar, and M. Maroncelli, Nature (London) **369**, 471 (1994).

[3] *Solvent Effects and Chemical Reactivity*, edited by O. Tapia and J. Bertrán (Kluwer, Dordrecht, 1996).

[4] M. Maroncelli and G. R. Fleming, J. Chem. Phys. **86**, 6221 (1987).

[5] E. W. Castner, Jr., M. Maroncelli, and G. R. Fleming, J. Chem. Phys. **86**, 1090 (1987).

[6] M. A. Kahlow, T. J. Kang, and P. F. Barbara, J. Phys. Chem. **91**, 6452 (1987).

[7] M. A. Kahlow, T. J. Kang, and P. F. Barbara, J. Chem. Phys. **88**, 2372 (1988).

[8] S. J. Rosenthal, X. Xie, M. Du, and G. R. Fleming, J. Chem. Phys. **95**, 4715 (1991).

[9] *Ultrafast Reaction Dynamics and Solvent Effects: Theoretical and Experimental Aspects*, edited by Y. Gauduel and P. J. Rossky (AIP, New York, 1994).

[10] M. L. Horng, J. A. Gardecki, A. Papazyan, and M. Maroncelli, J. Phys. Chem. **99**, 17311 (1995).

[11] P. J. Rossky and J. D. Simon, Nature **370**, 263 (1994).

[12] X. Song and D. Chandler, J. Chem. Phys. **108**, 2594 (1998).

[13] M. Maroncelli and G. R. Fleming, J. Chem. Phys. **89**, 5044 (1988).

[14] B. M. Ladanyi and M. Maroncelli, J. Chem. Phys. **109**, 3204 (1998).

[15] M. Maroncelli, J. Chem. Phys. **94**, 2084 (1991).

[16] T. Fonseca and B. M. Ladanyi, J. Phys. Chem. **95**, 2116 (1991).

[17] K. Ando and S. Kato, J. Chem. Phys. **95**, 5966 (1991).

[18] P. V. Kumar and M. Maroncelli, J. Chem. Phys. **103**, 3038 (1995).

[19] K. Ando, J. Chem. Phys. **107**, 4585 (1997).

[20] M. Maroncelli, J. Mol. Liq. **57**, 1 (1993).

[21] J. Tomasi and M. Persico, Chem. Rev. **94**, 2027 (1994).

[22] S. Ten-no, F. Hirata, and S. Kato, Chem. Phys. Lett. **214**, 391 (1993).

[23] S. Ten-no, F. Hirata, and S. Kato, J. Chem. Phys. **100**, 7443 (1994).

[24] H. Sato, F. Hirata, and S. Kato, J. Chem. Phys. **105**, 1546 (1996).

[25] J. Gao, Acc. Chem. Res. **29**, 298 (1996).

[26] F. O. Raineri, H. Resat, B.-C. Perng, F. Hirata, and H. L. Friedman, J. Chem. Phys. **100**, 1477 (1994).

[27] F. O. Raineri, B.-C. Perng, and H. L. Friedman, Chem. Phys. **183**, 187 (1994).

[28] H. L. Friedman, F. O. Raineri, F. Hirata, and B.-C. Perng, J. Stat. Phys. **78**, 239 (1995).

[29] F. Hirata and P. J. Rossky, Chem. Phys. Lett. **83**, 329 (1981).

[30] F. Hirata, B. M. Pettitt, and P. J. Rossky, J. Chem. Phys. **77**, 509 (1982).

[31] F. Hirata, P. J. Rossky, and B. M. Pettitt, J. Chem. Phys. **78**, 4133 (1983).

[32] O. S. Khalil, J. L. Meeks, and S. P. McGlynn, Chem. Phys. Lett. **39**, 457 (1976).

[33] Y. Dimitrova, J. Mol. Struct.: THEOCHEM **362**, 23 (1996).

[34] A. L. Sobolewski and W. Domcke, Chem. Phys. Lett. **79**, 3078 (1997).

[35] E. Lippert, W. Lüder, F. Moll, W. Nägele, H. Boos, H. Prigge, and I. Seibold-Blankenstein, Angew. Chem. **73**, 695 (1961).

[36] K. Rotkiewicz, K. H. Grellmann, and Z. R. Grabowski, Chem. Phys. Lett. **19**, 315 (1973).

[37] F. Hirata, J. Chem. Phys. **96**, 4619 (1992).

[38] F. Hirata, T. Munakata, F. Raineri, and H. L. Friedman, J. Mol. Liq. **65**, 15 (1995).

[39] T. H. Dunning, Jr. and P. J. Hey, in *Modern Electronic Structure Theory*, edited by H. F. Schaefer III (Plenum, New York, 1977).

[40] H. Nakano, Chem. Phys. Lett. **207**, 372 (1993).

[41] H. Nakano, J. Chem. Phys. **99**, 7983 (1993).

[42] H. J. C. Brendsen, J. P. M. Postma, W. F. von Gustern, and J. Hermas, in *Intermolecular Forces*, edited by B. Pullman (Reidel, Dordrecht, 1981).

[43] W. L. Jorgensen, J. Am. Chem. Soc. **103**, 335 (1981).

[44] F. Hirata and R. M. Levy, J. Phys. Chem. **91**, 4788 (1987).

[45] W. L. Jorgensen and J. M. Briggs, Mol. Phys. **63**, 547 (1988).

[46] W. L. Jorgensen and T. B. Nguyen, J. Comput. Chem. **14**, 195 (1993).

[47] R. D. Mountain, J. Chem. Phys. **107**, 3921 (1997).

[48] R. E. Rathbum and A. L. Babb, J. Phys. Chem. **65**, 1072 (1961).

[49] A. J. Easteal, A. V. Edge, and L. A. Woolf, J. Phys. Chem. **88**, 6060 (1984).

[50] J. Casado, L. Nygaard, and G. O. Sørensen, J. Mol. Struct. **8**, 211 (1971).

Figure Caption

Fig. 1. Optimized geometry for benzonitrile in the gas phase with site numbering. Values in parentheses are the experimental values.

Fig. 2. Time dependent radial distribution functions between the solute and solvent sites in water. Those before and after the solvent relaxation are denoted by $t = 0$ and ∞. (a) C_7-O and H, (b) N_8-O and H.

Fig. 3. Time dependent radial distribution functions between the solute and solvent sites in methanol. (a) C_7-O and H, (b) N_8-O and H. See Fig. 2.

Fig. 4. Time dependent radial distribution functions between the solute and solvent sites in acetonitrile. (a) C_7-CH_3 and N, (b) N_8-CH_3 and N. See Fig. 2.

Fig. 5. Solvation time correlation functions for H_2O, CH_3OH and CH_3CN solutions.

Fig. 6. Time-dependent variations of solute dipole moment after the vertical excitation.

Fig. 7. Solute charge time correlation function for C_1, C_6, C_7 and N_8 sites in benzonitrile. (a) in H_2O (b) in CH_3OH (c) in CH_3CN.

Fig. 8. Solvent charge polarization around C_1, C_6, C_7 and N_8 sites in water. (a) C_1 and C_6 sites (b) C_7 and N_8 sites.

Table.I: Parameters for Solvents and Solute

solvent[a]	site	q	σ/Å	$\epsilon/kcalmol^{-1}$
H_2O	H	0.41	1.000	0.056
	O	−0.82	3.166	0.155
CH_3OH	CH_3	0.285	3.86	0.181
	O	−0.685	3.08	0.175
	H	0.4	1.00	0.055
CH_3CN	CH_3	0.15	3.775	0.206
	C	0.28	3.650	0.150
	N	−0.43	3.200	0.169

solute[b]	σ/Å	$\epsilon/kcalmol^{-1}$
C	3.550	0.070
C(-C≡N)	3.550	0.070
C(in C≡N)	3.650	0.150
N(in C≡N)	3.200	0.170
H	2.420	0.030

[a] Data from refs 42 for H_2O, ref 43,44 for CH_3OH, ref 45 for CH_3CN.
[b] Reference 46.

Table.II: The Solute Site Charges (Units in Electronic Charges)

	gas		H_2O			CH_3OH			CH_3CN		
	S_0	vertical	S_0	vertical	$t=\infty$	S_0	vertical	$t=\infty$	S_0	vertical	$t=\infty$
C_1	0.061	0.212	0.011	0.061	−0.090	0.026	0.096	−0.004	0.035	0.118	0.052
C_2	−0.115	−0.328	−0.118	−0.283	−0.241	−0.113	−0.293	−0.265	−0.112	−0.301	−0.283
C_4	−0.103	0.079	−0.121	0.034	0.041	−0.109	0.057	0.058	−0.104	0.069	0.068
C_6	−0.089	0.001	−0.094	0.049	0.175	−0.090	0.038	0.113	−0.089	0.030	0.078
C_7	0.296	0.230	0.450	0.400	0.474	0.382	0.330	0.365	0.337	0.283	0.296
N_8	−0.422	−0.445	−0.583	−0.641	−0.775	−0.518	−0.567	−0.633	−0.473	−0.516	−0.547
H_9	0.124	0.139	0.143	0.163	0.155	0.133	0.152	0.146	0.128	0.146	0.140
H_{11}	0.116	0.079	0.138	0.106	0.108	0.128	0.095	0.098	0.124	0.090	0.094
H_{13}	0.110	0.064	0.132	0.091	0.090	0.122	0.081	0.085	0.118	0.077	0.083

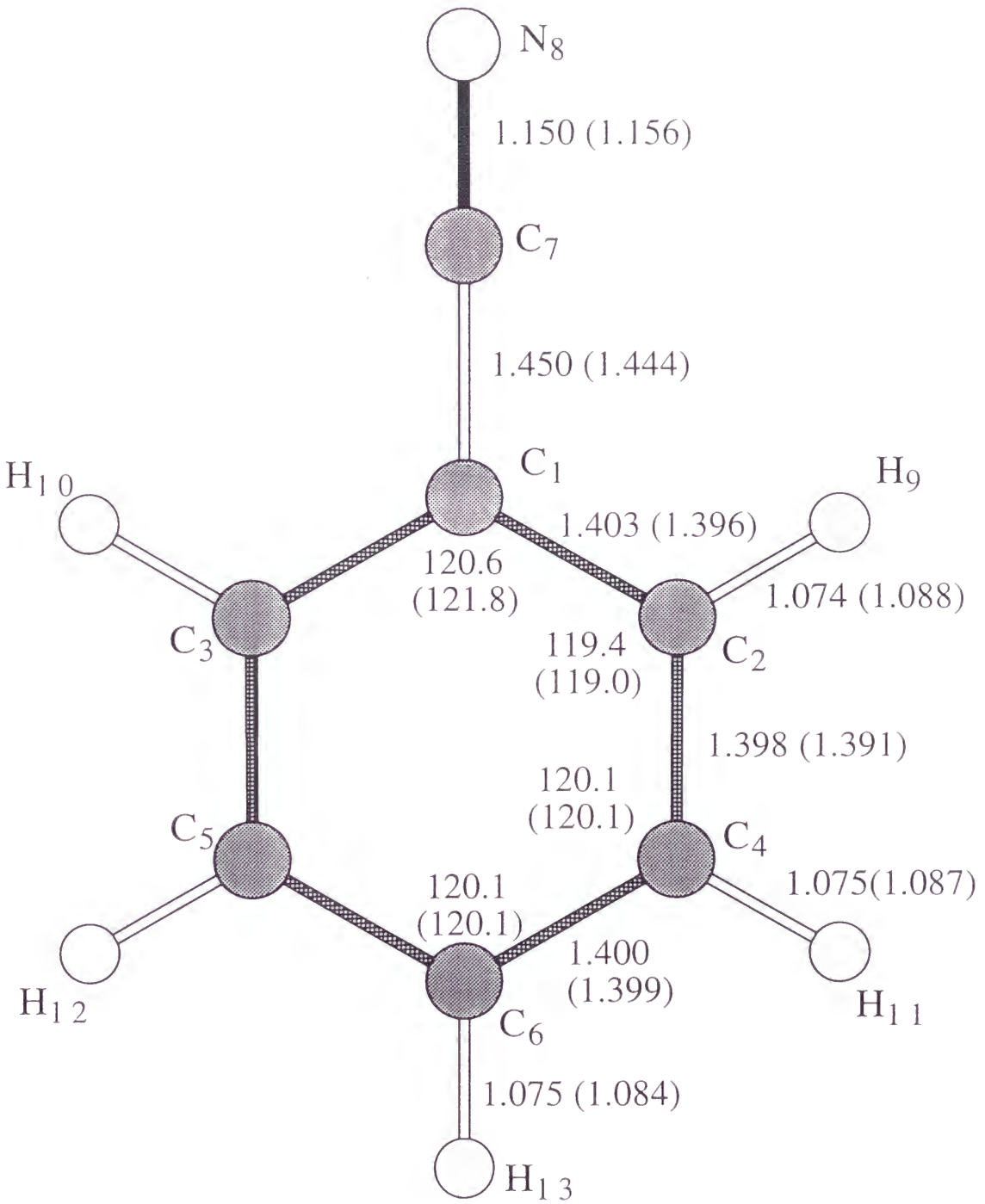
N8
1.150 (1.156)
C7
1.450 (1.444)
C1
H10
H9
1.403 (1.396)
120.6
(121.8)
1.074 (1.088)
C3
119.4
(119.0)
C2
1.398 (1.391)
120.1
(120.1)
C5
C4
120.1
(120.1)
1.075(1.087)
1.400
(1.399)
H12
H11
C6
1.075 (1.084)
H13

FIG.1.

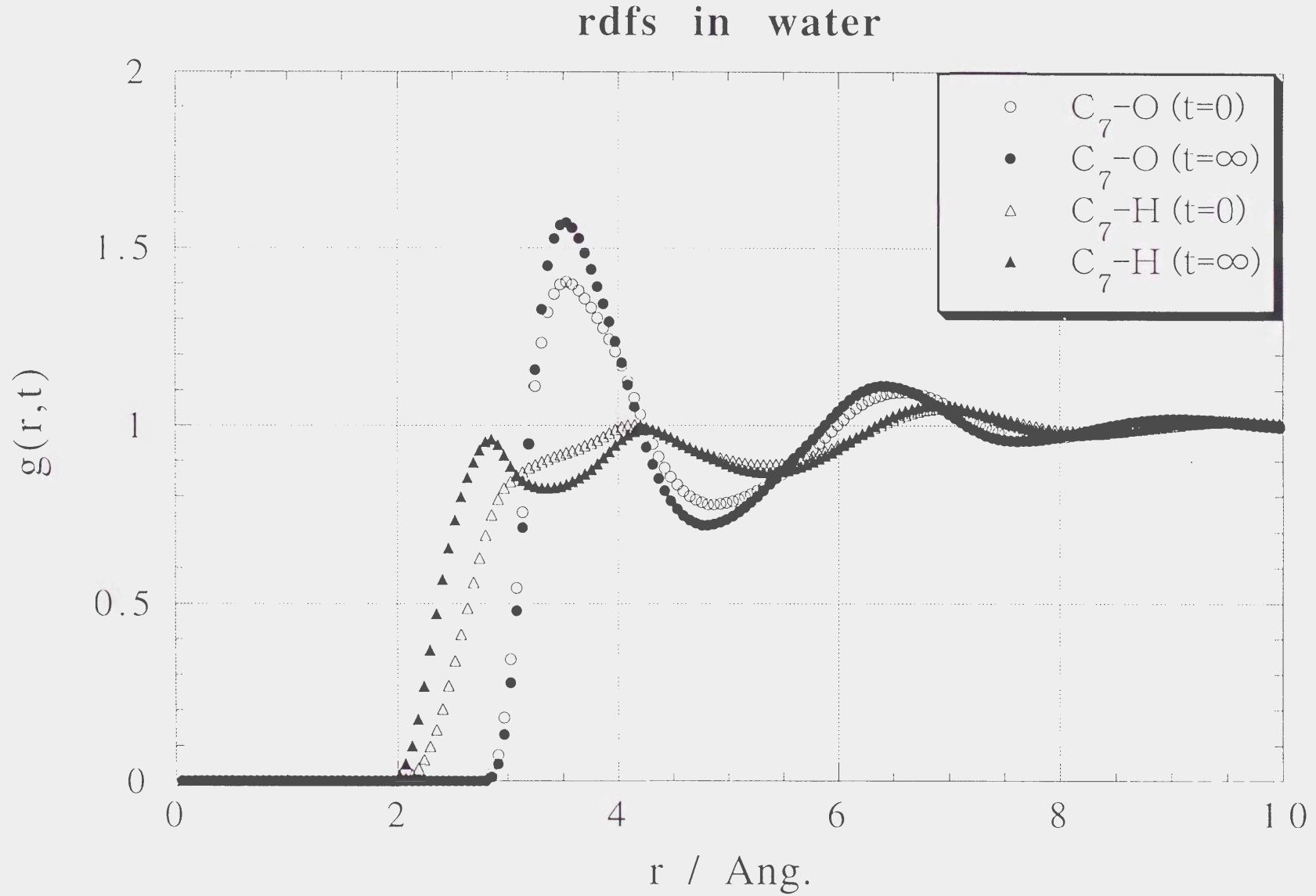
rdfs in water
g(r,t)
r / Ang.
0
0.5
1
1.5
2
0
2
4
6
8
10
C7-O (t=0)
C7-O (t=∞)
C7-H (t=0)
C7-H (t=∞)

FIG. 2. (a)

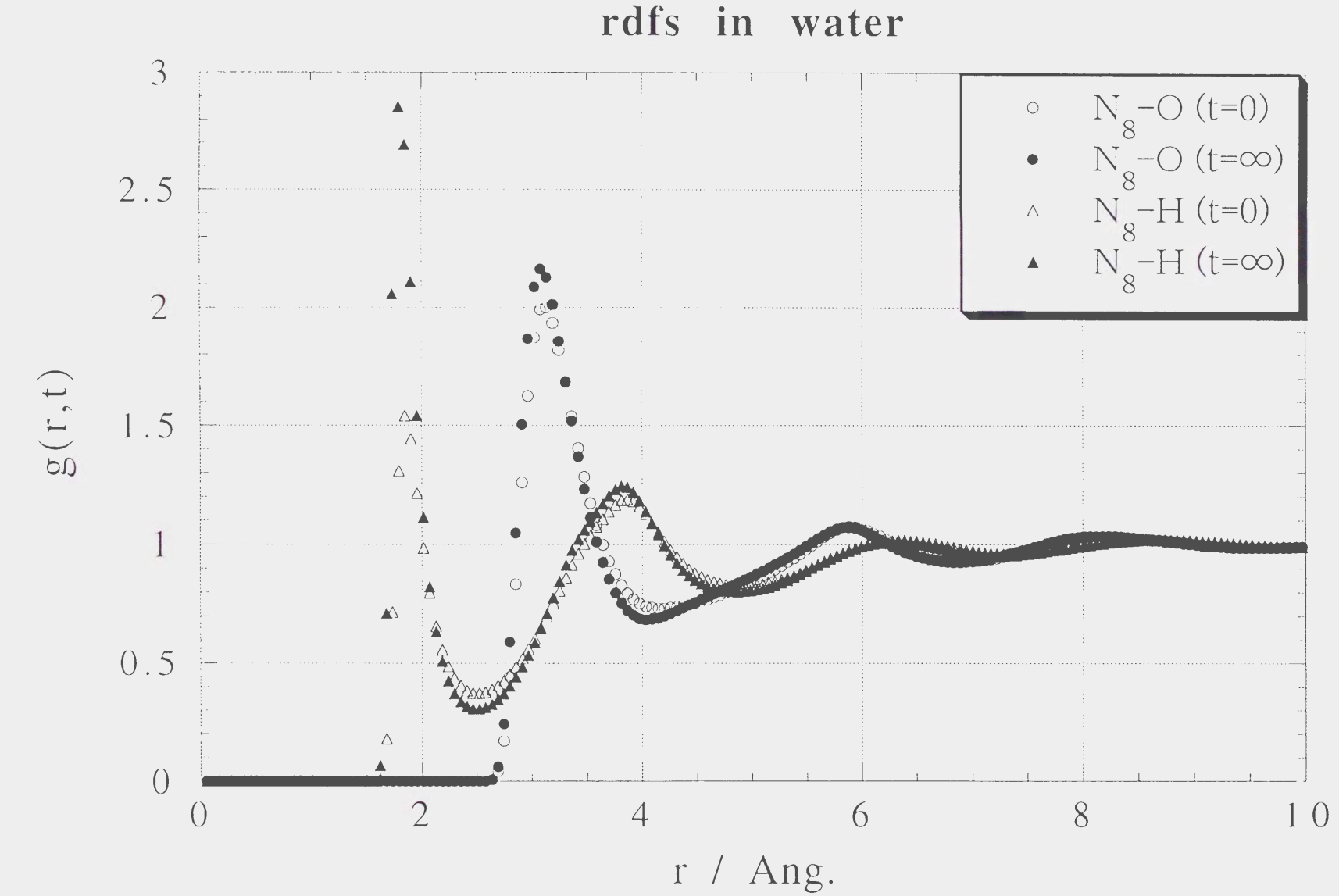
rdfs in water
g(r,t)
r / Ang.
0
0.5
1
1.5
2
2.5
3
0
2
4
6
8
10
N8-O (t=0)
N8-O (t=∞)
N8-H (t=0)
N8-H (t=∞)

FIG.2. (b)

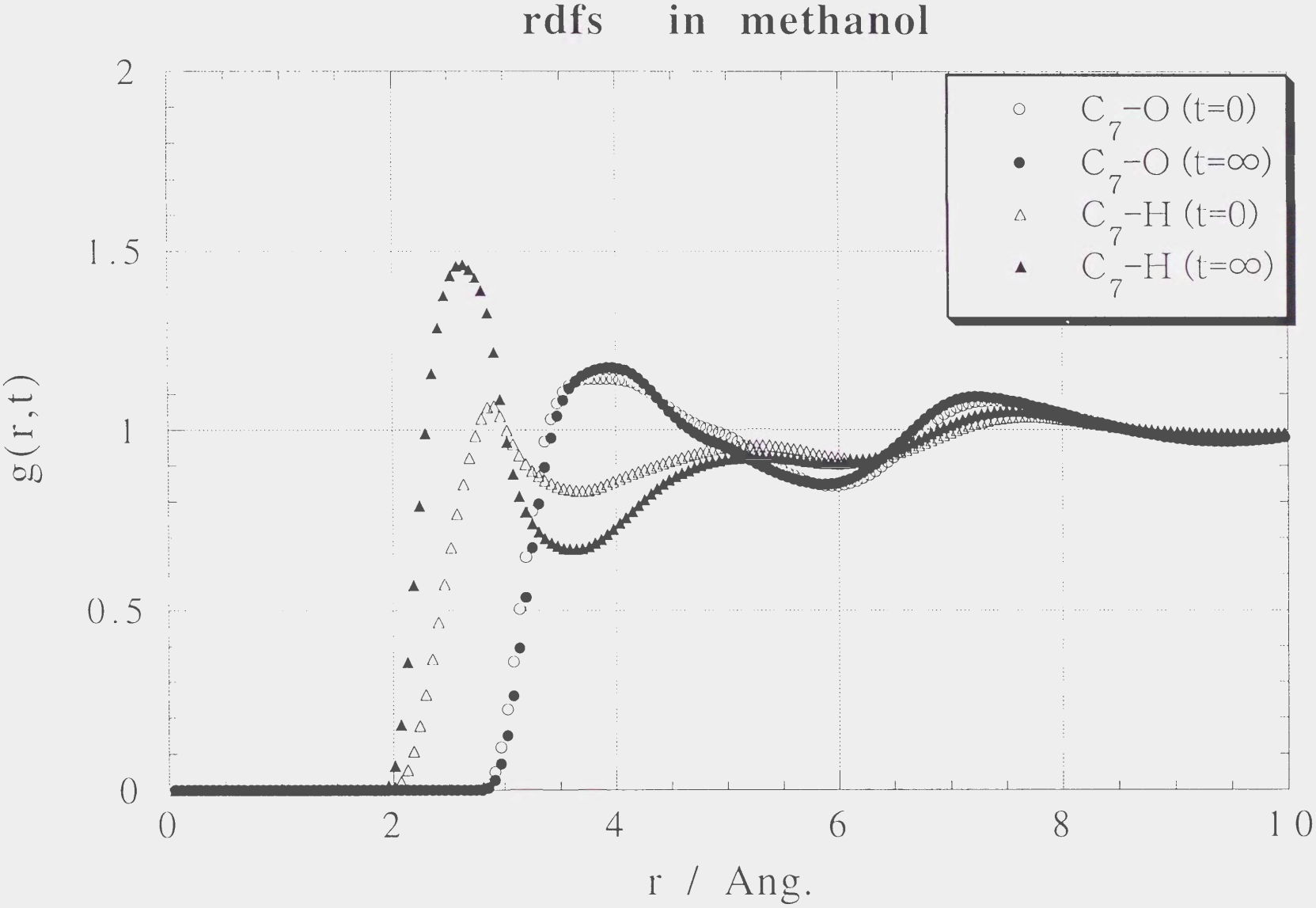
rdfs in methanol
C7-O (t=0)
C7-O (t=∞)
C7-H (t=0)
C7-H (t=∞)
g(r,t)
r / Ang.
0
0.5
1
1.5
2
0
2
4
6
8
10

FIG.3. (a)

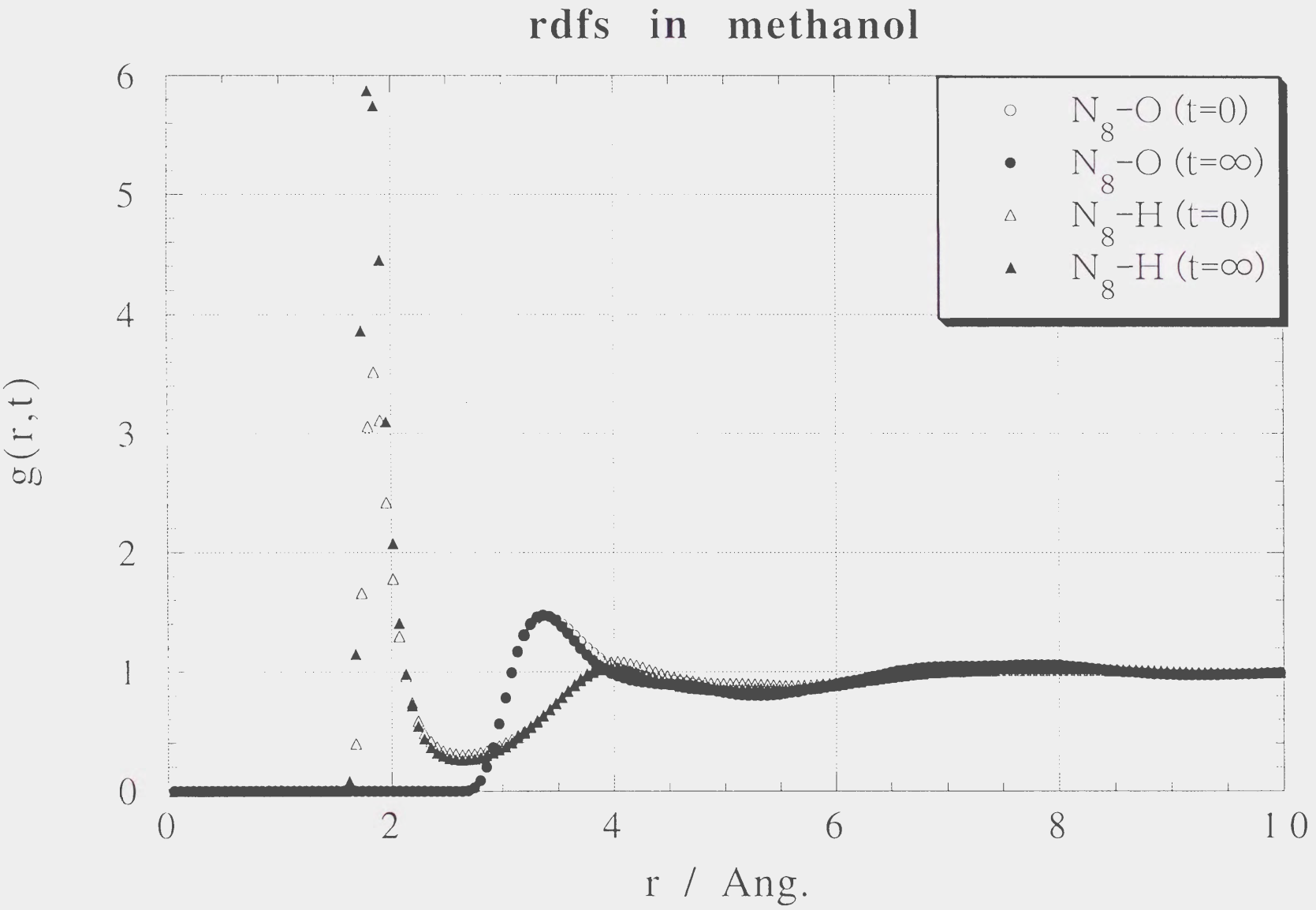
rdfs in methanol
g(r,t)
r / Ang.
0
1
2
3
4
5
6
0
2
4
6
8
10
N8-O (t=0)
N8-O (t=∞)
N8-H (t=0)
N8-H (t=∞)

FIG.3. (b)

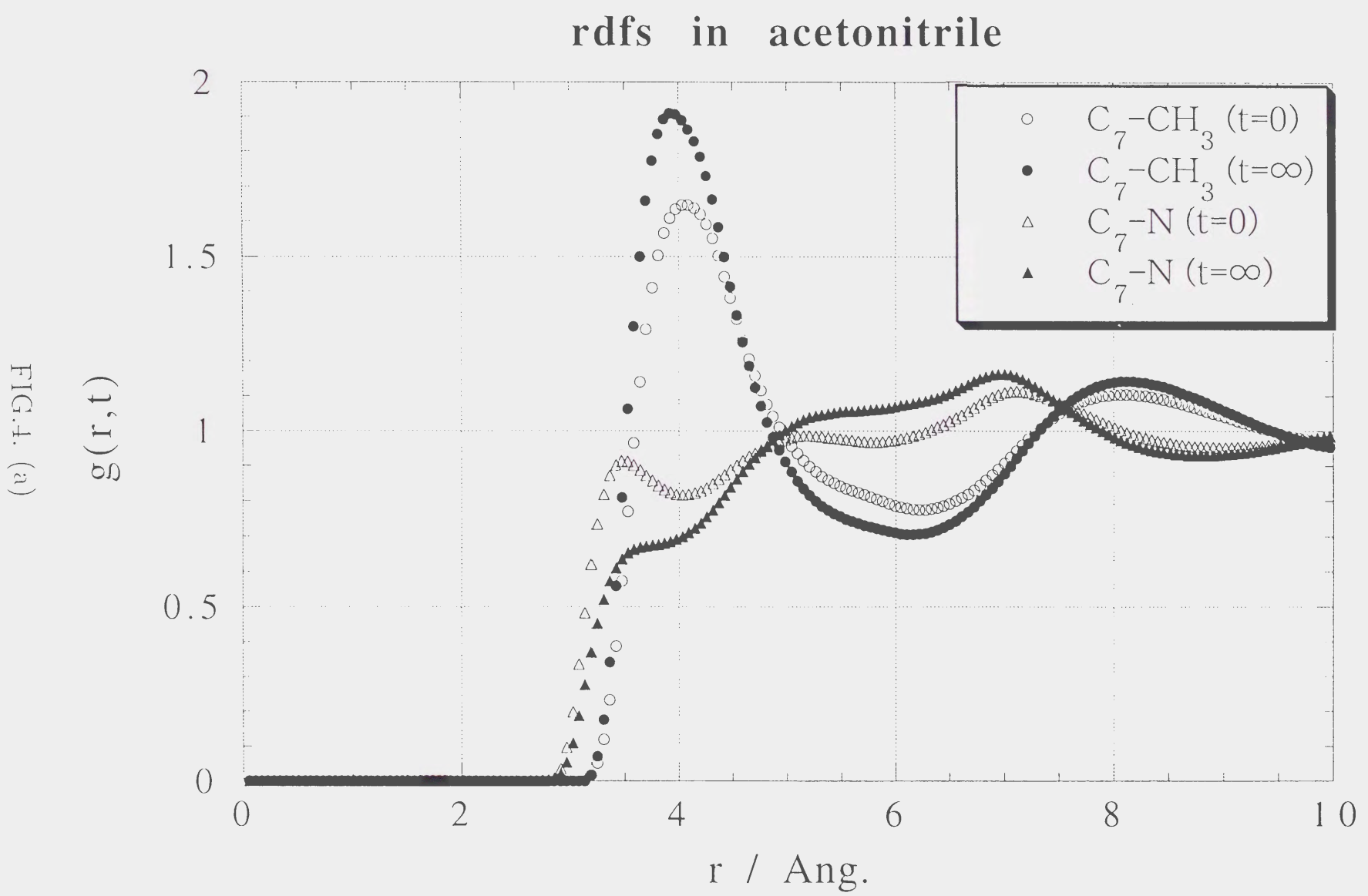
rdfs in acetonitrile
C7-CH3 (t=0)
C7-CH3 (t=∞)
C7-N (t=0)
C7-N (t=∞)
g(r,t)
r / Ang.
0
0.5
1
1.5
2
0
2
4
6
8
10

FIG.4. (a)

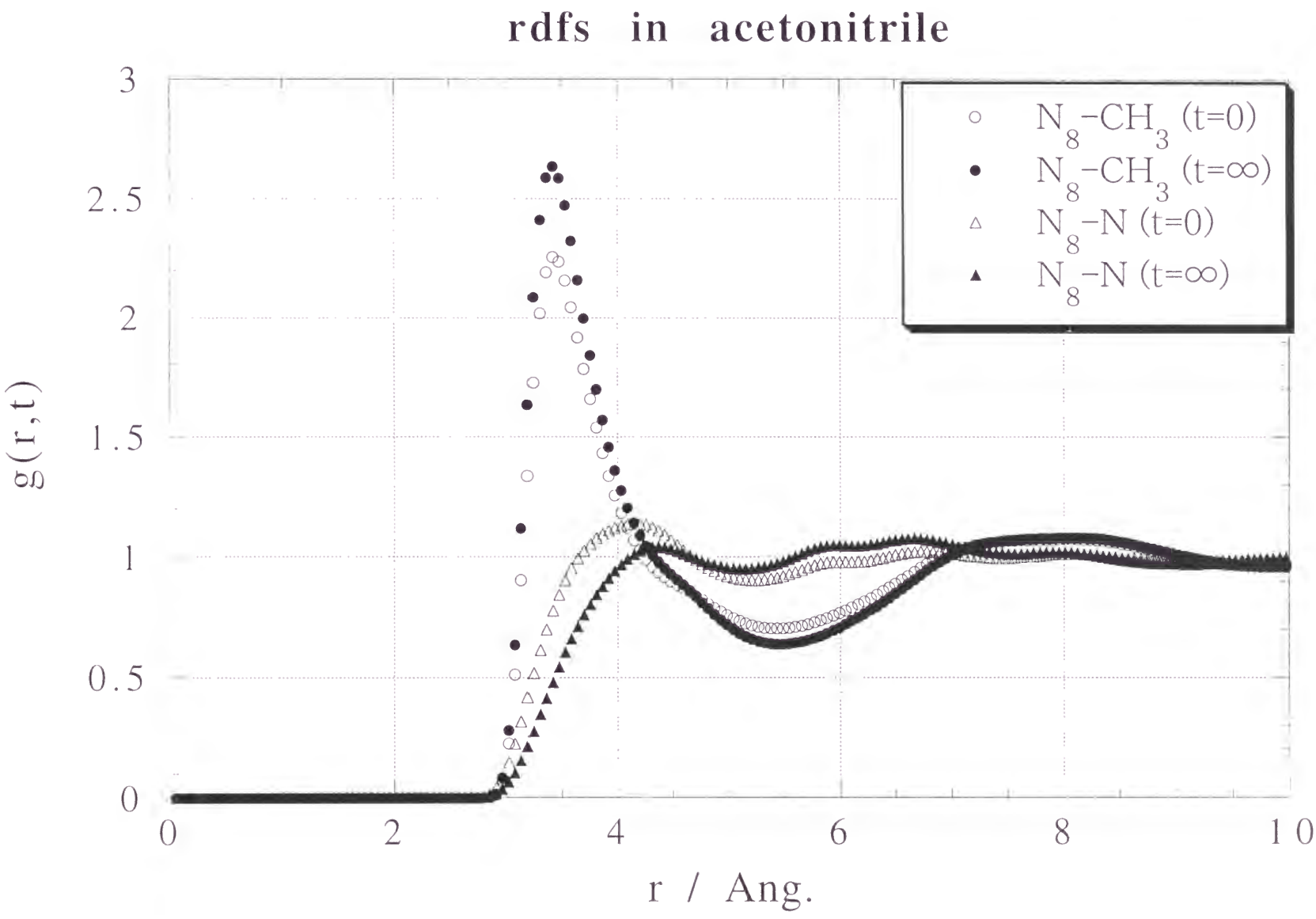
rdfs in acetonitrile
g(r,t)
r / Ang.
N8–CH3 (t=0)
N8–CH3 (t=∞)
N8–N (t=0)
N8–N (t=∞)
0
0.5
1
1.5
2
2.5
3
0
2
4
6
8
10

FIG.4. (b)

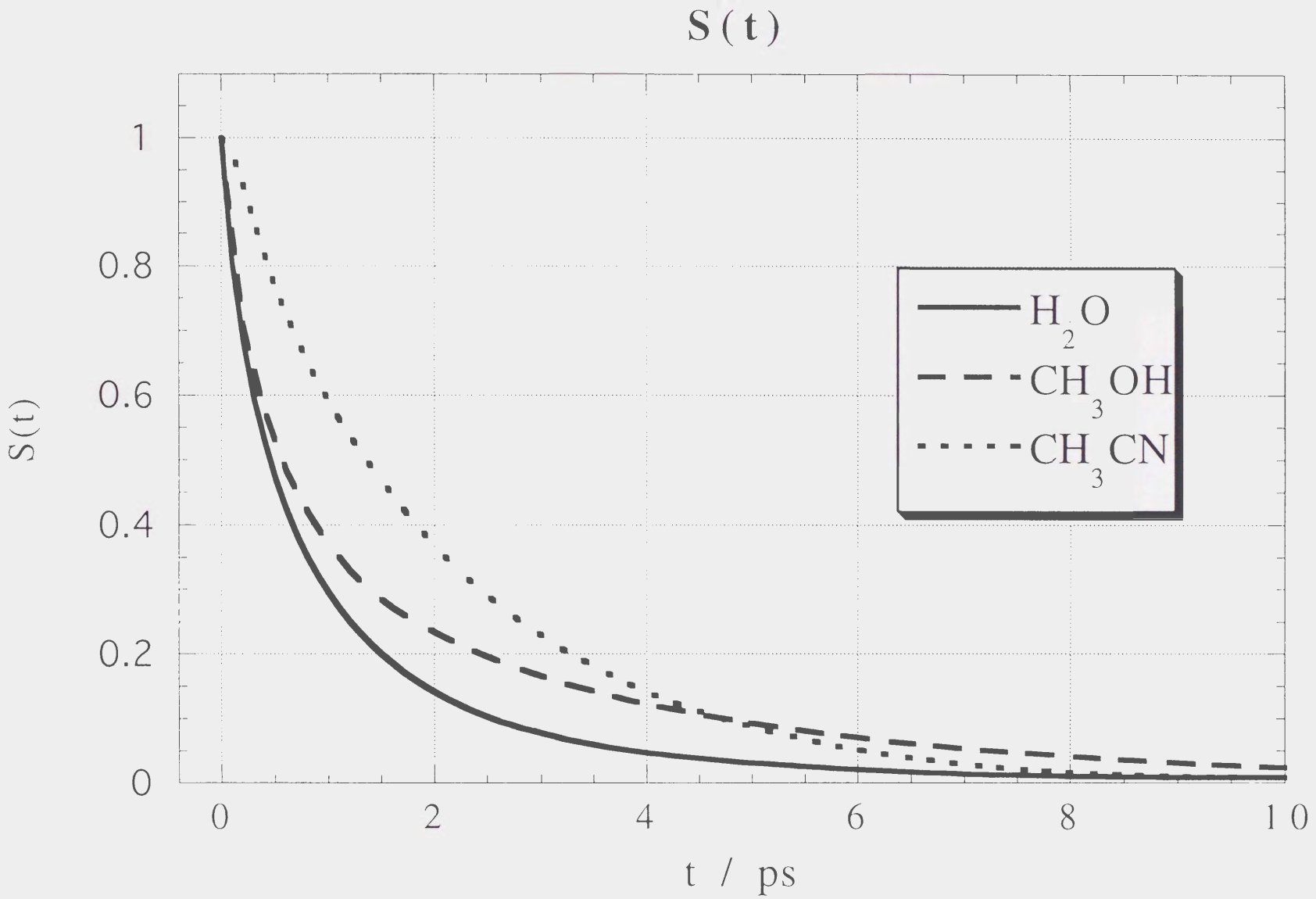

FIG.5.

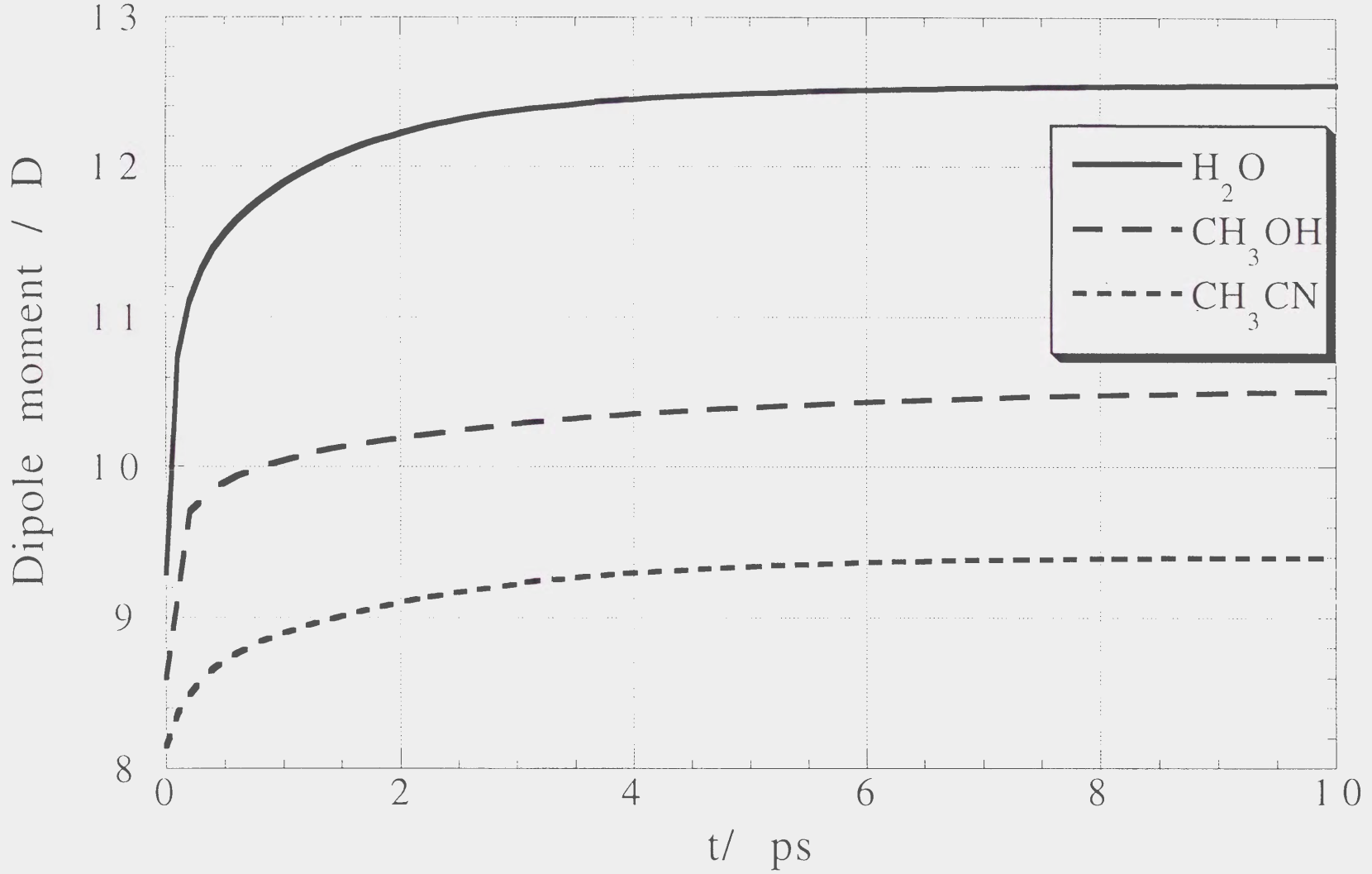

FIG.6.

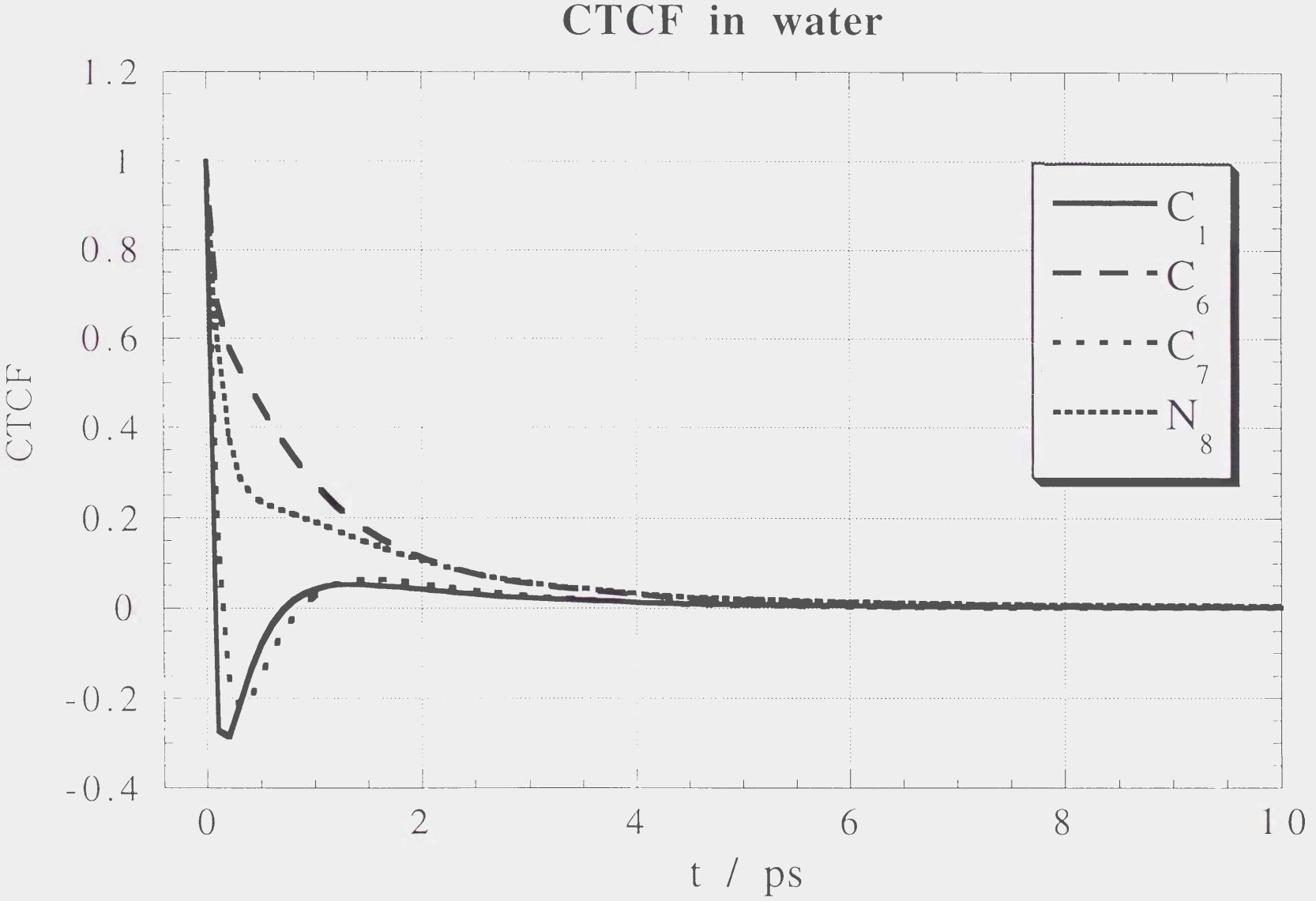

FIG. 7. (a)

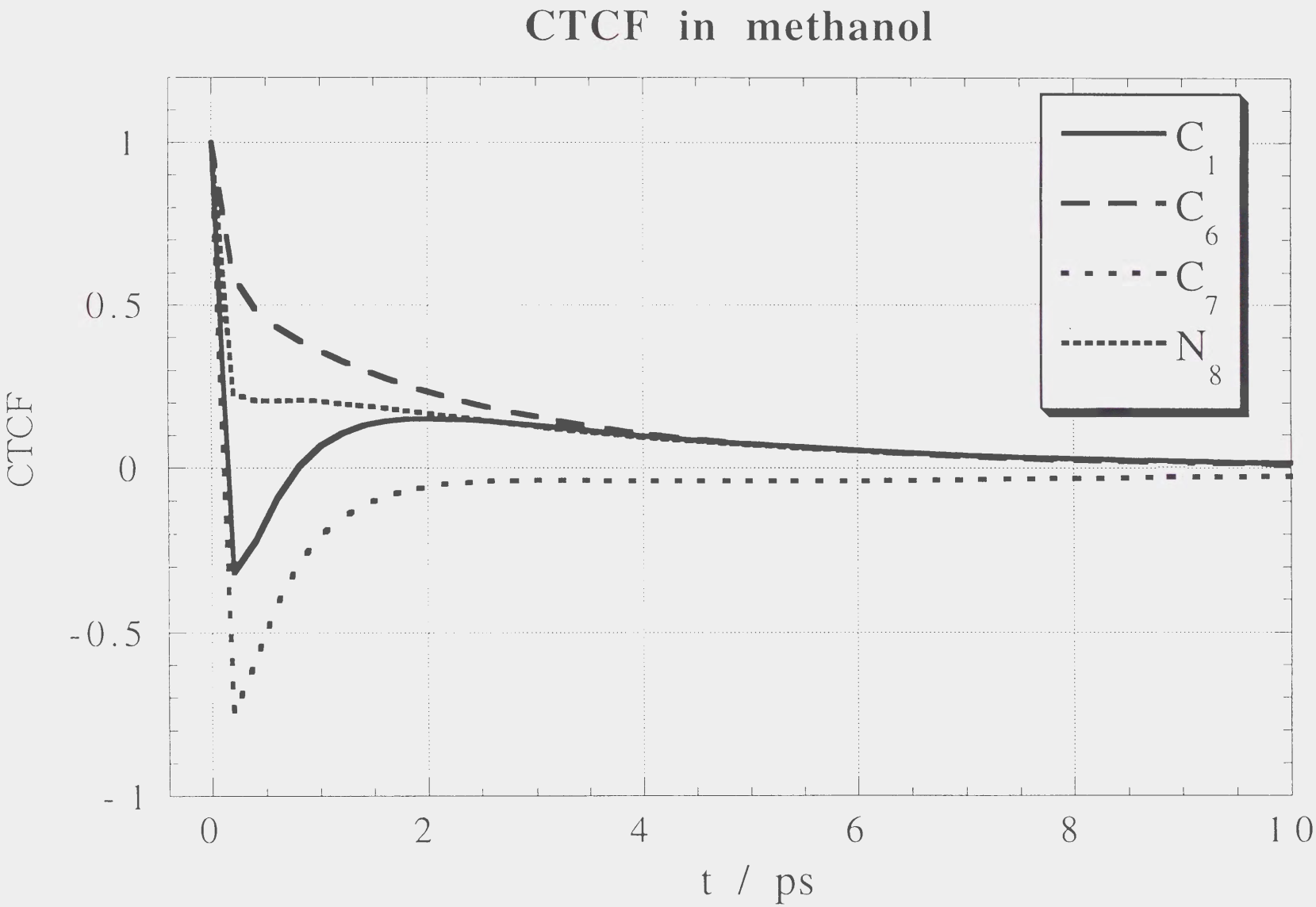

FIG.7. (b)

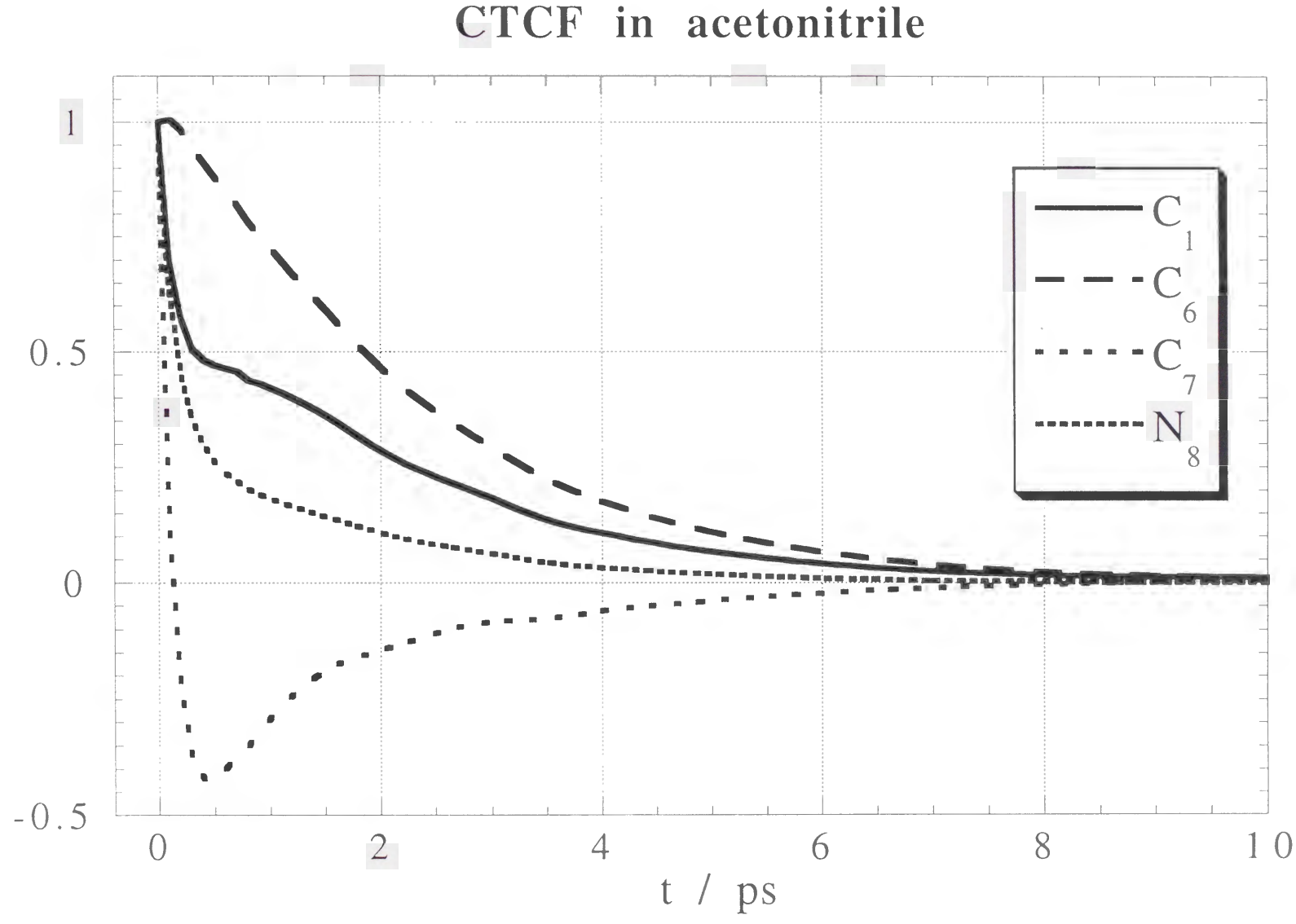

FIG.7. (c)

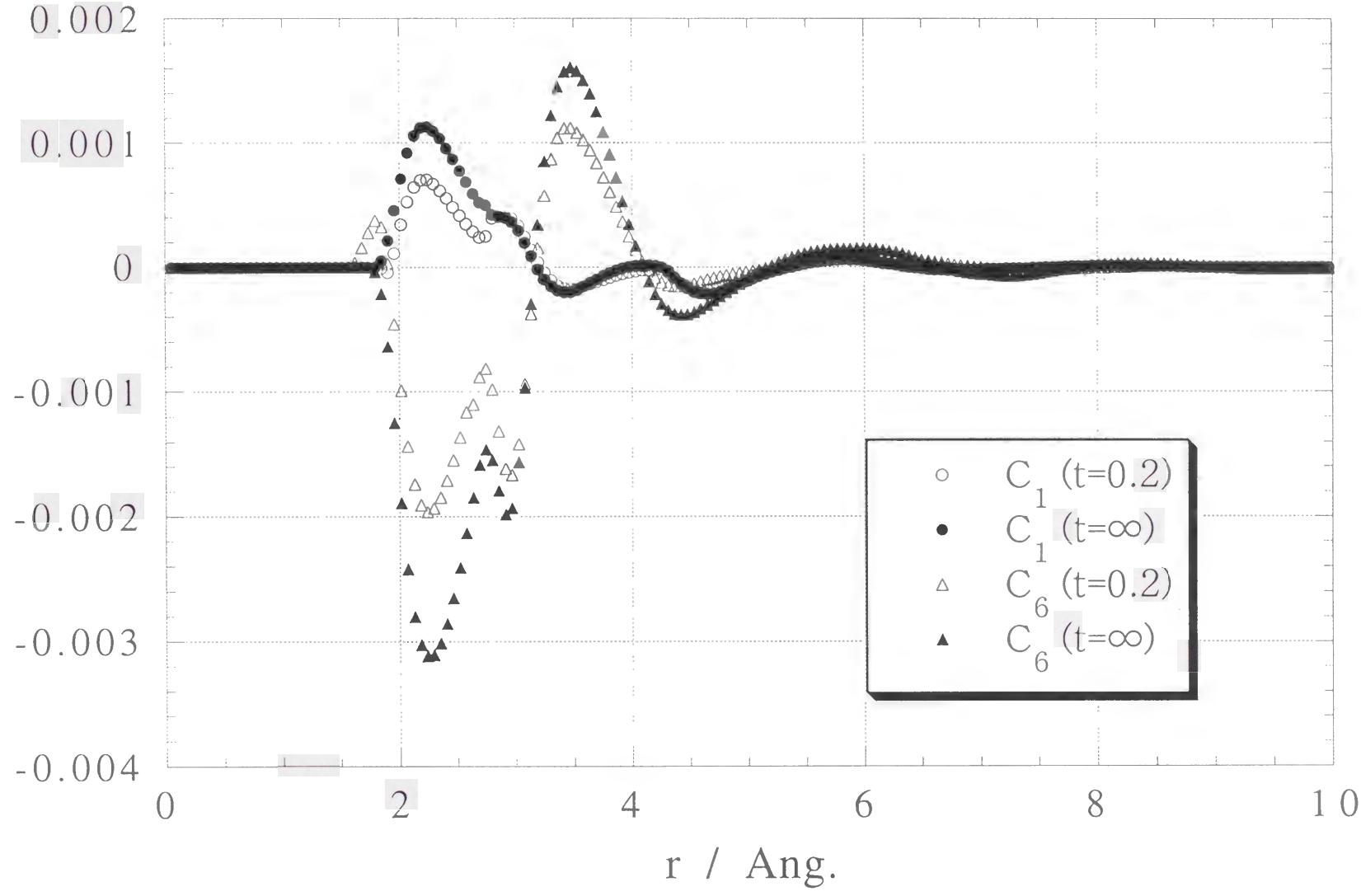
0.002
0.001
0
-0.001
-0.002
-0.003
-0.004
0
2
4
6
8
10
r / Ang.
$\Delta V_u(r,t)$ / e/Å^4
C_1 (t=0.2)
C_1 (t=∞)
C_6 (t=0.2)
C_6 (t=∞)

FIG.8. (a)

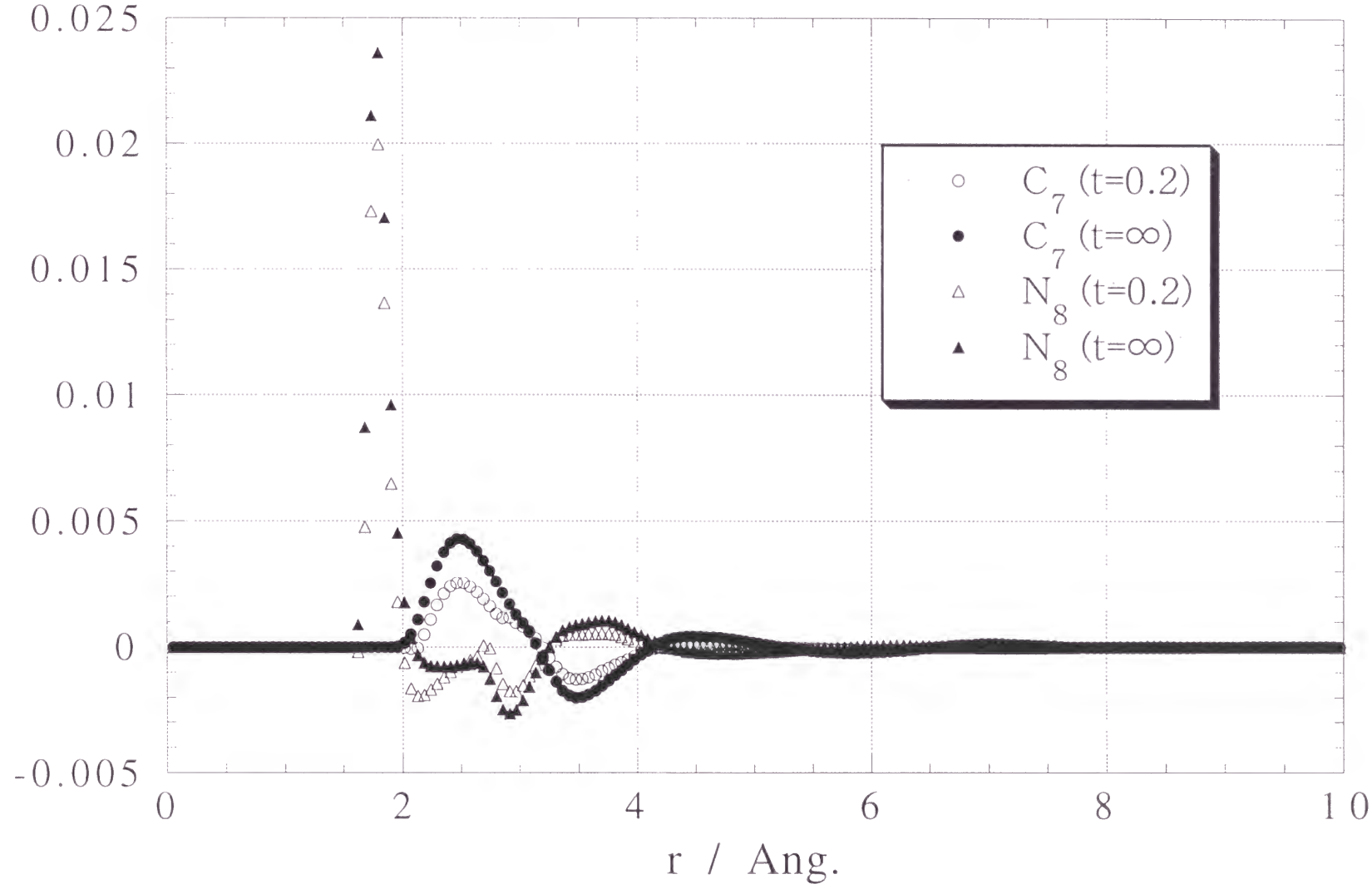
0.025
0.02
0.015
0.01
0.005
0
-0.005
0
2
4
6
8
10
r / Ang.
$\Delta V_u(r,t)$ / e/Å^4
C_7 (t=0.2)
C_7 (t=∞)
N_8 (t=0.2)
N_8 (t=∞)

FIG.8. (b)

Chapter 5

Conclusion

In the thesis, solvation processes in polar or nonpolar solvents by the electronic structure and statistical mechanical approach are studied, mainly focused on solvent effects on the solute electronic structure.

In the chapter 2, we investigated the optimized geometries and excess chemical potentials (Note that the latter is denoted as the solvation free energies in the chapter 2) of the keto and enol tautomers of formamide in six organic aprotic solvents: CS_2, CCl_4, dimethylether, THF, acetonitrile and DMSO, by the RISM-SCF method. It is found that the contribution of the solute-solvent hydrogen bonding to the solvation free energy is large and that the solvent ability to form hydrogen bonding is very important. It is also shown that Taft's β parameters (for the solvent ability to accept a proton in solute) is are well correlated to the calculated well-depth of the hydrogen bonding. The analysis indicates the irregularity in the acetonitrile solution for the solvation free energies for both tautomers. This can not be explained by the dielectric continuum theory, but our results are in qualitative accord with the solvent parameters determined empirically. Therefore, from our analyses, the empirical measure of the solvent ability to form hydrogen bonding

with solute is explained at a molecular level.

The solvent effects on the energy difference of total free energy between the keto-enol tautomers were studied. It is shown that the keto tautomer is stabilized largely compared to the enol one and that out results are consistent with the experimental and previous reported theoretical studies. For both tautomers, solute dipole moments are largely enhanced in polar solvents. Also, the solute geometry are changed so that its dipole moment is increased, and the tendency of solute dipole moments is correlated to the solvent polarity parameters determined by Taft *et al.*.

In the chapter 3, we studied the keto-enol tautomerization equilibrium of acetylacetone in CCl_4, DMSO and H_2O by the RISM-SCF method. Based on the results with the RISM-SCF procedure, the thermodynamic analysis of the solvation free energy by decomposing them into the enthalpy and entropy terms as well as the solute electronic and vibrational one was carried out. The geometry of keto tautomer shows a large change in polar solvents from that in the gas phase. The dihedral angle between the planes containing two carbonyl groups is decreased to be 56.4 and 75.2° in H_2O and DMSO, respectively. In CCl_4, the geometry was almost the same as in the gas phase. In the enol form, the geometry change due to the solvation was rather small even in polar solvents. The calculated keto-enol free energy difference in solution was in good agreement with the experiments, taking the vibrational free energy difference and zero-point energy contributions as well as the electron correlation effect of solute molecule.

The calculated solvation enthalpies for both tautomers were comparable to the experiment estimates in CCl_4 and DMSO, but a large discrepancy in solvation enthalpies in H_2O between the calculation and experiment was observed, and this was assigned to the overestimation of the solvent reorganization energy in water. Also, for large geometric

changes of the keto form in polar solvents, it was found that those are driven by the enthalpy term for aqueous solution while the entropy term is dominant in DMSO.

In the chapter 4, we proposed a time-dependent RISM-SCF approach with the time-depedent radial distribution functions based on the surrogate linear response theory and it is applied to the study of the solvation dynamics of the 2^1A_1 excited state of benzonitrile (C_6H_5CN) in H_2O, CH_3OH and CH_3CN solvents. The 2^1A_1 excited state was found to be of ionic character with the dipole moment of 6.75 D in the gas phase. In solutions, the solute dipole moment was enhanced to 9.29, 8.60 and 8.15 D in H_2O, CH_3OH and CH_3CN solvents just after the vertical excitation to this state. The red shift of 6230~6500 cm^{-1} for the vertical excitation energy in solution is attributed to a large difference of the dipole moment between the excited and ground states. The solute dipole moment increased to 12.6, 10.5 and 9.4 D in the respective solvent after the solvent relaxation. These indicate that the electron distribution of 2^1A_1 state is very sensitive to the change of electrostatic field caused by the solvent polarization. The calculated STCFs indicated that non-exponential behaviors characterized by the fast and slow components. Calculated fast components were consistent with those obtained by MD simulation studies for a benzene-like solute model. A long-time tail was observed with the decay rate of 24.7 ps in CH_3OH, while the solvent relaxation almost completed within 5 ps in H_2O and CH_3OH. The evolution of solute electronic structure during the solvation process was investigated, defining and observing the solute charge time correlation function (CTCF). The CTCF changes very rapidly at the initial stage of solvent relaxation particularly at solute C_1, C_7 and N_8 sites in contrast to the behavior of the STCFs. In the SSSV theory that we employ in the present study, the inertial term is neglected. Therefore, a rather slower relaxation at the initial region immediately after the vertical excitation was

resulted. It would be required to improve the present procedure considering the inertial effect correctly. Nevertheless, we could show the importance of treating solute electronic structure explicitly with the models taking account of molecular geometric aspects in the time-dependent (nonequilibrium) process, e.g. solvation processes.

Acknowledgements

The author is grateful to Professor Shigeki Kato for his valuable discussion, suggestions and continuous encouragement and also to Professor Fumio Hirata for his fruitful discussion, advices and continuous encouragement. The author also thanks to the members of the laboratory and the department.

Finally, the author expresses his gratitude to his parents and family.

February, 1999

Kyoto

Tateki Ishida